# GENERALIZED DISCONTINUOUS MULTISCALE METHODS FOR FLOWS IN HIGHLY HETEROGENEOUS POROUS MEDIA

A Dissertation

by

MINAM MOON

Submitted to the Office of Graduate and Professional Studies of
Texas A&M University
in partial fulfillment of the requirements for the degree of

DOCTOR OF PHILOSOPHY

| | |
|---|---|
| Chair of Committee, | Raytcho Lazarov |
| Co-Chairs of Committee, | Yalchin Efendiev |
| Committee Members, | Bojan Popov |
| | Jean Ragusa |
| Head of Department, | Emil J. Straube |

August 2015

Major Subject: Mathematics

ABSTRACT

This dissertation is devoted to the development, study and testing of numerical methods for elliptic and parabolic equations with heterogeneous coefficients. The motivation for this study is to meet the need for fast and robust methods for numerical upscaling and simulation of single and multi-phase fluid flow in highly heterogeneous porous media. We consider the multiscale model reduction technique in the framework of the discontinuous Galerkin (DG) and the hybridizable discontinuous Galerkin (HDG) finite element methods.

First, we design multiscale finite element methods for second order elliptic equations by applying the symmetric interior penalty discontinuous Galekin finite element method. We propose two different types of finite element spaces on the coarse mesh within DG framework. The first type of spaces is based on a local spectral problem that uses an interior weighted $L^2$-norm and a boundary weighted $L^2$-norm for computing the mass matrix. The second choice is based on generation of a snapshot space and subsequent selection of a subspace of a reduced dimension.

Second, we develop multiscale model reduction methods within the HDG framework. We provide construction of several multiscale finite element spaces (related to the coarse-mesh edges) that guarantee a reasonable approximation on a reduced dimensional space of the numerical traces. In these approaches, we use local snapshot spaces and local spectral decomposition following the concept of Generalized Multiscale Finite Element Methods. We also provide a general framework for systematic construction of multiscale spaces. By using local snapshots we were able to add local features to the solution space and to avoid high dimensional representation of trace spaces. Further, we extend multiscale finite element methods within HDG method

to nonlinear and/or time-dependent problems. These extensions demonstrate the potential of the proposed constructions for some advanced and more practical applications.

For most of the proposed methods, we investigate their stability and derive error estimates for the approximate solutions. Furthermore we study the performance of all proposed methods on a representative number of numerical examples. In the numerical tests, we use various permeability data of highly heterogeneous porous media and contrasts ranging from $10^3$ to $10^6$. Since the exact solution is in general unknown, we first generate solutions on a very fine mesh and use them as reference solutions in our tests. The numerical results confirm the theoretical study of the accuracy of the proposed methods and their robustness with respect to the media contrast. Our numerical experiments also show that the proposed methods could be implemented in a practical and efficient way.

# ACKNOWLEDGEMENTS

I would like to express my deep appreciation to Dr. Raytcho Lazarov and Dr. Yalchin Efendiev for providing wonderful support during my graduate career. Dr. Raytcho Lazarov showed me invaluable insights and encouraged me to achieve better results. He also guided me during my graduate process to keep me on the right track. Dr. Yalchin Efendiev gave me many great ideas for my research. In addition, I would like to thank my committee members, Dr. Bojan Popov and Dr. Jean Ragusa, for their detailed comments and directions throughout my PhD work.

I also would like to thank to Dr. Juan Galvis and Dr. Ke Shi for great discussions and technical help. I wish to express my gratitude to the Department of Mathematics, especially to Dr. Peter Howard, who was departmental graduate advisor during my graduate career. I also wish to present my appreciation to Ms. Monique Stewart for her incredible knowledge as a graduate program assistant.

I would like to thank my wife, my parents, and my daughter for their encouragement throughout my time at Texas A&M University. Without their love and support this work would never have been completed.

Finally, I would like to acknowledge the financial support I have received throughout my graduate studies. This work was supported by funding from Korean Army and the Department of Mathematics. I am grateful to the Department of Mathematics for providing my graduate teaching and research assistantships throughout my study.

TABLE OF CONTENTS

Page

LIST OF FIGURES

LIST OF TABLES

# 1. INTRODUCTION

Flows in porous media have wide ranging applications in many fields of industry, science, engineering and the environment. In many applications, flows are in highly heterogeneous media with properties that vary with different scales and have disparate values. Such are the flows in fractured and vuggy porous media, where the fractures and vugs are primary conduits. Conductivities of fractures can be many orders of magnitude higher than the conductivity of the surrounding media. The simplest model is based on the principle of conservation of mass and Darcy's law representing a relationship between pressure $u$ and Darcy velocity $\boldsymbol{q}$:

$$\nabla \cdot \boldsymbol{q} = f \quad \text{and} \quad \boldsymbol{q} = -\frac{\kappa}{\mu}\nabla u,$$

where $\kappa$ is the permeability of the media (in general a tensor), $\mu$ is the viscosity of the invading fluid and $f$ is the source term. Examples of media on a micro-level are shown in Figure 1.

The above system could be written in more compact form as an equation of second order

$$-\nabla \cdot \left(\frac{\kappa}{\mu}\nabla u\right) = f,$$

a popular model not just for flows in porous media, but also in heat and mass transfer, diffusion and dispersion processes in various media, in material sciences, etc.

In numerical simulations aimed at studying the behavior of the flow, the above model is discretized by using finite element, finite volume or finite difference methods. These lead to systems of algebraic equations for the unknown value of the pressure and/or velocity (at a discrete set of points). To resolve all scales present

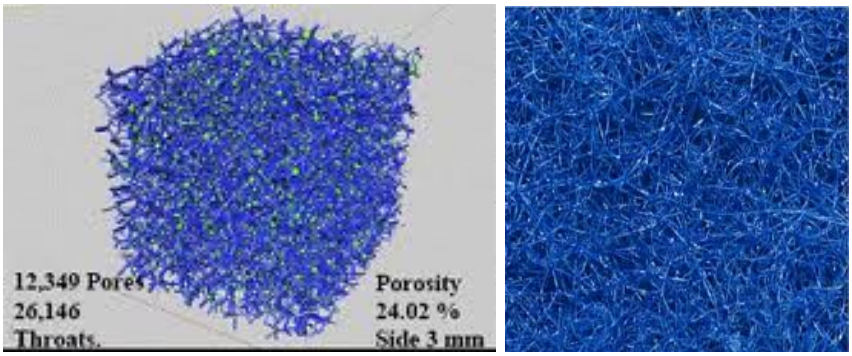


Figure 1: Illustrations of porous media: (left) 3-D image of computer generated media, (right) 3-D micro-scan of fibrous material

in the model one needs to introduce a very fine mesh. As a result, solving the systems arising in this approximation could be prohibitively expensive. Moreover, due to uncertainties, one often needs to solve the problem for each parameter value representing heterogeneities. This in general, will make the simulations unfeasible.

To solve the fine-grid systems, one can use multigrid methods (e.g., [8, 28]), multilevel methods (e.g., [54, 55]), and domain decomposition techniques (e.g., [29, 32, 37, 38, 41, 53]). However, regardless of the tremendous progress in all these techniques, due to disparity in the scales, high contrast in the media properties, and uncertainties the complexity of the problem could be very high and robustness with respect to the parameters could be lost. Thus, model reduction across small scales has become the most promising approach in reducing substantially the computational complexity.

Recently, a new class of accurate reduced-order methods has been introduced and used in various applications. These include Galerkin multiscale finite elements (e.g., [3, 16, 34, 35, 36]), mixed multiscale finite element methods (e.g., [1, 2, 5]), the multiscale finite volume method (see, e.g., [44]), mortar multiscale methods (see e.g., [9, 57]), and variational multiscale methods (see e.g., [42, 43]).

The purpose of the dissertation is to extend the concept of model reduction and to develop a systematic methodology for solving complex multiscale problems with high-contrast and no-scale separation by using discontinuous basis functions. For this framework, we use discontinuous Galerkin (DG) and hybridizable discontinuous Galerkin (HDG) methods as a finite element method.

In 1973, Reed and Hill developed the discontinuous Galerkin (DG) method for solving a problem of neutron transport [51]. In recent years, DG methods have become attractive as a competitive simulation tool for solving partial differential equations. The DG methods for diffusion equations introduced in the early seventies by Nische [47, 48]. Based on work, DG methods for diffusion problems used Interior Penalty (IP) techniques to enforce some conditions such as weak continuity of the solution or its derivatives across interfaces (see e.g. [26, 56, 49]). This work contributes to the development of Interior Penalty Discontinuous Galerkin (IPDG) methods. There are four IPDG versions: Symmetric Interior Penalty Galerkin (SIPG) [11, 56], Nonsysmmetric Interior Penaly Galerkin (NIPG) [52, 56], Incomplete Interior Penalty Galerkin (IIPG) [56], and Oden-Babuska-Baumann DG (OBB-DG) methods [49]. Within DG methods, we use SIPG emthods in the discontinuous FEM framework.

The DG methods have several advantages over the continuous Galerkin (CG) methods. DG methods can be implemented on general meshes and polynomials of arbitrary degree. Also they easily handle adaptivity (both $h$ and $p$) and lead to efficient parallelization. DG methods can be used to produce highly accurate discretization for convection-diffusion equations and can be applied for problems with unambiguous boundary conditions. Despite all these advantages, there are also some shortcomings for practical applications. The main issue among these is the higher number of globally coupled degrees of freedom for the same mesh since

there is no sharing of the degree of freedom at the element boundary. This results in higher computational cost compared to the continuous Galerkin method and/or finite difference schemes.

The HDG methods were recently developed to overcome this issue. A hybridized DG method results in an algebraic system that involves only the degrees of freedom associated with the numerical traces of the field variables. Since the numerical traces are defined on the inter-element boundaries only, this results in a substantial reduction in degrees of freedom. As a result, HDG methods can save computational cost significantly.

As the problem is expected to be solved for many input parameters such as source terms, boundary conditions, and spatial heterogeneities, we divide the computation into two stages (following known formalism [14]): offline and online. In the offline stage one constructs a reduced dimensional multiscale space, which used for rapid computations in the online stage. In the offline stage [33], we generate a snapshot space and propose some local spectral problem that allows selecting dominant modes. In the online stage, we use the functions computed in the offline stage to generate a suitable low-dimensional solution space that will still bring important features of the solution into this approximation. Our approach relies on local basis functions on each coarse-grid cell or face that are constructed independently in the offline stage. The coupling of these local functions is provided by the SIPG and HDG technology.

In both methods, SIPG and HDG, we construct several multiscale spaces that provide reasonable approximations of the solution and results in a stable multiscale method. The efficacy of the proposed methods is demonstrated on a set of numerical experiments of flows in high-contrast media where the permeability fields have subregions of high-conductivity, which form channels and islands. In all cases of permeability data considered in the dissertation, we observe that as the dimension of

the coarse-grid space increases, the error decreases. Further, we derive error estimates and discuss the convergence issues of the method.

In Chapter 2, we present the flow equations for heterogeneous porous media and two different discontinuous finite element methods that will be the base of our study. First, we give four different model problems the subject of our study in developing of model reduction technique. Second, we present an overview of SIPG and HDG methods (both are discontinuous Galerkin FEM), which will be used as a framework for generalized multiscale finite element methods. HDG methods, as outlined in [22], provide ample possibilities for "gluing" together various discontinuous finite element approximations. The mechanism of this "glue" is based on the notions of *numerical trace* and *numerical flux*. Numerical trace is a single valued function on the finite element interfaces and belongs to a certain Lagrange multiplier space which is used to solve the global problem. The well-posedness and accuracy are ensured by a proper choice of the numerical flux, that involves a stabilization parameter $\tau$ (see, e.g. [22]).

In Chapter 3, we develop generalized multiscale methods within the SIPG framework. We use spectral basis functions that are constructed in special ways in order to reduce the degrees of freedom of the coarse-grid approximation spaces. Further we discuss the use of a penalty parameter in the SIPG method and derive a stability estimate for a penalty parameter that scales as the inverse of the fine-scale mesh-size. We show that the constant in this estimate is independent of the contrast, which is important for problems that have high-contrast. We present some numerical experiments and report various errors of the Discontinuous Galerkin method that uses the constructed coarse-grid spaces. Finally, we derive error estimates (in a broken energy norm associated with the bilinear form of the discontinuous Galerkin FEM) for the proposed methods. These estimates take into account both, the approximation properties of both the fine-grid spares and the spectral properties of the reduced

coarse-grid spaces.

In Chapter 4, we design a generalized multiscale method within the framework of HDG for second order elliptic problems. Since the *numerical trace* plays the role of a Lagrange multiplier (provides the "glue") in this framework, the main focus of this Chapter is the construction of suitable spaces. Using this space, we derive the up-scaling method, which is independent of the choice of local spaces. Also, we provide a general framework for systematic construction of multiscale spaces and propose three different types of multiscale finite element spaces. We also present some numerical experiments and report error of HDG with examples of the constructed multiscale spaces. We show that the stability is independent of the choice of multiscale spaces. However, the error bounds depend on the choice of spaces. Finally, we provide error estimates for some specific spaces. These include spaces generated by splitting of the domain on subdomains that overlap (oversampling) or cover it with no overlapping (chess-board splitting). The error bounds are expressed in terms of the coarse and fine grid mesh-size and the spectral properties of the coarse-grid spaces.

In Chapter 5, we extend generalized multiscale HDG (GMsHDG) methods to nonlinear and time dependent partial differential equations. Here we consider as basic model a nonlinear parabolic equation with a high contrast coefficient that depends on the space variable and a solution. Comparing the nonlinear to linear case, we note three significant differences in deriving the approximation scheme. First, in the construction of a multiscale space for nonlinear problem, we use eigenvalue problems which depends on a parameter, while we have an standard (without a parameter) eigenvalue problem for linear problem. The second difference is that in the nonlinear problem we need to use iterative methods. A more significant difference is the choice of the stabilization parameter: to get efficient convergence rate in the case of linear problems we use the stabilization $\tau = 1$, while in the case of nonlinear problems,

we use $\tau = h$. Moreover, we needed to modify the constructions of the multiscale spaces introduced in Chapter 4. In the analysis and our numerical experiment we choose some specific cases for nonlinear porous media. Further, we derive some error estimates based on only space discritization (semi-discritization) and report the error decay as adding more multiscale basis function for each coarse face. The stability estimates give to be able to neglect the choice of multiscale spaces, which is similar to elliptic case.

Finally, in Chapter 6, we summarize our work and discuss possible future work.

# 2. GOVERNING EQUATIONS AND DISCRETIZATION

## 2.1 Governing equations

Multiscale finite element methods and their modifications have been used with success in flow simulation through heterogeneous porous media. First, we present the most popular model in flows in porous media, a single-phase flow while neglecting the effects of gravity, compressibility, and dispersion. In general, all quantities involved in this model depend on the spatial variable $x$ and the time $t$.

Here is a very brief description of flow in a porous media that fills the domain $\Omega \subset \mathbb{R}^n$, $n = 2, 3$. The macroscopic fluid pressure $u$ (dimension $[Pa] = [N/m^2]$) and the mass fluid flux $\boldsymbol{q}_w$ (dimension $[kg/(m^2 s)]$) are related through the Darcy law

$$\boldsymbol{q}_w = -\frac{k(x)}{\mu}(\nabla u - \rho \mathbf{g}), \tag{2.1}$$

where $k(x)$ is the absolute permeability of the porous media (dimension $[m^2]$), $\mathbf{g}$ (dimension $[m/s^2]$) is the gravity vector pointing in the direction of gravity (in the case of using the system of grams, meters and seconds $\mathbf{g} = (0, 0, -9.81)$), $\mu$ (dimension $[Pa\, s]$) and $\rho$ (dimension $[kg/m^3]$) are the fluid viscosity and density, respectively. This law was experimentally established for the one-dimensional case in 1856 by H. Darcy. Then the conservation of mass is expressed by the following partial differential equation

$$\frac{\partial \phi \rho}{\partial t} + \nabla \cdot (\rho \boldsymbol{q}_w) = \rho f, \tag{2.2}$$

where $\phi$ is the media porosity and $f$ is known source/sink term.

A simplified version of the equation (2.2) is obtained when neglecting the compressibility and the gravity effects and assuming that the fluid viscosity is constant,

so that we get the following steady-state model

$$-\nabla \cdot (\kappa(x)\nabla u(x)) = f(x), \quad x \in \Omega \tag{2.3}$$

with $\Omega$ a bounded domain in $\mathbb{R}^n$. This equation with a suitable boundary condition will be considered as the first model problem in the dissertation.

As we mentioned above, the equation (2.3) is a good model in the heat and mass transfer processes as well. However, often in such situations the process is time dependent, and therefore, the dependent variable (in this case temperature) is a function of space and also time $t$, i.e. $u(x,t)$. Our goal is to extend the multiscale finite element methods also to parabolic equations with heterogeneous coefficients of the following type:

$$\frac{d}{dt}u(x,t) - \nabla \cdot (\kappa(x)\nabla u(x,t)) = f(x,t) \quad (x,t) \in \Omega \times (0,T], \tag{2.4}$$

with appropriate boundary conditions and smooth initial conditions. Here, $T$ is a final time. In general, there are space and time heterogeneities (i.e., $\kappa = \kappa(x,t)$). However, here we only consider space heterogeneity (i.e., $\kappa = \kappa(x)$) and use the corresponding construction of multiscale approximation for elliptic equations.

The ultimate goal in this area is development, study, and testing discontinuous multiscale methods for nonlinear problems. We carry one possible extension to the case of some specific classes of nonlinear elliptic and parabolic problems. These constructions are quite similar to the one proposed for the linear case, since the heterogeneous coefficient $\kappa(x)$ in the linear equations (2.3) is replaced by $\kappa = \kappa(x,u)$ in the nonlinear case. However, the analysis of this case is much more complicated and is left for future studies.

## 2.2 Discontinuous Galerkin method : SIPG

In this section, we present an overview of the Symmetric Interior Penalty Galerkin (SIPG) method within discontinuous Galerkin (DG) methods for solving heterogeneous diffusion equations.

The SIPG method for elliptic problems was introduced by Arnold [11]. The model problem considered in this section has a heterogeneous coefficient. In order to approximate the model problem with the SIPG method, we follow the work of Dryja [27]. The approach is to use the harmonic average of the heterogeneous coefficient to formulate the symmetry term and penalty term, which are added to ensure consistency, symmetry and stabilization with penalty in regular SIPG method. The method has guaranteed coercivity and convergence when the penalty parameter is large enough.

### *2.2.1 Problem setting*

We consider the following second order elliptic differential equation for the unknown function $u(x)$

$$-\nabla \cdot (\kappa(x)\nabla u) = f, \quad x \in \Omega \tag{2.5}$$

with homogeneous Dirichlet boundary conditions. Here, $\kappa(x) \geq \kappa_0 > 0$ is a highly heterogeneous coefficient, $\Omega$ is a bounded polyhedral domain in $\mathbb{R}^n, n = 2, 3$ and $f \in L^2(\Omega)$.

Let $\mathcal{T}_h$ be a finite collection of disjoint polyhedra forming a partition of $\Omega$ with the mesh size $h$. We denote by $\partial\mathcal{T}_h$ the set $\{\partial T : T \in \mathcal{T}_h\}$. We say that a (closed) subset $F$ of $\overline{\Omega}$ is a face (an edge) if $F$ has positive $(n-1)$ Lebesgue measure (in dimension $n = 2$) and if either one of the two following condition is satisfied:

(i) There are two distinct elements $T_1$ and $T_2$ such that $F = \partial T_1 \cap \partial T_2$; in such

a case, $F$ called an *interface*.

(ii) There is $T \in \mathcal{T}_h$ such that $F = \partial T \cap \partial\Omega$; in such case, $F$ is called a *boundary face*. Let $\mathcal{E}_h^0$ and $\mathcal{E}_h^\partial$ denote the set of interfaces and boundary faces, respectively. We denote by $\mathcal{E}_h$ the union of $\mathcal{E}_h^0$ and $\mathcal{E}_h^\partial$. Moreover, for any element $T \in \mathcal{T}_h$, the set $\mathcal{E}_h^T$ the collection of the faces composing the boundary of $T$. The maximum number of faces composing the boundary of elements is denoted by

$$N_\partial = \max_{T \in \mathcal{T}_h} card(\mathcal{E}_h^T). \tag{2.6}$$

Let $u_1$ and $u_2$ be the traces of $u$ on $F$ from the interface of $T_1$ and $T_2$, respectively. Then, we define the averages $\{\cdot\}$ and jumps $[\![\cdot]\!]$ as follows. For an interface $F \in \mathcal{E}_h^0$, we set

$$\{u\} = \frac{1}{2}(u_1 + u_2), \quad [\![u]\!] = u_1 - u_2. \tag{2.7}$$

For a boundary face $F \in \mathcal{E}_h^\partial$, the set of boundary faces on which $u$ are single valued, we set

$$\{u\} = [\![u]\!] = u.$$

Let $\mathcal{P}_k(D)$ denote the set of polynomials of degree at most $k$ on a domain $D$. We introduce the broken finite element space

$$V_h = \{v \in L^2(\Omega) : v|_T \in \mathcal{P}_k(T), \quad T \in \mathcal{T}_h\}.$$

We use the following harmonic averages along the interface $F$ of $T_1$ and $T_2$ (i.e., $F = \partial T_1 \cap \partial T_2$).

$$\kappa_F = \frac{2\kappa_1\kappa_2}{\kappa_1 + \kappa_2} \quad h_F = \frac{2h_1h_2}{h_1 + h_2},$$

where $\kappa_i = \kappa|_{T_i}, i = 1, 2$, while, for all boundary face $F = \partial T \cap \partial\Omega$,

$$\kappa_F = \kappa|_T \quad h_F = h|_T.$$

We observe that, for any $F \in \mathcal{E}_h^0$,

$$\min\{\kappa_1, \kappa_2\} \leq \kappa_F \leq 2\min\{\kappa_1, \kappa_2\}.$$

### *2.2.2 SIPG formulation*

The SIPG method [11] is : Find $u_h \in V_h$ such that

$$a_h(u_h, v_h) = \int_\Omega f v_h \quad \text{for all} \quad v_h \in V_h. \tag{2.8}$$

Here, the bilinear form $a_h$ is given as a sum of three symmetric bilinear forms :

$$a_h(u, v) = a(u, v) + s(u, v) + p(u, v), \tag{2.9}$$

where the $a$ is the bilinear form related to the energy,

$$a(u, v) = \sum_{T \in \mathcal{T}_h} \int_T \kappa(x) \nabla u \cdot \nabla v, \tag{2.10}$$

the $s$ is the bilinear form ensuring consistency and symmetry

$$s(u, v) = \sum_{F \in \mathcal{E}_h} \int_F \kappa_F \left( \frac{\partial u}{\partial n} [\![v]\!] + \frac{\partial v}{\partial n} [\![u]\!] \right) ds, \tag{2.11}$$

and the $p$ is the penalty bilinear form for stability

$$p(u,v) = \sum_{F\in\mathcal{E}_h} \frac{\delta}{h_F} \int_F \kappa_F [\![u]\!][\![v]\!] ds. \tag{2.12}$$

The equations (2.10), (2.11), and (2.12) are respectively called *energy, consist-symmetry*, and *penalty* terms.

To derive stability and error estimates, we define the following broken norm : For all $v \in V_h$,

$$\|v\|_{\mathrm{DG}} := \left(a(v,v) + p(v,v)\right)^{1/2}. \tag{2.13}$$

**Lemma 2.2.1.** *For any $v_h \in V_h$, $T \in \mathcal{T}_h$, and $F \in \mathcal{E}_h^T$, the trace estimate*

$$\|v_h\|_{L^2(F)} \le C_{tr} h_T^{-\frac{1}{2}} \|v_h\|_{L^2(T)} \tag{2.14}$$

*holds.*

In [50], it has been proved that the SIPG bilinear form is coercive when the penalty parameter $\delta$ is large enough and the bilinear form is bounded.

**Lemma 2.2.2.** *For all $\delta > \delta_0 := C_{tr}^2 N_\partial$ where $C_{tr}$ is the constant of trace inequality* (2.14) *and $N_\partial$ is defined by* (2.6)*, the SIPG bilinear form defined by* (2.9) *is coercive on $V_h$ with respect to the $\|\cdot\|_{DG}$-norm, i.e.,*

$$a_h(v_h, v_h) \ge C_\delta \|v_h\|_{DG}, \quad \textit{for all} \quad v_h \in V_h, \tag{2.15}$$

*where $C_\delta = \frac{\delta-\delta_0}{1+\delta}$ is independent of $h$ and $\kappa$.*

**Lemma 2.2.3.** *There is $C$, independent of $h$ and $\kappa$, such that*

$$a_h(v_h, w_h) \le C \|v_h\|_{DG} \|w_h\|_{DG}, \quad \textit{for all} \quad (v_h, w_h) \in V_h \times V_h. \tag{2.16}$$

By the Lax-Milgram Lemma, the discrete problem (2.8) obtained by the SIPG methods is well-posed. For convergence analysis, we have the following theorem shown in [50]. Here we do not provide the proof.

**Theorem 2.2.4.** *Let $u$ and $u_h$ be the solution of Problem* (2.5) *and* (2.8)*, respectively. Assume that the penalty parameter $\delta > \delta_0$ where $\delta_0$ defined in Lemma 2.2.2. Then, we have*

$$\|u - u_h\|_{DG} \leq C_1 \inf_{v_h \in V_h} \|u - v_h\|_{DG}.$$

*Moreover, if $u \in H^{k+1}$,*

$$\|u - u_h\|_{DG} \leq C_2 \|\kappa\|^{1/2}_{L^\infty(\Omega)} h^k \|u\|_{H^{k+1}(\Omega)}.$$

*Here, $C_1$ and $C_2$ are independent of $h$ and $\kappa$.*

## 2.3 Hybridizable discontinuous Galerkin method

In this section, we present an overview of hybridizable discontinuous Galerkin (HDG) methods for solving second order elliptic equations.

The first HDG methods were introduced for second order elliptic problems [21, 22]. The error estimates based on a projection were developed for elliptic problems [23]. Optimal convergence order for convection-diffusion equations were established in the $L^2$-norm of $k+1$ if plynomials of degree $k$ are used and the exact solution is smooth enough [24, 25]. The choices of stabilization parameter was numerically presented and analyzed in sense of the optimal convergence order of numerical solutions [20, 46]. Based on the optimal convergence and superconvergence of HDG methods, local postprocessing were developed to increase the convergence order of numerical solutions [46].

### *2.3.1 Problem setting*

Here we describe concepts of the HDG method using the second order elliptic differential equation (2.5) with a high contrast coefficient. To describe the HDG method, we consider model equation (2.5) with homogeneous Drichlet boundary condition in a mixed form:

$$\alpha \boldsymbol{q} + \nabla u = 0 \quad \text{in} \quad \Omega, \tag{2.17a}$$

$$\nabla \cdot \boldsymbol{q} = f \quad \text{in} \quad \Omega, \tag{2.17b}$$

$$u = 0 \quad \text{on} \quad \partial\Omega. \tag{2.17c}$$

Here, $\alpha(x) = \kappa(x)^{-1}$, $\Omega \subset \mathbb{R}^n, n = 2, 3$ is a bounded polyhedral domain, and $f \in L^2(\Omega)$.

Let $\mathcal{T}_h$ be a finite collection of disjoint polyhedra forming a partition of $\Omega$ with the mesh size $h$. We denote by $\partial\mathcal{T}_h$ the set $\{\partial T : T \in \mathcal{T}_h\}$. Similarly, for $\mathcal{E}_h^0$, $\mathcal{E}_h^\partial$ and $\mathcal{E}_h$, we use the same definition defined in SIPG methods.

We introduce discontinuous finite element spaces that are used in the HDG method :

$$W_h = \{w \in L^2(\Omega) : w|_T \in W(T), \quad T \in \mathcal{T}_h\},$$

$$\boldsymbol{V}_h = \{\boldsymbol{v} \in \boldsymbol{L}^2(\Omega) : \boldsymbol{v}|_T \in \boldsymbol{V}(T), \quad T \in \mathcal{T}_h\}.$$

Also, we introduce a finite element space for a numerical trace

$$M_h = \{\mu \in L^2(\mathcal{E}_h) : \mu|_F \in M(F), \quad F \in \mathcal{E}_h^0, \quad \mu|_F = 0, \quad F \in \mathcal{E}_h^\partial\}.$$

Here for $T \in \mathcal{T}_h$ the spaces $W(T), \boldsymbol{V}(T)$, and $M(F)$ are suitable finite element spaces (see, e.g. [22]). On each element $T \in \mathcal{T}_h$, let local spaces $W(T) \times \boldsymbol{V}(T) \times M(F)$ be any set of spaces presented in [24, Tables 1 – 9]. It could be any classical mixed

elements or the HDG elements defined on different triangulations. In Table 1, we give examples of local spaces for the classical mixed element and HDG element defined on a simplex.

Table 1: Possible choices for the finite element spaces for $T$ a simplex.

| method | $\boldsymbol{V}(T)$ | $W(T)$ | $M(F),\ F \in \partial T$ |
|---|---|---|---|
| $\mathbf{BDFM}_{k+1}$ | $\{\boldsymbol{q} \in \boldsymbol{P}^{k+1}(T) :$ $\boldsymbol{q}\cdot\boldsymbol{n}\vert_{\partial T} \in P^k(F),\ \forall F \in \partial T\}$ | $P^k(T)$ | $P^k(F)$ |
| $\mathbf{RT}_k$ | $\boldsymbol{P}^k(T) \oplus \boldsymbol{x}\widetilde{P}^k(T)$ | $P^k(T)$ | $P^k(F)$ |
| $\mathbf{HDG}_k$ | $\boldsymbol{P}^k(T)$ | $P^k(T)$ | $P^k(F)$ |

### *2.3.2 HDG formulation*

The discrete problem obtained by the HDG method [22] is : Find $(u_h, \boldsymbol{q}_h, \widehat{u}_h) \in W_h \times \boldsymbol{V}_h \times M_h$ such that

$$(\alpha \boldsymbol{q}_h\,,\,\boldsymbol{v})_{\mathcal{T}_h} - (u_h\,,\,\nabla\cdot\boldsymbol{v})_{\mathcal{T}_h} + \langle \widehat{u}_h\,,\,\boldsymbol{v}\cdot\boldsymbol{n}\rangle_{\partial\mathcal{T}_h} = 0, \tag{2.18a}$$

$$-(\boldsymbol{q}_h\,,\,\nabla w)_{\mathcal{T}_h} + \langle \widehat{\boldsymbol{q}}_h\cdot\boldsymbol{n}\,,\,w\rangle_{\partial\mathcal{T}_h} = (f\,,\,w)_{\mathcal{T}_h}, \tag{2.18b}$$

$$\langle \widehat{\boldsymbol{q}}_h\cdot\boldsymbol{n}\,,\,\mu\rangle_{\partial\mathcal{T}_h} = 0 \tag{2.18c}$$

$$\widehat{u}_h = 0 \quad \text{on} \quad \partial\Omega, \tag{2.18d}$$

for all $(w, \boldsymbol{v}, \mu) \in W_h \times \boldsymbol{V}_h \times M_h$, with a numerical trace for the flux defined

$$\widehat{\boldsymbol{q}}_h\cdot\boldsymbol{n} = \boldsymbol{q}_h\cdot\boldsymbol{n} + \tau(u_h - \widehat{u}_h) \quad \text{on} \quad \partial\mathcal{T}_h, \tag{2.18e}$$

where $\tau$ is a local stabilization parameter. We write

$$(\eta\,,\,\zeta)_{\mathcal{T}_h} := \sum_{T\in\mathcal{T}_h}(\eta,\zeta)_T \quad \text{and} \quad \langle\eta\,,\,\zeta\rangle_{\partial\mathcal{T}_h} := \sum_{T\in\mathcal{T}_h}\langle\eta,\zeta\rangle_{\partial T}$$

where $(\eta,\zeta)_D$ denotes the integral of $\eta\zeta$ over the domain $D\in\mathbb{R}^n$ and $\langle\eta,\zeta\rangle_{\partial D}$ denotes the integral of $\eta\zeta$ over the boundary of the domain $\partial D\subset\mathbb{R}^{n-1}$.

For implementation, we insert (2.18e) and (2.18d) into (2.18a)-(2.18c) and obtain, after some manipulations, that $(u_h,\boldsymbol{q}_h,\widehat{u}_h)\in W_h\times\boldsymbol{V}_h\times M_h$ is the solution of the following weak formulation:

$$a(\boldsymbol{q}_h,\boldsymbol{v}) - b(u_h,\boldsymbol{v}) + c(\widehat{u}_h,\boldsymbol{v}) = 0, \tag{2.19a}$$

$$-b(w,\boldsymbol{q}_h) - d(u_h,w) + e(\widehat{u}_h,w) = -f(w), \tag{2.19b}$$

$$c(\mu,\boldsymbol{q}_h) + e(\mu,u_h) - g(\mu,\widehat{u}_h) = 0, \tag{2.19c}$$

for all $(w,\boldsymbol{v},\mu)\in W_h\times\boldsymbol{V}_h\times M_h$. Here, the bilinear forms and the linear functional are defined by

$$\begin{aligned} a(\boldsymbol{q},\boldsymbol{v}) = (\alpha\boldsymbol{q}\,,\,\boldsymbol{v})_{\mathcal{T}_h}, \quad b(u,\boldsymbol{v}) = (u\,,\,\nabla\cdot\boldsymbol{v})_{\mathcal{T}_h},\\ c(\widehat{u},\boldsymbol{v}) = \langle\widehat{u}\,,\,\boldsymbol{v}\cdot\boldsymbol{n}\rangle_{\partial\mathcal{T}_h}, \quad d(u,w) = \langle w\,,\,\tau u\rangle_{\partial\mathcal{T}_h},\\ e(\mu,u) = \langle\mu\,,\,\tau u\rangle_{\partial\mathcal{T}_h}, \quad g(\mu,\widehat{u}) = \langle\mu\,,\,\tau\widehat{u}\rangle_{\partial\mathcal{T}_h}, \quad f(w) = (f\,,\,w)_{\mathcal{T}_h}, \end{aligned} \tag{2.20}$$

for all $(u,\boldsymbol{q},\widehat{u})$ and $(w,\boldsymbol{v},\mu)$ in $W_h\times\boldsymbol{V}_h\times M_h$.

The discretization of the system of equations (2.19) give rise to a matrix equation

of the following form

$$\begin{bmatrix} A & -B^T & C^T \\ -B & -D & E \\ C & E^T & G \end{bmatrix} \begin{bmatrix} Q \\ U \\ \widehat{U} \end{bmatrix} = - \begin{bmatrix} 0 \\ F \\ 0 \end{bmatrix} \tag{2.21}$$

Here $Q, U$ and $\widehat{U}$ are the vectors of degrees of freedom for $\boldsymbol{q}_h, u_h, \widehat{u}_h$, respectively. The matrices in (2.21) corresponding to the bilinear forms in (2.20) in the order they appear in the system of equation (2.19).

Since the HDG methods produce a final system in terms of globally coupled degrees of freedom of the numerical trace $\widehat{u}_h$ (or $\widehat{U}$) only, the equations (2.18a) and (2.18b) can be used to remove both $\boldsymbol{q}_h$ and $u_h$ in an element by element sense. Then, we obtain a reduced globally coupled matrix equation only for $\widehat{U}$ as

$$\mathbb{K}\widehat{U} = \mathbb{F} \tag{2.22}$$

where

$$\mathbb{K} = - \begin{bmatrix} C & E^T \end{bmatrix} \begin{bmatrix} A & -B^T \\ -B & -D \end{bmatrix}^{-1} \begin{bmatrix} C^T \\ E \end{bmatrix} + G,$$

and

$$\mathbb{F} = \begin{bmatrix} C & E^T \end{bmatrix} \begin{bmatrix} A & -B^T \\ -B & -D \end{bmatrix}^{-1} \begin{bmatrix} 0 \\ F \end{bmatrix}$$

After solving the equation (2.22), $Q$ and $U$ can be obtained from the following matrix equation.

$$\begin{bmatrix} Q \\ U \end{bmatrix} = \begin{bmatrix} A & -B^T \\ -B & -D \end{bmatrix}^{-1} \left( \begin{bmatrix} 0 \\ -F \end{bmatrix} - \begin{bmatrix} C^T \\ E \end{bmatrix} \widehat{U} \right).$$

### *2.3.3 Characterization of the numerical trace*

We introduce the local solver which is related to each function $(\eta, f) \in M_h \times L^2(\Omega)$ in order to look into the nature of the matrix equation (2.21). This concept will be used in establishing the upscaling structure of generalized multiscale HDG methods. For each element $T$, let $\widehat{u}_h = \eta$, where $\eta \in M_h$. Then we can find the pair $(\boldsymbol{q}_h^{\eta,f}, u_h^{\eta,f})$ by restricting the equations (2.18) to an element $T$:

$$(\alpha \boldsymbol{q}_h(\eta, f)\,,\, \boldsymbol{v})_{\mathcal{T}_h} - (u_h(\eta, f)\,,\, \nabla \cdot \boldsymbol{v})_{\mathcal{T}_h} = -\langle \eta\,,\, \boldsymbol{v} \cdot \boldsymbol{n} \rangle_{\partial \mathcal{T}_h}, \tag{2.23a}$$

$$-(\boldsymbol{q}_h(\eta, f)\,,\, \nabla w)_{\mathcal{T}_h} + \langle \widehat{\boldsymbol{q}}_h(\eta, f) \cdot \boldsymbol{n}\,,\, w \rangle_{\partial \mathcal{T}_h} = (f\,,\, w)_{\mathcal{T}_h}, \tag{2.23b}$$

for all $(\boldsymbol{v}, w) \in \boldsymbol{V}_h(T) \times W_h(T)$, where

$$\widehat{\boldsymbol{q}}_h(\eta, f) \cdot \boldsymbol{n} = \boldsymbol{q}_h(\eta, f) \cdot \boldsymbol{n} + \tau(u_h(\eta, f) - \eta). \tag{2.23c}$$

Since the solution $(u_h, \boldsymbol{q}_h) \in W_h \times \boldsymbol{V}_h$ satisfies

$$\boldsymbol{q}_h = \boldsymbol{q}_h(\widehat{u}_h, f), \quad u_h = u_h(\widehat{u}_h, f),$$

where $\widehat{u}_h \in M_h$ is such that

$$\langle \widehat{\boldsymbol{q}}_h(\eta, f) \cdot \boldsymbol{n}\,,\, \mu \rangle_{\partial \mathcal{T}_h} = 0, \quad \text{for all} \quad \mu \in M_h. \tag{2.24}$$

The solution of system (2.23) can be split into two parts as follows

$$(u_h(\widehat{u}_h, f), \boldsymbol{q}_h(\widehat{u}_h, f)) = (u_h(\widehat{u}_h, 0), \boldsymbol{q}_h(\widehat{u}_h, 0)) + (u_h(0, f), \boldsymbol{q}_h(0, f)).$$

Then, for all $\eta, \mu \in M_h$, we set

$$a_h(\eta, \mu) = \langle \widehat{\boldsymbol{q}}_h(\eta, 0) \cdot \boldsymbol{n}\,,\, \mu \rangle_{\partial \mathcal{T}_h}, \quad b_h(\mu) = -\langle \widehat{\boldsymbol{q}}_h(0, f) \cdot \boldsymbol{n}\,,\, \mu \rangle_{\partial \mathcal{T}_h}. \tag{2.25}$$

By the equation (2.24) and the linearity of the system (2.23), the equation (2.18) reduces to finding $\widehat{u}_h \in M_h$ such that

$$a_h(\widehat{u}_h, \mu) = b_h(\mu), \quad \text{for all} \quad \mu \in M_h. \tag{2.26}$$

We note that the bilinear form $a_h(\cdot, \cdot)$ is associated with the matrix $\mathbb{K}$, and the linear functional $b_h(\cdot)$ is associated with the vector $\mathbb{F}$ in (2.21).

The existence and uniqueness of the numerical trace $\widehat{u}_h$ is presented in [22]. We only state the stability result without the proof of the following theorem.

**Theorem 2.3.1.** *Assume that the stabilization parameter $\tau > 0$. Then the system* (2.18) *has unique solution.*

Although a positive stabilization parameter promises the existence and uniqueness, the choice of the stabilization parameter is significant if this is associated with the optimal convergence order. Numerical experiment and analysis (see [20, 46]) confirm the optimal the stabilization parameter is $\tau = \frac{\kappa}{l}$ where $l$ denotes a representative diffusive length scale which is typically of unit order and independent of the mesh size. With this stabilization parameter, we can obtain the optimal convergence order $k + 1$ of both the numerical solutions $u_h$ and $\boldsymbol{q}_h$ when using polynomials of degree $k$.

In [46], prostprocessing procedure has been introduced to obtain new solution with high order accuracy, denoted $u_h^*$, that is following . We define a new approxi-

mation $u_h^*$ in the space

$$W_h^* = \{w \in L^2(\Omega) : w|_T \in W^*(T), K \in \mathcal{T}_h\}$$

When we use the $\mathbf{HDG}_k$, $W(T)$ is a polynomial of degree $k$ and $W^*(T)$ is a polynomial of degree $k+1$.

On each element $T \in \mathcal{T}_h$, we find the function $u_h^* \in W_h^*$ such that

$$\begin{aligned} (\kappa \nabla u_h^*, \nabla w)_T &= -(\boldsymbol{q}_h, \nabla w)_T \quad \text{for all} \quad w \in W^*(T), \\ (u_h^*, 1)_T &= (u_h, 1)_T. \end{aligned} \tag{2.27}$$

We note that we can implement the local postprocessing (2.27) in parallel on each element $T \in \mathcal{T}_h$ and reduce the computation time. Moreover, this postprocessing shows that $\boldsymbol{q}_h$ converges of optimal order of $k+1$ and $u_h^*$ of super-convergent order $k+2$ when polynomials of degree $k$ are used (e.g., see [46]).

# 3. GENERALIZED MULTISCALE DISCONTINUOUS GALERKIN METHOD*

In this chapter, we design a multiscale model reduction technique within the framework of the discontinuous Galerkin framework. As the problem is expected to be solved for many input parameters such as source terms, boundary conditions, and spatial heterogeneities, we divide the computation into two stages (following known formalism [14, 45]): offline and online, where our goal in the offline stage is to construct a reduced dimensional multiscale space to be used for rapid computations in the online stage. In the offline stage [33], we generate a snapshot space and propose a local spectral problem that allows selecting dominant modes in the space of snapshots. In the online stage, we use the basis functions computed offline to solve the problem for current choice of the parameters (a further spectral selection may be done in the online step in each coarse block). As a result, the basis functions generated by coarse block computations are discontinuous along the coarse-grid inter-element faces/edges. In the previous research (see, e.g. [33]) multiplication by partition of unity functions has been used in order to generate conforming basis functions. However, our procedure modifies original spectral basis functions and is found to be difficult to apply for more complex flow problems. In this chapter, we propose and explore the use of local model reduction techniques within the framework of the discontinuous Galerkin finite element methods.

We use the Symmetric Interior Penalty Galerkin (SIPG) method by utilizing spectral basis functions that are constructed in a special way in order to reduce the globally coupled degrees of freedom of the coarse-grid approximation spaces. Also

*This chapter is reprinted with permission from Y. Efendiev, J. Gavis, R. Lazarov, M. Moon, M. Sarkis. Generalized multiscale finite element method. Symmetric interior penalty coupling. *Journal of Computational Physics*, 255:1-15, 2013

we discuss the choice of the penalty parameter in the SIPG method and derive a stability result for a penalty that scales as the inverse of the fine-scale mesh-size and show that the stability constant is independent of the contrast. The latter is important as the problems under consideration have high contrast.

Further, we derive error estimates and discuss the accuracy of the method. Additionally, the efficacy of the proposed methods is demonstrated on a set of numerical experiments with flows in highly heterogeneous porous media where the permeability fields have subregions of high conductivity, which form channels and islands. In all cases, we observe that as the dimension of the coarse-grid space increases, the error decreases. In particular, we present results when the snapshot space consists of local solutions.

## 3.1 Model problem and discretization

We consider the following problem: Find $u^* \in H_0^1(\Omega)$ such that

$$a(u^*, v) = f(v) \quad \text{for all } v \in H_0^1(\Omega) \tag{3.1}$$

where

$$a(u, v) := \int_\Omega \kappa(x) \nabla u \cdot \nabla v dx \quad \text{and} \quad f(v) := \int_\Omega f v dx.$$

Here $\Omega$ is a bounded domain in $R^d$, $d = 2, 3$ with polygonal boundary. We assume that $f \in L_2(\Omega)$ and the coefficient $\kappa(x)$ represents the permeability of a highly heterogeneous porous media with high contrast, that is high ratio between the maximum and minimum values. Our main goal in this chapter is to develop an approximation method for (3.1) on a coarse grid using certain "low energy" local eigenfunctions within the discontinuous Galerkin framework.

We consider the two dimensional case. The method and results presented here

extend for the three dimensional case in a similar manner. We split the domain $\Omega$ into disjoint polygonal subregions $\{\Omega_i\}_{i=1}^N$ of diameter $O(H_i)$ so that $\overline{\Omega} = \cup_{i=1}^N \overline{\Omega}_i$. We assume that the substructures $\{\Omega_i\}_{i=1}^N$ form a geometrically conforming partition of $\Omega$. In this case, for $i \neq j$, the intersection $\partial\Omega_i \cap \partial\Omega_j$ is either empty, a vertex of $\Omega_i$ and/or $\Omega_j$, or a common edge/face of $\partial\Omega_i$ and $\partial\Omega_j$.

Further, in each $\Omega_i$ we introduce a shape regular triangulation $\mathcal{T}_h(\Omega_i)$ with triangular elements and maximum mesh-size $h_i$. The resulting triangulation of $\Omega$ is in general non-matching across $\partial\Omega_i$. Let $X_h(\Omega_i)$ be the regular finite element space of piecewise linear and continuous functions in $\mathcal{T}_h(\Omega_i)$. We do not assume that functions in $X_h(\Omega_i)$ vanish on $\partial\Omega_i \cap \partial\Omega$. We define

$$X_h(\Omega) = X_h(\Omega_1) \times \cdots \times X_h(\Omega_N)$$

and represent functions $v$ of $X_h(\Omega)$ as $v = \{v_i\}_{i=1}^N$ with $v_i \in X_h(\Omega_i)$. For simplicity, we also assume that the permeability $\kappa(x)$ is constant over each fine-grid element.

Due to the fact that $\mathcal{T}_h(\Omega_i)$ and $\mathcal{T}_h(\Omega_j)$ are independent from each other on a common edge $E = \partial\Omega_i \cap \partial\Omega_j$ they may introduce two different partitions of $E$, which are merged to obtain a set of faces $E_{ij} \subset E$. Since the functions in $X_h(\Omega)$ are discontinuous along the interfaces, it is necessary to distinguish between $E \subset \overline{\Omega}_i$ and $E \subset \overline{\Omega}_j$. From now on the $\Omega_i$-side of $E$ will be denoted by $E_{ij}$ while on the $\Omega_j$-side of $E$ will be denoted by $E_{ji}$. Geometrically, $E_{ij}$ and $E_{ji}$ are the same object.

We use the following harmonic averages along the edges $E_{ij}$. For $i, j \in \{1, \ldots, N\}$ define

$$\kappa_{ij} = \frac{2\kappa_i\kappa_j}{\kappa_i + \kappa_j} \quad \text{and} \quad h_{ij} = \frac{2h_ih_j}{h_i + h_j}. \tag{3.2}$$

We note that the functions $\kappa_{ij}$ and $h_{ij}$ are piecewise constants over the edge $E_{ij}$ on

a mesh that is obtained by merging the partitions $\mathcal{T}_h(\Omega_i)$ and $\mathcal{T}_h(\Omega_j)$ along their common edge $E_{ij}$.

The discrete problem obtained by the DG method (see [12, 27]) is: Find $u_h^* = \{u_{h,i}^*\}_{i=1}^N \in X_h(\Omega)$, (i.e., $u_{h,i}^* \in X_h(\Omega_i)$, $i = 1, \ldots, N$), such that

$$a_h^{DG}(u_h^*, v_h) = f(v_h) \quad \text{for all} \quad v_h = \{v_{h,i}\}_{i=1}^N \in X_h(\Omega), \tag{3.3}$$

where $a_h^{DG}(u_h, v_h)$, defined on $X_h(\Omega) \times X_h(\Omega)$, and $f(v)$, defined on $X_h(\Omega)$, are given by

$$a_h^{DG}(u, v) = \sum_{i=1}^N a_i^{DG}(u, v) \quad \text{and} \quad f(v) = \sum_{i=1}^N \int_{\Omega_i} f v_i dx. \tag{3.4}$$

Here, each local bilinear form $a_i^{DG}$ is given as a sum of three symmetric bilinear forms:

$$a_i^{DG}(u, v) := a_i(u, v) + s_i(u, v) + p_i(u, v), \tag{3.5}$$

where $a_i$ is the bilinear form associated with the "energy" in $\Omega_i$,

$$a_i(u, v) := \int_{\Omega_i} \kappa(x) \nabla u_i \cdot \nabla v_i dx, \tag{3.6}$$

the $s_i$ is the bilinear form ensuring consistency and symmetry on $\partial\Omega_i$

$$s_i(u, v) := \sum_{E_{ij} \subset \partial\Omega_i} \frac{1}{l_{ij}} \int_{E_{ij}} \kappa_{ij} \left( \frac{\partial u_i}{\partial n_i}(v_j - v_i) + \frac{\partial v_i}{\partial n_i}(u_j - u_i) \right) ds, \tag{3.7}$$

and $p_i$ is the penalty bilinear form that is added for stability

$$p_i(u, v) := \sum_{E_{ij} \subset \partial\Omega_i} \frac{1}{l_{ij}} \frac{\delta}{h_{ij}} \int_{E_{ij}} \kappa_{ij}(u_j - u_i)(v_j - v_i) ds. \tag{3.8}$$

Here $\kappa_{ij}$ is defined in (3.2) and $\frac{\partial}{\partial n_i}$ denotes the outward normal derivative on $\partial\Omega_i$.

The parameter $\delta$ is a positive penalty parameter. In order to simplify notation we included the index $j = \partial$ in the definition of the bilinear forms $s_i$ and $p_i$ above. In order to include $E_{i\partial} := \partial\Omega_i \cap \partial\Omega$ in the summation sign, we set $l_{ij} = 2$ when $i, j \neq \partial$ and $l_{ij} = 1$ when $j = \partial$. We also let $v_\partial = 0$ for all $v \in X_h(\Omega)$, and define $\kappa_{i\partial} = \kappa_i$ and $h_{i\partial} = h_i$. We note that when $\kappa_{ij}$ is given by the harmonic average, then $\min\{\kappa_i, \kappa_j\} \leq \kappa_{ij} \leq 2\min\{\kappa_i, \kappa_j\}$.

For later use, we define the positive bilinear forms $d_i$ as

$$d_i(u, v) = a_i(u, v) + p_i(u, v), \tag{3.9}$$

and the broken bilinear form $d_h$ for $X_h(\Omega)$:

$$d_h(u, v) := \sum_{i=1}^{N} d_i(u, v). \tag{3.10}$$

For $u = \{u_i\}_{i=1}^N \in X_h(\Omega)$ the associated broken norm is then defined by

$$\|u\|_{h,\delta}^2 = d_h(u, u) = \sum_{i=1}^{N} \left\{ \| \kappa_i^{\frac{1}{2}} \nabla u_i \|_{L^2(\Omega_i)}^2 + \sum_{E_{ij} \subset \partial\Omega_i} \frac{1}{l_{ij}} \frac{\delta}{h_{ij}} \int_{E_{ij}} \kappa_{ij}(u_i - u_j)^2 ds \right\}. \tag{3.11}$$

## 3.2 Generating multiscale spaces

In this section, we will construct a local multiscale basis function. We will follow the ideas of GMsFEM (e.g. [30, 31]) where one needs the snapshot space. Based on the construction of the snapshot space, we generate two different type of multiscale spaces. In the construction of the snapshot space, some local spectral problems are designed and solved to generate suitable basis functions for a multiscale space. We first use the the snapshot space to be fine-grid functions within each coarse region. Thus, the local spectral problems will be posed on the fine grid independently on

some subregions related to the coarse grid. For the construction of the second type of the snapshot spaces, we solve a specific snapshot equation.

### *3.2.1 Fine-grid snapshot space*

We first consider the snapshot space that consists of all fine-grid functions in $\Omega_i$. We generate the multiscale space by solving a local spectral problem described below. Following [34, 30], for a given $i$, $i = 1, \ldots, N$ we consider the following spectral problem in $\Omega_i$: find the eigenvalues $\lambda^I_{i,\ell}$ and the eigenfunctions $\psi^{I_a}_{i,\ell}(x)$ such that

$$a_i(\psi^{I_a}_{i,\ell}, z) = \lambda^{I_a}_{i,\ell} m_i(\psi^{I_a}_{i,\ell}, z) \quad \text{for all } z \in X_h(\Omega_i). \tag{3.12}$$

Here, $a_i$ is defined in (3.6), the bilinear form $m_i(\cdot, \cdot)$ is defined by

$$m_i(v, z) = \int_{\Omega_i} \widetilde{\kappa} v z, \tag{3.13}$$

where $\widetilde{\kappa}$ is a properly selected weight; for scalar permeability, we select $\widetilde{\kappa} = \kappa$ while for tensor permeability we refer to [34]. The super-index $I$ is used to distinguish from the other snapshot space we develop here (with index $II$).

Now we present a modification of the above eigenvalue problem. This modification is motivated by the error analysis developed below in Section 3.4.2 and results in the ability to bound the terms involving integral of functions over boundaries of the subdomains. More precisely, for any given subdomain $\Omega_i$, we find $\lambda^{I_b}_{i,\ell}$ and $\psi^{I_b}_{i,\ell} \in X_h(\Omega_i)$ such that

$$a_i(\psi^{I_b}_{i,\ell}, z) = \lambda^{I_b}_{i,\ell}\Big(m_i(\psi^{I_b}_{i,\ell}, z) + m^{\delta}_i(\psi^{I_b}_{i,\ell}, z)\Big) \quad \text{for all } z \in X_h(\Omega_i). \tag{3.14}$$

Here, the (boundary) bilinear form $m_i^{\delta}(\cdot,\cdot)$ is given by

$$m_i^{\delta}(v,z) = \sum_{E_{ij}\subset\partial\Omega_i} \frac{1}{l_{ij}}\frac{\delta}{h_{ij}} \int_{E_{ij}} \kappa_{ij} v z ds. \tag{3.15}$$

These eigenvalue problems allow us to obtain simple error estimates since the eigenvectors can approximate fine-grid functions simultaneously in a norm that includes interior weighted semi-norm in the coarse-grid block and weighted $L^2$-norm on the interfaces.

We order the eigenvalues so that $0 \leq \lambda_{i,1}^I \leq \lambda_{i,2}^I \leq .... \leq \lambda_{i,N_i}^I$, where $N_i$ is the number of vertices of $\mathcal{T}_h(\Omega_i)$, i.e., the number of degrees of freedom associated to $X_h(\Omega_i)$. Then, in each subdomain $\Omega_i$, we take the $L_i$ eigenfunctions corresponding to the smallest eigenvalues and use them as the multiscale basis. More precisely, define

$$X_H^I(\Omega_i) := \text{span}\left\{\psi_{i,\ell}^I, 1 \leq l \leq L_i\right\} \subset X_h(\Omega_i), \quad i = 1,\ldots,N.$$

Finally, the coarse space is defined as

$$X_H^I(\Omega) := X_H^I(\Omega_1) \times \cdots \times X_H^I(\Omega_N) \subset X_h(\Omega).$$

We refer to $X_H^I(\Omega)$ as a spectral coarse space.

Now the coarse-grid problem is to find $u_H^I \in X_H^I(\Omega)$ such that

$$a_h^{DG}(u_H^I, v_H) = f(v_H) \quad \text{for all} \quad v_H \in X_H^I(\Omega). \tag{3.16}$$

Note that the dimension of $X_H^I(\Omega)$ depends on the number of eigenvectors chosen in each coarse block $\Omega_i$. An ideal situation would be when a small select number of eigenvectors in $\Omega_i$ represent (approximate) the restriction of the solution to that

subdomain accurately.

**Remark 3.2.1** (On the original weighted eigenvalue problem)**.** *We refer to the eigenvalue problem (3.14) as "the amended eigenvalue problem" due to the introduced modification on the right hand side. This modification is done with respect to the simpler eigenvalue problem* (3.12)*. We refer to this eigenvalue problem as the (original) weighted eigenvalue problem. Although the convergence of the method using this simpler eigenvalue problem is not guaranteed by our analysis, the resulting method was tested numerically where we observed good results in comparison with the amended eigenvalue problem. See Section 3.3.*

### *3.2.2 General snapshot space*

One can consider a more general snapshot space by solving local eigenvalue problems. As we discussed in the Introduction, the use of general snapshot space can have an advantage when additional information is known about the local solutions. The subset of all functions that have desired properties of the solution can be taken as a possible snapshot space. In this way we solve the eigenvalue problem on more relevant (smaller dimension) subspaces instead of the space involving all fine degrees of freedom. For example, if solutions need to be computed only for a subspace of possible source terms, one can restrict the snapshot space to the space of local solutions for those sources only. To demonstrate the possibility of using a snapshot space strictly smaller than $X_h(\Omega)$, we consider an example where the snapshot space consists of all local solutions of the homogeneous equation with boundary conditions restricted on the boundary of the finite element nodal basis functions (or the set of all discrete $a_i-$harmonic functions in each block). More precisely, for the nodal basis

function $\delta_k(x)$ corresponding to the $k-$th node on $\partial\Omega_i$, we consider the problem

$$-\nabla \cdot (\kappa \nabla \phi_{i,k}) = 0 \quad \text{in } \Omega_i, \quad \phi_{i,k} = \delta_k \quad \text{on } \partial\Omega_i. \tag{3.17}$$

The $\phi_{i,k} \in X_h(\Omega_i)$, $k = 1, \ldots, n_i$, is the (finite element) solution of this local problem. Here $n_i$ denotes the number of the nodal basis function corresponding to nodes on $\partial\Omega_i$. Then the snapshot space is defined by

$$X_h^{\text{snap}}(\Omega_i) = \text{span}\{\phi_{i,k}, 1 \leq k \leq n_i\}, \quad i = 1, \ldots, N. \tag{3.18}$$

**Remark 3.2.2.** *The reference solution we want to approximate on a coarse grid is the Galerkin projection of $u_h^*$, solution of (3.3), into the global snapshot space $X_h^{snap}(\Omega) = X_h^{snap}(\Omega_1) \times \cdots \times X_h^{snap}(\Omega_N)$.*

Our objective is to construct a possibly smaller dimension space $X_H^{\text{snap}}(\Omega_i)$ which is a subspace of $X_h^{\text{snap}}(\Omega_i)$. The construction is done using an appropriate spectral decomposition. For this, we define the matrices

$$A_i^{\text{snap}} = [a_i(\phi_{i,k}, \phi_{i,k'})]_{k,k'=1,}^{n_i} \quad \text{and} \quad M_i^{\text{snap}} = [m_i^{\delta}(\phi_{i,k}, \phi_{i,k'})]_{k,k'}^{n_i}$$

and solve the following algebraic eigenvalue problem

$$A_i^{\text{snap}} \alpha_{i,\ell} = \lambda_{i,\ell}^{\text{snap}} M_i^{\text{snap}} \alpha_{i,\ell}. \tag{3.19}$$

We write $\alpha_{i,\ell} = (\alpha_{i,\ell;1}, \ldots, \alpha_{i,\ell;M_i}) \in \mathbb{R}^{M_i}$ and define the corresponding finite element functions, $\psi_{i,\ell}^{II} \in X_h(\Omega_i)$ as

$$\psi_{i,\ell}^{II} = \sum_{k=1}^{n_i} \alpha_{i,\ell;k} \phi_{i,k}, \quad \ell = 1, \ldots, n_i.$$

Note that the matrices $A_i^{\text{snap}}$ and $M_i^{\text{snap}}$ are computed in the space of snapshots in $\Omega_i$. Assume that $0 \leq \lambda_{i,1}^{\text{snap}} \leq ... \leq \lambda_{i,n_i}^{\text{snap}}$, and choose the $L_i$ eigenvectors $\psi_{i,1}^{II}, \ldots, \psi_{i,L_i}^{II}$ that correspond to the smallest $L_i$ eigenvalues. We introduce

$$X_H^{II}(\Omega_i) = \text{span}\left\{\psi_{i,\ell}^{II} : l = 1, \ldots, L_i\right\} \text{ for } i = 1, \ldots, N$$

and define the global coarse space by

$$X_H^{II}(\Omega) := X_H^{II}(\Omega_1) \times \cdots \times X_H^{II}(\Omega_N) \subset X_h(\Omega).$$

Then the coarse problem is to find $u_H^{II} \in X_H^{II}(\Omega)$ such that

$$a_h^{DG}(u_H^{II}, v_H) = f(v_H) \quad \text{for all} \quad v_H \in X_H^{II}(\Omega). \tag{3.20}$$

**Remark 3.2.3.** *Note that according to the definition of $m_i^{\delta}$ in (3.15), the matrix $M_i^{snap}$ scales with $1/h_{ij}$. Then, the resulting eigenvalues scale with $h_{ij}$ while the eigenspaces do not depend on $h_{ij}$. A similar situation is also valid for Method II and the eigenvalue problem (3.14). It is easy to see from our main Theorem 3.4.4 (stated and proved in Section 3.4.2) that this scaling does not affect the convergence rate with respect to the number of eigenvectors used in the coarse space.*

**Remark 3.2.4.** *Instead of the defined above $M_i^{snap} = [m_i^{\delta}(\phi_{i,k}, \phi_{i,k'})]_{k,k'=1}^{n_i}$, we can use $M_i^{snap} = [m_i(\phi_{i,k}, \phi_{i,k'})]_{k,k'=1}^{n_i}$.*

## 3.3 Numerical experiments

In this section, we present some representative numerical experiments. In particular, we compute the coarse (or upscaled) solution and study the error with respect to the reference solution (or the fine-grid solution of (3.3)). In all the numerical tests

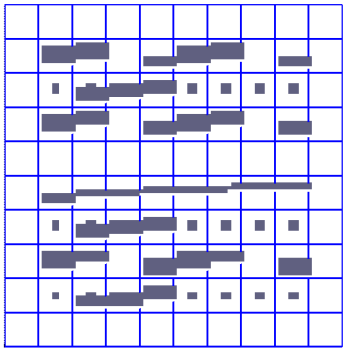

Figure 2: High-contrast coefficient. Topology 1.

presented here we choose $\delta = 4$. We note that the solution of (3.3) depends on both fine-scale and coarse-scale parameters, $h$ and $H$. We are mainly interested in the convergence (to the reference solution) when adding more basis functions. We study the error behavior due to the increase of the numbers of coarse basis functions for fixed values of $h$ and $H$.

We consider the domain $\Omega = (0,1)^2$ and divide $\Omega$ into $N = M \times M$ square coarse blocks, $\{\Omega_i\}_{i=1}^N$, which are unions of fine elements. In this case $H = 1/M$ is the coarse mesh parameter. Inside each subdomain $\Omega_i$ we generate a structured triangulation with $m$ subintervals in each coordinate direction (and thus $h = 1/(Mm)$ is the fine mesh parameter). We consider the solution of Equation (3.3) with $f = 1$ and a high-contrast coefficient described in Figure 2. This coefficient equals one in the white background and $\eta$ in the gray regions representing high-contrast channels and high-contrast inclusions. Thus, $\eta$ represents the contrast of the media, namely the ratio of the maximum and minimum values of $\kappa(x)$.

In the numerical experiments we compute the norm of the error $e = u_h^* - u_H$ between the reference solution (fine-grid solution) obtained by solving (3.3) and the coarse-grid solutions $u_H$: 1. $u_H^I$ solution of (3.16) (with original eigenvalue problem

and also with amended eigenvalue problem) or 2. $u_H^{II}$ the solution of (3.20). The total error is $\|e\|_{h,1}^2$ where $\|\cdot\|_{h,\delta}^2$ defined in (3.11). The relative error is computed as $\|e\|_{h,1}^2/\|u_h^*\|_{h,1}^2$. The error is divided into two quantities:

- *Interior Error*: (square of the) broken $H^1-$semi-norm of the error

$$\sum_{i=1}^{N} a_i(e,e) = \sum_{i=1}^{N} \| \kappa_i^{\frac{1}{2}} \nabla e_i \|_{L^2(\Omega_i)}^2 .$$

- *Interface Error*: (square of the) $L^2-$norm of the jump of the error across the edges

$$\sum_{i=1}^{N} \sum_{E_{ij}\subset\partial\Omega_i} \frac{1}{l_{ij}} \frac{1}{h_{ij}} \int_{E_{ij}} \kappa_{ij}(e_i - e_j)^2.$$

- *Energy error*: (square of the) DG bilinear form, that is, $a_h^{DG}(e,e)$.

### *3.3.1 Fine-grid snapshot space and original eigenvalue problem*

We present the numerical experiments for the method that uses the original weighted eigenvalue problem (3.12). We recall that the convergence of this method is not covered by our analysis. We numerically show the error obtained when the dimension of the coarse space is increased.

First, we recall that for high-contrast problems we include the eigenvectors corresponding to small eigenvalues (that asymptotically vanish as the contrast increases). We denote by $L_i^{small}$ the number of these small eigenvalues in $\Omega_i$. For the coefficient $\kappa(x)$ and the coarse mesh shown on Figure 2, $L_i^{small} = 1$, $i = 1, 2, \ldots, N$. To see the effect of adding more basis functions, we select additional $L_i^{add}$ eigenvectors so the total number of eigenfunctions selected in the block $\Omega_i$ is $L_i^{small} + L_i^{add}$. We show that the error decays as $L_i^{add}$ increases. The Figure 3 illustrates the effect of using an increasing number of eigenvectors in the solution space. We show the fine-

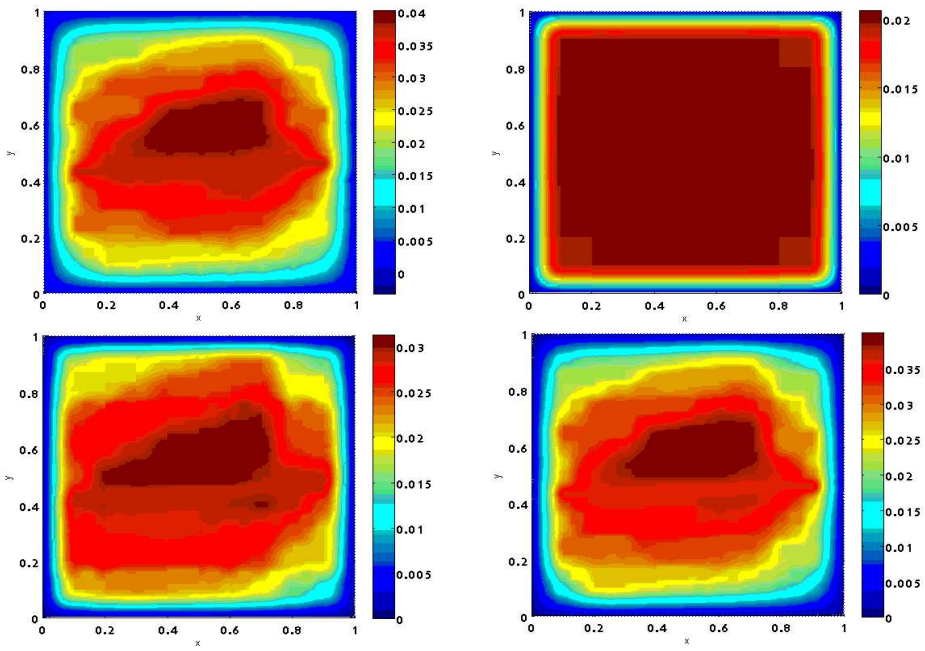

Figure 3: Illustration of fine and coarse solutions. Fine-scale solution $u_h^*$ (top left). Coarse-scale solution $u_H^{ms,I}$ with $L_i^{add} = 0$ eigenvalues (top right). Coarse-scale solution $u_H^{ms,I}$ with $L_i^{add} = 3$ eigenvalues (bottom left). Coarse-scale solution $u_H^{ms,I}$ with $L_i^{add} = 11$ eigenvalues (bottom right).

scale solution and coarse-scale solutions computed with three different coarse spaces $L_i^{add} = 0, 2, 11$.

The results for the computation of interior and interface errors are presented in Table 2 for $h = 1/100$ and $H = 1/10$ and two different contrasts. In this table, we also report the dimension of the coarse spaces (denoted by "Dim") and the number of eigenvectors that are added for each subdomain to form the coarse space. The convergence with respect to the minimum left out the eigenvalue is shown in Figure 4 (left). In this case, we solve a local eigenvalue problem in each coarse block. From the results, we see a convergence to the reference solution (fine-grid solution). We also observe that the error is inversely proportional to the $\lambda_{min}$ (the minimum left

Table 2: Numerical results using the original weighted eigenvalue problem in Remark 3.2.1. Here, $h = 1/100$, $H = 1/10$, $\eta = 10^4$ and $\eta = 10^6$ (in parenthesis). "Dim" stands for the dimension of the coarse space.

| $L_i^{add}$ | Dim. | Interface error | Interior error | Total error | $\lambda_{\min}$ |
|---|---|---|---|---|---|
| 0 | 100 (100) | 0.026 (0.026) | 0.326 (0.326) | 0.3522 (0.3522) | 689.4 ( 689.3) |
| 2 | 300 (300) | 0.031 (0.032) | 0.221 (0.220) | 0.2523 (0.2516) | 1562.2 (1561.7) |
| 4 | 500 (500) | 0.028 (0.029) | 0.171 (0.170) | 0.1991 (0.1984) | 2607.5 (2607.0) |
| 6 | 700 (700) | 0.027 (0.027) | 0.133 (0.131) | 0.1600 (0.1581) | 5199.4 (5199.3) |
| 8 | 900 (900) | 0.026 (0.027) | 0.114 (0.113) | 0.1399 (0.1392) | 7237.9 (7237.6) |
| 10 | 1100 (1100) | 0.025 (0.025) | 0.104 (0.103) | 0.1293 (0.1283) | 9509.1 (9509.0) |

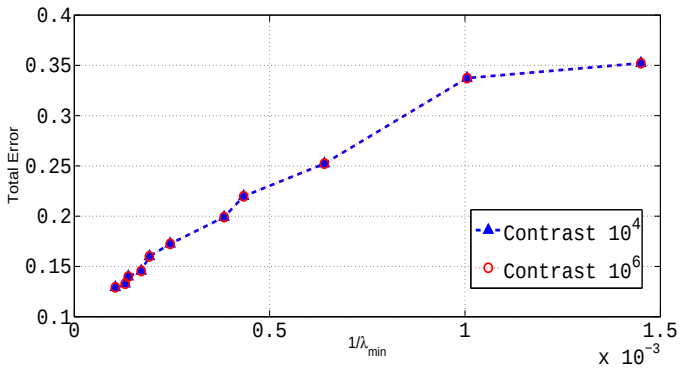


Figure 4: Total error of Method I (in Section 3.2.1) vs. $1/\lambda_{min}$. Here $h = 1/100$ and the contrast is $10^6$. Coarse mesh size $H = 1/10$ and contrast $10^4$ and $10^6$.

out eigenvalue). In particular, for $H = 1/10$, we only need coarse space of dimension 300 to 400 to get an interior error of 17%. This error is computed with respect to the fine-grid solution with fine-grid mesh size $h = 1/100$. The dimension of fine-scale system is $12,980$. Note that, in this case, we have four or five basis functions per subdomain that is comparable to the number of degrees of freedom of a classical DG method on the coarse grid.

Next, we test the error when we change the scaling of the penalty term. We recall that the fine-scale problem in (3.3) uses a penalty term scaled by $\delta \frac{1}{l_{ij}} \frac{1}{h_{ij}}$. In the classical SIPG formulation on the coarse grid one uses a penalty scaled by $\delta \frac{1}{l_{ij}} \frac{1}{H}$.

Here we experiment by computing the coarse solutions with several penalties in the range from $1/H$ to $1/h$ to identify a good penalty parameter for the coarse problem.

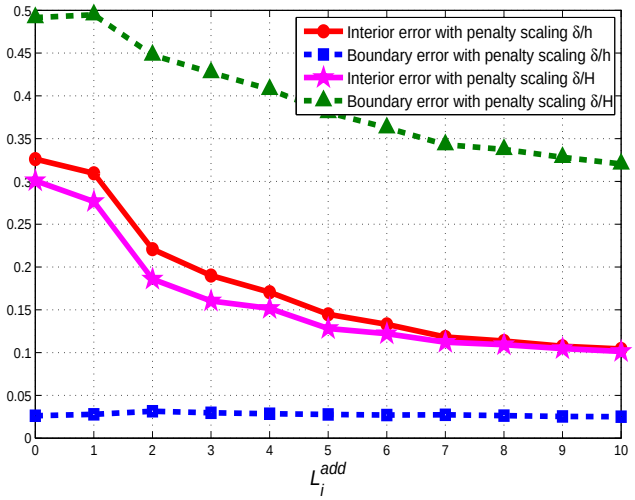


Figure 5: The error for values of $L_i^{add} = 0, 1, \ldots, 10$ and the two different penalty scalings: $\frac{\delta}{h}$ and $\frac{\delta}{H}$. Here $h = 1/100$, $H = 1/10$ and $\eta = 10^4$.

For this experiment we set the contrast $\eta = 10^4$, $M = 10$, $n_i = 10$, $i = 1, \ldots, N$ (and thus $H = 1/10$ and $h = 1/100$). Then, recalling that $\delta = 4$ for the numerical experiments, we have $\delta\frac{1}{H} = 40$ and $\delta\frac{1}{h_{ij}} = 400$. For these two choices of the penalty in Figure 5 we show the decay of the interior and interface error when adding more eigenfunctions. We observe a reduction of the error as we add more additional coarse-grid basis functions. Also, we observe that the interior error are of comparable size (with either scaling) and that the interface error is bigger if we use penalty scaled by the coarse-grid size

### *3.3.2 Fine-grid snapshot space and amended eigenvalue problem*

Next, we consider the method introduced in Subsection 3.2.1 with the amended eigenvalue problem. The convergence of this method, with respect to the number of eigenvectors used in the construction of the coarse space, follows from Theorem 3.4.4. We repeat the experiment described in Subsection 3.3.1 using the amended local eigenvalue problem. The results are displayed in Table 3 for contrast $\eta = 10^4$. Similar results were observed for higher contrast ratios. We observe an error reduction when more eigenfunctions are added. Note that the results obtained by using the amended eigenvalue problem in Subsection 3.2.1 are slightly better compared when using the original eigenvalue problem. Our numerical results agree with our theoretical error estimates in Theorem 3.4.4. We also report the energy error.

Table 3: Numerical results for Method I (Subsection 3.2.1) with increasing dimension of the coarse space, $h = 1/100$, $H = 1/10$, and $\eta = 10^4$. "Dim" stands for the dimension of the coarse space.

| $L_i^{add}$ | Dim | Interface | Interior | Total | Energy | $\lambda_{\min}$ |
|---|---|---|---|---|---|---|
| 0 | 100 | 0.0318 | 0.2854 | 0.3172 | 0.3172 | 0.0528 |
| 2 | 300 | 0.0342 | 0.1679 | 0.2020 | 0.2646 | 0.0933 |
| 4 | 500 | 0.0257 | 0.1066 | 0.1323 | 0.1793 | 0.1165 |
| 6 | 700 | 0.0214 | 0.0800 | 0.1014 | 0.1444 | 0.2459 |
| 8 | 900 | 0.0194 | 0.0581 | 0.0775 | 0.1164 | 0.3514 |
| 10 | 1100 | 0.0185 | 0.0566 | 0.0751 | 0.1132 | 0.4551 |

Next, we consider different permeability field shown on Figure 6 with the contrast $\eta = 10^4$. For this permeability field, long channels of the domain are added to introduce a long-range effect in the solution. We note that there are more asymptotically small eigenvalues in some subdomains as we observe in our numerical simulations. The numerical results are presented in Table 4, where we present interface, interior,

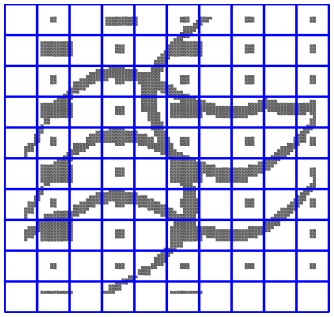

Figure 6: High-contrast coefficient. Topology 2.

total, and energy errors. We note that the convergence behavior is similar to the previous case with errors that are slightly smaller. These two high-contrast permeability examples show that the proposed approach is capable of approximating the solution well when using local spectral multiscale basis functions.

Table 4: Numerical results for Method I (Subsection 3.2.1) with increasing dimension of the coarse space, $h = 1/100$, $H = 1/10$, and $\eta = 10^4$. The coefficient is depicted in Figure 6. "Dim" stands for the dimension of the coarse space.

| $L_i^{add}$ | Dim | Interface | Interior | Total | Energy | $\lambda_{\min}$ |
|---|---|---|---|---|---|---|
| 0 | 111 | 0.0643 | 0.2445 | 0.3088 | 0.4479 | 0.0237 |
| 2 | 311 | 0.0331 | 0.1072 | 0.1403 | 0.2048 | 0.0972 |
| 4 | 511 | 0.0228 | 0.0588 | 0.0817 | 0.1230 | 0.1946 |
| 6 | 711 | 0.0200 | 0.0437 | 0.0637 | 0.1014 | 0.2521 |
| 8 | 911 | 0.0189 | 0.0379 | 0.0567 | 0.0912 | 0.2838 |
| 10 | 1111 | 0.0187 | 0.0374 | 0.0560 | 0.0907 | 0.4613 |

### *3.3.3 Local solutions as snapshot space*

Next, we consider the snapshot space given as in Subsection 3.2.2 that consists of $a_i-$harmonic functions defined in (3.17). We note that this snapshot space is used in the generalized multiscale finite element method for the wave equation in [17].

The objective of presenting these results is to show that the proposed DG method is flexible and one can use various snapshot spaces.

Table 5: Numerical results for Method II (see Subsection 3.2.2) with increasing dimension of the coarse space, $h = 1/100$, $H = 1/10$ and $\eta = 10^4$. "Dim" stands for the dimension of the coarse space.

| $L_i^{add}$ | Dim | Interface | Interior | Total | Energy | $\lambda_{\min}$ |
|---|---|---|---|---|---|---|
| 0 | 100 | 0.032 | 0.285 | 0.317 | 0.373 | 0.0528 |
| 2 | 300 | 0.034 | 0.168 | 0.202 | 0.265 | 0.0933 |
| 4 | 500 | 0.026 | 0.107 | 0.133 | 0.181 | 0.1165 |
| 6 | 700 | 0.021 | 0.079 | 0.101 | 0.144 | 0.2459 |
| 8 | 900 | 0.019 | 0.058 | 0.077 | 0.116 | 0.3514 |
| 10 | 1100 | 0.018 | 0.057 | 0.075 | 0.114 | 0.4552 |

In Table 5, we present the numerical results with contrast $\eta = 10^4$. In this example, we choose $H = 1/10$, $h = 1/100$, and $\delta = 4$. Simliarly, we see the convergence to the fine-grid solution of (3.3). We also observe errors decay proportional to increase eigenfunctions across all coarse blocks. Note that, we are report the error not with respect to the reference solution (on the snapshot space) but with respect to the fine-grid solution.

We will need to use the bilinear form $m_i^\delta$ in the eigenvalue problem in order to obtain error estimates in Section 3.4.2 . We also observe convergence in the numerical tests if we use $M_i^{\text{snap}}$ introduced in Remark 3.2.4. In this case, we use $m_i$ bilinear form instead of $m_i^\delta$ to generate $M_i^{\text{snap}}$. These results are reported in Table 6.

## 3.4 Analysis of the method

In this section, we investigate the stability and derive error estimates for the proposed methods in Section 3.2. We also show that constants for stability and error estimates are independent of the high contrast.

Table 6: Numerical results for snapshot space and bilinear form $m_i$ (instead of $m_i^\delta$). Here $h = 1/100$, $H = 1/10$, and $\eta = 10^4$. "Dim" stands for the dimension of the coarse space.

| $L_i^{add}$ | Dim. | Interface | Interior | Total |
|---|---|---|---|---|
| 2 | 300 | 0.0301 | 0.1750 | 0.2051 |
| 4 | 500 | 0.0278 | 0.1104 | 0.1382 |
| 6 | 700 | 0.0257 | 0.0905 | 0.1162 |
| 8 | 900 | 0.0243 | 0.0763 | 0.1007 |
| 10 | 1100 | 0.0223 | 0.0663 | 0.0986 |

### *3.4.1 Stability analysis*

We have the following lemma shown in [27, Lemma 3.1]. Here we provide a sketch of the proof for the sake of completeness.

**Lemma 3.4.1.** *Let the bilinear forms $d_i(\cdot,\cdot)$ and $d_h(\cdot,\cdot)$ be defined by* (3.9) *and* (3.10)*, respectively. Then there exists a $\delta_0 > 0$ such that for $\delta \geq \delta_0$ and all $u \in X_h(\Omega)$ the following inequalities hold:*

$$\gamma_0 d_i(u,u) \leq a_i^{DG}(u,u) \leq \gamma_1 d_i(u,u), \qquad i = 1,\ldots,N,$$

*and*

$$\gamma_0 d_h(u,u) \leq a_h^{DG}(u,u) \leq \gamma_1 d_h(u,u), \tag{3.21}$$

*where $\gamma_0$ and $\gamma_1$ are positive constants independent of the $\kappa_i$, $h_i$ $H_i$ and $u$.*

*Proof.* First, we want to prove that $\gamma_0 d_i(u,u) \leq a_i^{DG}(u,u)$. Since $a_i^{DG}(u,u) = a_i(u,u) + s_i(u,u) + d_i(u,u)$, the proof reduces to bound $|s_i(u,u)|$. Note that

$$s_i(u,u) = 2\sum_{E_{ij}\subset\partial\Omega_i} \frac{1}{l_{ij}} \int_{E_{ij}} \kappa_{ij} \frac{\partial u_i}{\partial n_i}(u_j - u_i) = 2\sum_{E_{ij}\subset\partial\Omega_i} \frac{1}{l_{ij}} I_{ij}$$

where we have defined $I_{ij} := \int_{E_{ij}} \kappa_{ij} \frac{\partial u_i}{\partial n_i}(u_j - u_i)ds$. We have

$$I_{ij} \leq \left\| \kappa_{ij}^{1/2} \nabla u_i \right\|_{L^2(E_{ij})} \left\| \kappa_{ij}^{1/2} (u_j - u_i) \right\|_{L^2(E_{ij})}.$$

Using the following inequality for $u_i \in X_h(\Omega_i)$

$$h_i \left\| \kappa_{ij}^{1/2} \nabla u_i \right\|^2_{L^2(E_{ij})} \leq C \left\| \kappa_i^{1/2} \nabla u_i \right\|^2_{L^2(\Omega_i)},$$

the Young's inequality with arbitrary $\epsilon > 0$ and the fact $h_{ij} \leq 2h_i$ , we get

$$I_{ij} \leq C \left\{ \epsilon \left\| \kappa_i^{1/2} \nabla u_i \right\|^2_{L^2(\Omega_i)} + \frac{1}{4\epsilon} \frac{1}{2h_{ij}} \left\| \kappa_{ij}^{1/2} (u_j - u_i) \right\|^2_{L^2(E_{ij})} \right\}.$$

Then, multiplying by $1/l_{ij}$ and summing over the edges $E_{ij} \subset \Omega_i$, we get

$$\begin{aligned} |s_i(u,u)| &\leq 2CN_{CE}\epsilon \left\| \kappa_i^{1/2} \nabla u_i \right\|^2_{L^2(\Omega_i)} + \frac{C}{4\epsilon} \sum_{E_{ij} \subset \partial\Omega_i} \frac{1}{l_{ij}} \frac{1}{h_{ij}} \left\| \kappa_{ij}^{1/2} (u_j - u_i) \right\|^2_{L^2(E_{ij})} \\ &= 2CN_{CE}\epsilon a_i(u,u) + \frac{C}{4\epsilon\delta} p_i(u,u). \end{aligned}$$

Here $N_{CE}$ denotes the number of *coarse edges* of subdomain $\Omega_i$ (for instance, $N_{CE} = 4$ if the coarse subdomains have rectangular shape). Choosing $\epsilon = 1/(4CN_{CE})$ we get

$$|s_i(u,u)| \leq 0.5 a_i(u,u) + \frac{C^2 N_{CE}}{\delta} p_i(u,u)$$

and then

$$0.5 a_i(u,u) + (1 - \frac{C^2 N_{CE}}{\delta}) p_i(u,u) \leq a^{DG}(u,u) \leq 1.5 a_i(u,u) + (1 + \frac{C^2 N_{CE}}{\delta}) p_i(u,u).$$

Therefore the result holds if we take $\delta \geq \delta_0 > C^2 N_{CE}$, $\gamma_0 = \min\{0.5, 1 -$

$(C^2 N_{CE})/\delta\}$ and $\gamma_1 = \max\{1.5, (C^2 N_{CE})/\delta\}$. □

**Remark 3.4.2.** *We note that $\gamma_1/\gamma_0$ in Lemma 3.4.1 deteriorates when $\delta$ gets larger. In practice, however, $\delta \geq \delta_0$ is chosen such that $\delta = O(1)$; therefore, from now on we assume that all the estimates will not depend on $\delta$.*

For the coarse-grid approximate solution we have the following lemma, which could be considered as an analogue of Cea's Lemma.

**Lemma 3.4.3.** *Let $u_h^* \in X_h(\Omega)$ and $u_H^I \in X_H^I(\Omega)$ be the solutions of (3.3) and (3.16), correspondingly. Then*

$$d_h(u_h^* - u_H^I, u_h^* - u_H^I) \leq C_1 d_h(u_h^* - v, u_h^* - v) \quad \textit{for all} \quad v \in X_H^I(\Omega) \tag{3.22}$$

*with $C_1$ is independent of $\kappa_i, h_i, H_i, u_h^*$ and $u_H^I$.*

*Proof.* For all $v \in X_H^I(\Omega)$,

$$a_h^{DG}(u_h^*, v) = f(v) \quad \text{and} \quad a_h^{DG}(u_H^I, v) = f(v). \tag{3.23}$$

Then $a_h^{DG}(u_h^* - u_H^I, v) = 0$ and since $u_H^I \in X_H^I(\Omega)$,

$$a_h^{DG}(u_h^* - u_H^I, u_h^* - u_H^I) = a_h^{DG}(u_h^* - u_H^I, u_h^* - v). \tag{3.24}$$

Using a Cauchy-Schwarz inequality and (3.21) in Lemma 3.4.1,

$$\begin{aligned}
\gamma_0 d_h(u_h^* - u_H^I, u_h^* - u_H^I) &\leq a_h^{DG}(u_h^* - u_H^I, u_h^* - u_H^I) \\
&= a_h^{DG}(u_h^* - u_H^I, u_h^* - v) \\
&\leq a_h^{DG}(u_h^* - u_H^I, u_h^* - u_H^I)^{1/2} a_h^{DG}(u_h^* - v, u_h^* - v)^{1/2} \\
&\leq \gamma_1 d_h(u_h^* - u_H^I, u_h^* - u_H^I)^{1/2} d_h(u_h^* - v, u_h^* - v)^{1/2}.
\end{aligned}$$

Taking $C_1 = (\gamma_1/\gamma_0)^2$, we get

$$d_h(u_h^* - u_H^I, u_h^* - u_H^I) \leq C_1 d_h(u_h^* - v, u_h^* - v)$$

and this completes the proof. □

Analogous best approximation results, with respect to the fine-grid reference solutions, hold true for the coarse problem (3.20) and even for the coarse problem of the method using the original weighted eigenvalue problem (see Remark 3.2.1).

### *3.4.2 Error analysis*

The theorem below gives an error bound with respect to the number of eigenvectors used in the construction of the clears-grid space. Thus, we obtain improvement of the numerical solution when we add more eigenvectors to the coarse space. The error estimates are written in terms of the local energy norm (of the reference solution).

**Theorem 3.4.4.** *Let $u_h^* = \{u_i^*\}_{i=1}^N$ and $u_H^I$ be the solutions of problems (3.3) and (3.16), respectively. In each subdomain we write*

$$u_i^* = \sum_{\ell=1}^{N_i} c_\ell(u_i^*)\psi_{i,\ell}^I \quad \text{and} \quad a_i(u_i^*, u_i^*) = \sum_{\ell=1}^{N_i} \lambda_{i,\ell}^I c_\ell(u_i^*)^2,$$

*where $c_\ell(u_i^*) = m_i(u_i^*, \psi_{i,\ell}^I) + m_i^\delta(u_i^*, \psi_{i,\ell}^I)$. Then the following error estimate holds*

$$d_h(u_h^* - u_H^I, u_h^* - u_H^I) \leq C_1 \left(1 + \frac{4}{\min\limits_{1\leq i\leq N} \lambda_{i,L_i+1}^I}\right) \sum_{i=1}^{N} \sum_{\ell=L_i+1}^{N_i} \lambda_{i,\ell}^I c_\ell(u_i^*)^2.$$

*Proof.* Define the "interpolant" $I_H(u_h^*)$ of $u_h^*$ by truncating the expansion of solutions

with respect to the eigenfunction $\psi^I_{i,\ell}$:

$$I_H(u_h^*) = \{I_H^i(u_i^*)\}_{i=1}^N \text{ where } I_H^i(u_i^*) = \sum_{\ell=1}^{L_i} c_\ell(u_i^*)\psi^I_{i,\ell},$$

where $c_\ell(u_i^*) = m_i(u_i^*, \psi^I_{i,\ell}) + m_i^\delta(u_i^*, \psi^I_{i,\ell})$, $i = 1, \ldots, N$. Note that $I_H^i(u_i^*)$ is the projection of $u_i^*$ into the space spanned by the first $L_i$ eigenvectors. Now we take $v = I^H(u_h^*)$ in Lemma 3.4.3 to obtain

$$d_h(u_h^* - u_H^I, u_h^* - u_H^I) \leq C_1 d_h(u_h^* - I_H(u_h^*), u_h^* - I_H(u_h^*)) = d_h(e, e), \tag{3.25}$$

where we have defined $e = \{e_i\}_{i=1}^N$ as

$$e_i = u_i^* - I_H^i(u_i^*) = \sum_{\ell=L_i+1}^{N_i} c_\ell(u_i^*)\psi^I_{i,\ell}.$$

Now we bound $d_h(e, e)$. First, we observe that

$$d_h(e, e) = \sum_{i=1}^N \big(a_i(e_i, e_i) + p_i(e, e)\big). \tag{3.26}$$

The second term in this sum can be bounded as follows

$$\begin{aligned} p_i(e, e) &= \sum_{E_{ij} \subset \delta\Omega_i} \frac{1}{l_{ij}} \frac{\delta}{h_{ij}} \int_{E_{ij}} \kappa_{ij}(e_j - e_i)^2 ds \\ &\leq 2 \sum_{E_{ij} \subset \partial\Omega_i} \left( \frac{1}{l_{ij}} \frac{\delta}{h_{ij}} \int_{E_{ij}} \kappa_{ij}(e_j)^2 ds + \frac{1}{l_{ij}} \frac{\delta}{h_{ij}} \int_{E_{ij}} \kappa_{ij}(e_i)^2 ds \right) \\ &\leq 2 \sum_{E_{ij} \subset \partial\Omega_i} \frac{1}{l_{ij}} \frac{\delta}{h_{ij}} \int_{E_{ij}} \kappa_{ij}(e_j)^2 ds + 2m_i^\delta(e_i, e_i). \end{aligned}$$

Adding over all subdomains we get

$$\begin{aligned}\sum_{i=1}^{N} p_i(e,e) &\leq 2\sum_{i=1}^{N}\sum_{E_{ij}\subset\partial\Omega_i}\frac{1}{l_{ij}}\frac{\delta}{h_{ij}}\int_{E_{ij}}\kappa_{ij}(e_i)^2 ds + 2\sum_{i=1}^{N} m_i^{\delta}(e_i,e_i)\\ &= 4\sum_{i=1}^{N} m_i^{\delta}(e_i,e_i). \end{aligned} \tag{3.27}$$

On the other hand, if we use the increasing order of eigenvalues of eigenvalue problem (3.14), we get,

$$m_i^{\delta}(e_i,e_i) \leq m_i(e_i,e_i) + m_i^{\delta}(e_i,e_i) \leq \frac{1}{\lambda^I_{i,L_i+1}} a_i(e_i,e_i) \tag{3.28}$$

which, together with (3.26) and (3.27), gives

$$\begin{aligned}\sum_{i=1}^{N}\big(a_i(e_i,e_i)+p_i(e,e)\big) &\leq \sum_{i=1}^{N}\big(a_i(e_i,e_i)+4m_i^{\delta}(e_i,e_i)\big)\\ &= \sum_{i=1}^{N}\left(1+\frac{4}{\lambda^I_{i,L_i+1}}\right)\sum_{\ell=L_i+1}^{N_i}\lambda^I_{i,\ell}c_\ell(u_i^*)^2\\ &\leq \left(1+\frac{4}{\min\limits_{1\leq i\leq N}\lambda^I_{i,L_i+1}}\right)\sum_{i=1}^{N}\sum_{\ell=L_i+1}^{N_i}\lambda^I_{i,\ell}c_\ell(u_i^*)^2. \end{aligned}$$

This completes the proof. □

**Remark 3.4.5.** *In order to obtain further bounds for the error we have to study the convergence of the sum* $\sum_{\ell=1}^{N_i}\lambda^I_{i,\ell}c_\ell(u_i^*)^2$ *(that is, the decay of the coefficients* $c_\ell(u_i^*)^2$ *with increasing* $\ell$*). This can depend on various factors including the smoothness of the solution and it will be a subject of future research and study.*

**Remark 3.4.6.** *A similar result holds for the method constructed with snapshot space presented in Subsection 3.2.2. In this case the reference solution is the solution obtaining by a Galerkin projection on the snapshot space. See Remark 3.2.2.*

# 4. GENERALIZED MULTISCALE HDG METHODS FOR ELLIPTIC EQUATIONS [†]

In this chapter, we introduce a multiscale model reduction technique within the hybridizable discontinuous Galerkin finite element method (HDG). We use the generalized multiscale finite element [31] framework to construct a coarse-grid space that produces low dimensional solution space. In this approach, the local snapshot functions or/and spectral decomposition of the snapshot space are constructed to bring some small scale features of the solution through local approximations on each coarse patch. The multiscale finite element method allows to bring the local properties of the solution into a global coarse-grid problem in a systematic way that substantially reduces the number of coupled degrees of freedom in the algebraic system we need to solve. The local snapshot solutions are computed separately (possibly in parallel and/or offline) on each coarse block. In general, these solutions are discontinuous along the coarse grid interfaces and, consequently, a flexible and efficient method for gluing together this discontinuous functions is necessary in a global Galerkin type method is needed. In our work we use the hybridizable discontinuous Gelerkin method for this task.

The first efficient mixed multiscale finite element methods were devised by Arbogast in [7] as multi-block grid approximations using the framework of mortaring technique. Mortaring techniques (e.g. see the pioneering work [13]) were introduced to accommodate methods that can be defined in each subdomain that could have been independently meshed. We impose as a constrain the continuity along the in-

[†]Part of this chapter is reprinted with permission from Y. Efendiev, R. Lazarov, M. Moon, K. Shi. A spectral multiscale hybridizable discontinuous Galerkin method for second order elliptic problems. *Computer Methods in Applied Mechanics and Engineering*, 2014

terfaces of the coarse-grid mesh. This constrain is imposed in a weak sense by using an auxiliary space for the Lagrange multiplier. The classical mortaring, devised for the needs of domain decomposition methods, has been adapted recently as a multi-scale finite element approximation, e.g. [4, 9, 10]. In a two-scale (two-grid, fine and coarse) implementation we aim to resolve the local heterogeneities on the fine grid on each coarse block and then "glue" these approximations together via mortaring technique. The mortar spaces play the role of Lagrange multipliers, defined of the boundaries of the coarse partition. In order to design a stable method the mortar spaces have to satisfy proper inf-sup condition. This approach has shown to be well suited for problems with heterogeneous media and a number of efficient methods have been proposed, studied, implemented, and used for solving a variety of applied problems, see, e.g. [3, 4, 6, 9].

The hybridization of the finite element methods, as outlined in [22], represents another technique, which provides ample possibilities for "gluing" together various finite element approximations. The mechanism of this "glue" is based on the notions of *numerical trace* and *numerical flux*. Numerical trace is a single valued function on the finite element interfaces and belongs to a certain Lagrange multiplier space defined on the coarse-grid skeleton. Then the global problem is reduced to the solution of an algebraic problem for the degrees of freedom for the Lagrange multiplier space. The well-posedness and accuracy are ensured by a proper choice of the numerical flux, that involves a stabilization parameter $\tau$ (see, e.g. [22]). Standard approaches for selecting numerical traces involve the use of piecewise polynomials. However, the solution along the boundaries of a coarse grid can not have an arbitrary form and can be represented by a much lower dimensional space. In this paper, we seek a low dimensional representation of trace spaces. Our approach relies on local basis functions that are constructed independently (and in an offline stage) on each

coarse-grid cell (subdomain). The coupling of these local functions is provided by the HDG technology, where the role of the "glue" plays the space of the *numerical trace* whose construction is the main goal of this chapter. Here, we construct several spaces for the *numerical trace* that provide reasonable approximations of the solution and also results in a stable multi-scale method. Further, derive error estimates and discuss the convergence issues for some specific choices. Additionally, the efficacy of the proposed spaces is demonstrated on a set of numerical experiments on flows in highly heterogeneous porous media with high contrast.

## 4.1 Generalized multiscale HDG method

In this section, we present the multiscale structure of HDG finite element approximation. For this, we shall need two grid partitions of domain into finite elements, the corresponding multiscale finite element spaces, and some notations and norms form Sobolev spaces.

### *4.1.1 Model problem and discretization*

We consider the second-order elliptic differential equation

$$-\nabla \cdot (\kappa(x)\nabla u) = f(x) \ \text{ in } \ \Omega, \tag{4.1}$$

where $\Omega$ is a bounded polyhedral domain in $\mathbb{R}^n, n = 2, 3$. We assume that $f \in L^2(\Omega)$ and the coefficient $\kappa(x) \geq \kappa_0 > 0$ represents the permeability of a highly heterogeneous porous media with multiple scales and high contrast (the ratio between the maximum and minimum values of $\kappa$).

The multiscale finite element method for the equation (4.1) is based on the HDG methods and uses the concept of two-grid approximation.

We split the domain $\Omega$ into disjoint polygonal subdomains $\{\Omega_i\}_{i=1}^N$ of diameter

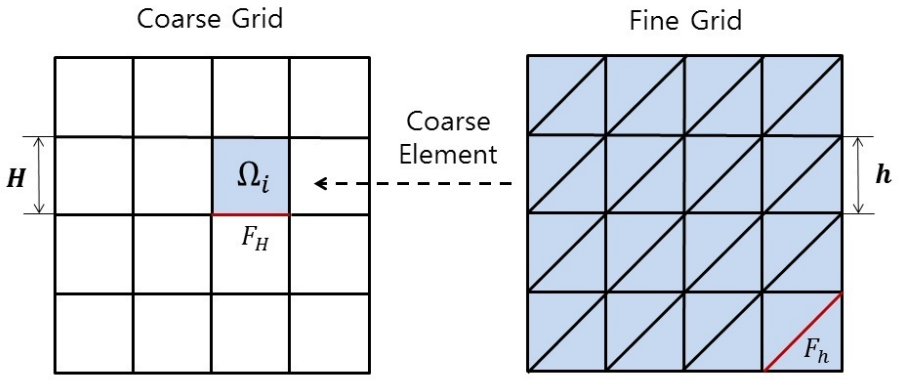


Figure 7: Fine and coarse grids: the coarse-grid blocks are squares while the fine grid finite elements are triangles.

$O(H_i)$ so that $\overline{\Omega} = \cup_{i=1}^{N} \overline{\Omega}_i$, see e.g. Figure 7. We denote by $F_H$ an face (edge) of the subdomain $\Omega_i$, if $F_H$ is either shared by $\Omega_i$ and its neighboring subdomain $\Omega_j$, i.e. $F_H = \overline{\Omega}_i \cap \overline{\Omega}_j$ or $F_H = \overline{\Omega}_i \cap \partial\Omega$. From now on the $\Omega_i$-side of $F_H$ will be denoted by $F_{ij}$ while on the $\Omega_j$-side of $F_H$ will be denoted by $F_{ji}$. Geometrically, $F_{ij}$ and $F_{ji}$ are the same object. Then $\mathcal{E}_H(\Omega_i)$ denotes the set of all coarse edges of a subdomain $\Omega_i$ and $\mathcal{E}_H = \cup_{i=1}^{N} \mathcal{E}_H(\Omega_i)$.

In each subdomain $\Omega_i$, we introduce a shape regular triangulation $\mathcal{T}_h(\Omega_i)$ with triangular elements and maximum mesh-size $h_i$. Faces (edges) of this triangulation are denoted by $F_h$. Let $\mathcal{T}_h = \cup_{i=1}^{N} \mathcal{T}_h(\Omega_i)$, $\mathcal{E}_h(\Omega_i)$ be the set of all edges/faces of the triangulation $\mathcal{T}_h(\Omega_i)$ and $\mathcal{E}_h^0(\Omega_i)$ be the set of all interior edges/faces of the triangulation $\mathcal{T}_h(\Omega_i)$. Then, we define the global sets as $\mathcal{E}_h = \cup_{i=1}^{N} \mathcal{E}_h(\Omega_i)$, $\mathcal{E}_h^0 := \{F \in \mathcal{E}_h : F \cap \partial\Omega_i = \emptyset, \quad i = 1, \cdots N\}$ and $\mathcal{E}_{h,H} = \mathcal{E}_h^0 \cup \mathcal{E}_H$. Further $\boldsymbol{x}_i$, $i = 1, \ldots, N_v$, denote the nodes in the partition $\mathcal{T}_h$. Note that the scale $H_i$ is associated only with the subdomains $\Omega_i$. Similar construction is assumed in 3-D with $\Omega_i$ being polyhedra while the fine-grid elements are simplices or hexahedra.

Now we present HDG method for the model problem (4.1) on the fine-grid $\mathcal{T}_h$. In

order to apply HDG method, we first consider the equation (4.1) with homogeneous Dirichlet boundary condition in mixed form:

$$\alpha \boldsymbol{q} + \nabla u = 0 \qquad \text{in } \Omega, \tag{4.2a}$$

$$\nabla \cdot \boldsymbol{q} = f \qquad \text{in } \Omega \tag{4.2b}$$

$$u = 0 \qquad \text{on } \partial\Omega. \tag{4.2c}$$

Here $\alpha(x) = \kappa(x)^{-1}$ and further introduce the finite element spaces that are used in the HDG method:

$$\begin{aligned} W_h &:= \{w \in L^2(\Omega) : w|_T \in W(T),\, T \in \mathcal{T}_h\}, \\ \boldsymbol{V}_h &:= \{\boldsymbol{r} \in \boldsymbol{L}^2(\Omega) : \boldsymbol{r}|_T \in \boldsymbol{V}(T),\, T \in \mathcal{T}_h\}, \\ M_{h,H} &:= M_h^0 \oplus M_H, \end{aligned}$$

where the spaces $M_h^0, M_H$ are defined as

$$\begin{aligned} M_h^0 &:= \{\mu \in L^2(\mathcal{E}_h) : \mu|_{F_h} \in M_h(F_h), \quad F_h \in \mathcal{E}_h, \;\; \mu|_{\partial\Omega_i} = 0, i = 1 \cdots N\}, \\ M_H &:= \{\mu \in L^2(\mathcal{E}_H) : \mu|_{F_H} \in M(F_H), \quad F_H \in \mathcal{E}_H, \;\; \mu|_{\partial\Omega} = 0\}. \end{aligned}$$

Here for $T \in \mathcal{T}_h$ the spaces $W(T)$, $\boldsymbol{V}(T)$, and $M_h(F_h)$ are suitable finite element spaces (see, Figure 1). The focus in this chapter will be the choice of the space $M_H$.

The multiscale HDG method is: Find $(u_h, \boldsymbol{q}_h, \widehat{u}_{h,H}) \in W_h \times \boldsymbol{V}_h \times M_{h,H}$ such that

$$(\alpha \boldsymbol{q}_h\,,\,\boldsymbol{v})_{\mathcal{T}_h} - (u_h\,,\,\nabla\cdot\boldsymbol{v})_{\mathcal{T}_h} + \langle \widehat{u}_{h,H}\,,\,\boldsymbol{v}\cdot\boldsymbol{n}\rangle_{\partial\mathcal{T}_h} = 0, \tag{4.3a}$$

$$-(\boldsymbol{q}_h\,,\,\nabla w)_{\mathcal{T}_h} + \langle \widehat{\boldsymbol{q}}_{h,H}\cdot\boldsymbol{n}\,,\,w\rangle_{\partial\mathcal{T}_h} = (f\,,\,w)_{\mathcal{T}_h}, \tag{4.3b}$$

$$\langle \widehat{\boldsymbol{q}}_{h,H}\cdot\boldsymbol{n}\,,\,\mu\rangle_{\partial\mathcal{T}_h} = 0 \tag{4.3c}$$

$$\widehat{u}_{h,H} = 0 \quad \text{on} \quad \partial\Omega, \tag{4.3d}$$

for all $(w,\boldsymbol{v},\mu)\in W_h\times\boldsymbol{V}_h\times M_h$, with a numerical trace for the flux defined

$$\widehat{\boldsymbol{q}}_{h,H}\cdot\boldsymbol{n} = \boldsymbol{q}_h\cdot\boldsymbol{n} + \tau(u_h - \widehat{u}_{h,H}) \quad \text{on} \quad \partial\mathcal{T}_h, \tag{4.3e}$$

where $\tau$ is a non-negative stabilization parameter.

We recall $(\eta\,,\,\zeta)_{\mathcal{T}_h} = \sum_{T\in\mathcal{T}_h}(\eta,\zeta)_T$, and $\langle\eta\,,\,\zeta\rangle_{\partial\mathcal{T}_h} = \sum_{T\in\mathcal{T}_h}\langle\eta,\zeta\rangle_{\partial T}$. Consequently, $\langle\eta\,,\,\zeta\rangle_{\partial\mathcal{T}_H} := \sum_{i=1}^{N}\langle\eta,\zeta\rangle_{\partial\Omega_i}$. We remark that if there is only one coarse grid (i.e. $\Omega_i=\Omega$, $i=1$) then this is the standard HDG method [22].

Now we present some notation from Sobolev spaces and define specific norms used in error estimates. We first use the standard notations for Sobolev spaces and their norm on the domain $\Omega$, subdomains $\Omega_i\subset\Omega$ or their boundaries. For example, $\|\cdot\|_{s,D}, |\cdot|_{s,D}, \|\cdot\|_{s,\partial D}, |\cdot|_{s,\partial D}, s>0$, denote the Sobolev norms and semi-norm on a region $D$ and it boundary $\partial D$. For an integer $s$, the Sobolev spaces are Hilbert spaces and the norms are defined by the $L^2$-norms of their weak derivatives up to order $s$. For a non-integer $s$, the spaces are defined by interpolation [39]. For $s=0$ and $D=\Omega$ instead of $\|\cdot\|_{0,\Omega}$, we use $\|\cdot\|$. Moreover, we define the following norms:

$$\|\boldsymbol{q}\|_{\alpha}^2 := (\alpha\boldsymbol{q}\,,\,\boldsymbol{q})_{\mathcal{T}_h} \quad \text{and} \quad \|u\|_{\tau}^2 := \langle\tau u\,,\,u\rangle_{\partial\mathcal{T}_h}.$$

Further, we shall use various inequalities between norms and semi-norms related to embedding of Sobolev spaces. If $D \subset \Omega$ and $diam(D) = d$ then we have the following inequality :

$$\|v\|^2_{\partial D} \leq C(d\|\nabla v\|^2_D + d^{-1}\|v\|^2_D). \tag{4.4}$$

### *4.1.2 Upscale structure of GMsHDG methods*

The main feature of this method is that it could be implemented in such a way that we need to solve global system on the coarse mesh only. To do this, we split the third equation of (4.3c) into two equations by testing separately with $\mu \in M_h^0$ and $\mu \in M_H$ so that

$$\langle \widehat{\boldsymbol{q}}_{h,H} \cdot \boldsymbol{n}\,,\, \mu\rangle_{\partial\mathcal{T}_h} = 0 \quad \text{for all} \quad \mu \in M_h^0 \tag{4.5}$$

and

$$\langle \widehat{\boldsymbol{q}}_{h,H} \cdot \boldsymbol{n}\,,\, \mu\rangle_{\partial\mathcal{T}_H} = 0 \quad \text{for all} \quad \mu \in M_H. \tag{4.6}$$

Now because of the structure of the space $M_h^0$ we can implement the solution of equation (4.3) independently on each subdomain $\Omega_i$. Indeed, for a particular subdomain $\Omega_i$, let $\widehat{u}_{h,H} = \xi_H$, where $\xi_H \in M_H$. Then on $\Omega_i$, we can find the solution $(u_h, \widehat{\boldsymbol{q}}_h, \widehat{u}_{h,H})|_{\Omega_i}$ by restricting the equation (4.3) to $\Omega_i$:

$$\begin{aligned}
(\alpha\boldsymbol{q}_h\,,\, v)_{\mathcal{T}_h(\Omega_i)} - (u_h\,,\, \nabla\cdot v)_{\mathcal{T}_h(\Omega_i)} + \langle \widehat{u}_{h,H}\,,\, \boldsymbol{v}\cdot\boldsymbol{n}\rangle_{\partial\mathcal{T}_h(\Omega_i)} &= 0,\\
-(\boldsymbol{q}_h\,,\, \nabla w)_{\mathcal{T}_h(\Omega_i)} + \langle \widehat{\boldsymbol{q}}_{h,H}\cdot\boldsymbol{n}\,,\, w\rangle_{\partial\mathcal{T}_h(\Omega_i)} &= (f\,,\, w)_{\mathcal{T}_h(\Omega_i)},\\
\langle \widehat{\boldsymbol{q}}_{h,H}\cdot\boldsymbol{n}\,,\, \mu\rangle_{\partial\mathcal{T}_h(\Omega_i)} &= 0,\\
\widehat{u}_{h,H} &= \xi_H \quad \text{on} \quad \partial\Omega_i
\end{aligned}$$

for all $(w, \boldsymbol{r}, \mu) \in W_h \times \boldsymbol{V}_h \times M_h^0$.

Here, we have used the relation (4.3e) for the "numerical flux" $\widehat{\boldsymbol{q}}_{h,H}$. In fact,

the above system is the regular HDG methods defined on $\Omega_i$. From [22], we already know that under proper choice of the spaces $W(T)$, $\boldsymbol{V}(T)$, and $M(F_h)$ this problem is stable. Using superposition principle the solution of equation (4.3) can be further split into two parts, namely,

$$(\boldsymbol{q}_h, u_h, \widehat{u}_{h,H}) = (\boldsymbol{q}_h(f), u_h(f), \widehat{u}_{h,H}(f)) + (\boldsymbol{q}_h(\xi_H), u_h(\xi_H), \widehat{u}_{h,H}(\xi_H)), \tag{4.7}$$

where $(\boldsymbol{q}_h(f), u_h(f), \widehat{u}_{h,H}(f))$ satisfies

$$\begin{aligned}
(\alpha \boldsymbol{q}_h(f)\,,\, \boldsymbol{v})_{\mathcal{T}_h(\Omega_i)} - (u_h(f)\,,\, \nabla\cdot\boldsymbol{v})_{\mathcal{T}_h(\Omega_i)} + \langle \widehat{u}_{h,H}(f)\,,\, \boldsymbol{v}\cdot\boldsymbol{n}\rangle_{\partial\mathcal{T}_h(\Omega_i)} &= 0,\\
-(\boldsymbol{q}_h(f)\,,\, \nabla w)_{\mathcal{T}_h(\Omega_i)} + \langle \widehat{\boldsymbol{q}}_{h,H}(f)\cdot\boldsymbol{n}\,,\, w\rangle_{\partial\mathcal{T}_h(\Omega_i)} &= (f\,,\, w)_{\mathcal{T}_h(\Omega_i)},\\
\langle \widehat{\boldsymbol{q}}_{h,H}(f)\cdot\boldsymbol{n}\,,\, \mu\rangle_{\partial\mathcal{T}_h(\Omega_i)} &= 0,\\
\widehat{u}_{h,H}(f) &= 0 \quad \text{on} \quad \partial\Omega_i,
\end{aligned}$$

for all $(w, \boldsymbol{r}, \mu) \in W_h \times \boldsymbol{V}_h \times M_h^0$ and $(\boldsymbol{q}_h(\xi_H), u_h(\xi_H), \widehat{u}_{h,H}(\xi_H))$ satisfies

$$\begin{aligned}
(\alpha \boldsymbol{q}_h(\xi_H)\,,\, \boldsymbol{v})_{\mathcal{T}_h(\Omega_i)} - (u_h(\xi_H)\,,\, \nabla\cdot\boldsymbol{v})_{\mathcal{T}_h(\Omega_i)} + \langle \widehat{u}_{h,H}(\xi_H)\,,\, \boldsymbol{v}\cdot\boldsymbol{n}\rangle_{\partial\mathcal{T}_h(\Omega_i)} &= 0,\\
-(\boldsymbol{q}_h(\xi_H)\,,\, \nabla w)_{\mathcal{T}_h(\Omega_i)} + \langle \widehat{\boldsymbol{q}}_{h,H}(\xi_H)\cdot\boldsymbol{n}\,,\, w\rangle_{\partial\mathcal{T}_h(\Omega_i)} &= 0,\\
\langle \widehat{\boldsymbol{q}}_{h,H}(\xi_H)\cdot\boldsymbol{n}\,,\, \mu\rangle_{\partial\mathcal{T}_h(\Omega_i)} &= 0,\\
\widehat{u}_{h,H}(\xi_H) &= \xi_H \quad \text{on} \quad \partial\Omega_i,
\end{aligned}$$

for all $(w, \boldsymbol{r}, \mu) \in W_h \times \boldsymbol{V}_h \times M_h^0$.

Then the equation (4.6) reduces to finding $\xi_H \in M_H$ such that

$$a(\xi_H, \mu) = l(\mu) \quad \text{for all} \quad \mu \in M_H, \tag{4.8}$$

where the bilinear form $a(\xi_H, \mu) : M_H \times M_H \to \mathbb{R}$ and the linear form $l(\mu) : M_H \to \mathbb{R}$ are defined as

$$a(\xi_H, \mu) := \langle \widehat{\boldsymbol{q}}_{h,H}(\xi_H)\,,\, \mu \rangle_{\partial \mathcal{T}_H} \quad \text{and} \quad l(\mu) := -\langle \widehat{\boldsymbol{q}}_{h,H}(f)\,,\, \mu \rangle_{\partial \mathcal{T}_H}.$$

We note that the same procedure can be applied for the case of non-homogeneous boundary data $u = g$ on $\partial\Omega$ as well.

### 4.2 General framework for constructing the multiscale space $M_H$

To motivate the need for multiscale spaces for $M_H$, we first present numerical examples using polynomial functions for $M_H$. In Figure 8, the high-contrast coefficient $\kappa(x)$, fine-scale solution, and multiscale solution with polynomial $M_H$ space are shown. In Figure 8a, the black region indicates the coefficient $\kappa(x) = \eta$ and the white region the coefficient $\kappa(x) = 1$. The error between the fine-scale solution and the multiscale solution with polynomial space $M_H$ is 37.4%. This representative example shows a need to go beyond piece-wise polynomial functions for $M_H$. In particular, when using spectral basis introduced in next sections, one can reduce the error below 5%. Next, we will discuss the construction of new multiscale spaces.

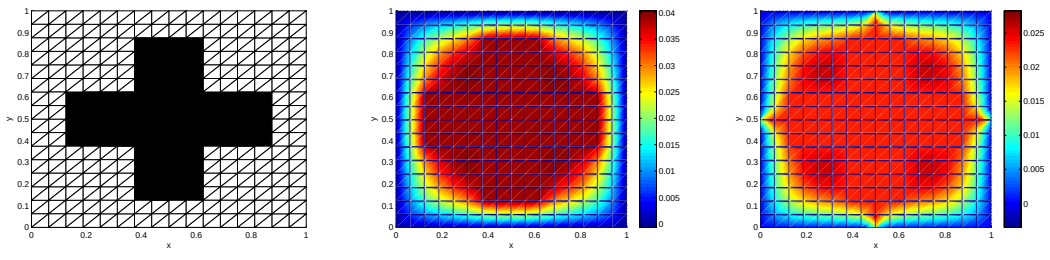

(a) Coefficient (b) Fine-scale solution (c) Coarse-scale solution

Figure 8: Numerical results for mutiscale HDG framework with $M_H(F) = \mathcal{P}_2(F)$, $h = 1/32, H = 1/2$, and $\eta = 10^4$.

Although the multiscale space $M_H$ lives only on the coarse skeleton $\mathcal{E}_H$, it needs to involve some information of the permeability field within coarse blocks. A reasonable approach is to construct a number of snapshots using local solutions defined on a subdomain around a face $F$ (or set of faces) and then take the traces of those functions on $\mathcal{E}_H$ to form the space $M_H$. This will resemble traces of the global solution and avoid a high-dimensional representation of the traces. In what follows, we present a general strategy of the construction of $M_H$:

**Step 1: Partition of skeleton.** First, we decompose the skeleton $\mathcal{E}_H$ by defining a covering $\mathcal{E}_H = \cup\mathcal{E}_i$, where the summation is over all partitions $\mathcal{E}_i$. Here each $\mathcal{E}_i$ can be a single coarse edge or a union of several coarse edges. We allow overlaps between $\mathcal{E}_i, \mathcal{E}_j$, for some $i$ and $j$, $\mathcal{E}_i \bigcap \mathcal{E}_j \neq 0$. For each $\mathcal{E}_i$, we associate a support domain $\omega_i$ such that $\mathcal{E}_i \subset \overline{\omega}_i$. For instance, if $\mathcal{E}_i$ is a single coarse face then $\omega_i$ can be any one of the neighboring coarse blocks sharing this face or the union of the neighboring blocks that share the face.

**Step 2: Local snapshot spaces $V^{\mathbf{snap}}(\omega_i)$.** For each $\omega_i$, we introduce the local snapshots $\{\phi_j\}_{j=1}^{N_i}$ that are defined on $\overline{\omega}_i$ and take

$$V^{\text{snap}}(\omega_i) = \text{span}\{\phi_j\}_{j=1}^{N_i}. \tag{4.9}$$

The snapshots can be given explicitly or computed via solutions of local boundary value or local spectral problems in $\omega_i$. The snapshots can represent the fine-scale features of the solution and thus the choice of the snapshot space seriously impacts the dimension of the local spectral problems.

Now, we present two cases for computing the snapshot space. These cases will be used in later sections.

The simplest choice would be a snapshot space $V^{\text{snap}}(\omega_i)$ that consists of all

fine-grid basis functions defined on $\omega_i$. Such choice substantially reduces the computational cost associated with calculating the snapshot vectors.

A second approach is based on local solutions of the problem. Let $\{\boldsymbol{x}_l\}_{l=1}^{N_i}$ be the set of all fine nodes on $\partial\omega_i$. For each $\omega_i$ we define the function $\phi_l$ as the finite element solution of the following local problem (in a discrete setting):

$$\nabla \cdot (\kappa \nabla \phi_l) = 0 \quad \text{in} \quad \omega_i, \quad \phi_l = \delta_l \quad \text{on} \quad \partial\omega_i. \tag{4.10}$$

Here $\delta_l$ is a continuous piecewise linear function defined on $\partial\omega_i$ such that $\delta_l(x) = 1$ on $\boldsymbol{x}_l$ and vanishes on all other nodes.

**Step 3: Form the multiscale space** $M_H$. For each $\omega_i$, we perform a spectral decomposition of $V^{\text{snap}}(\omega_i)$ via some generalized eigenvalue problem

$$\boldsymbol{A}\psi = \lambda \boldsymbol{M}\psi. \tag{4.11}$$

Choices of the (stiffness) matrix $\boldsymbol{A}$ and the (mass) matrix $\boldsymbol{M}$ will be discussed in the following section. If the snapshot space consists of all fine-grid basis functions in $\omega_i$, the eigenvalue problem (4.11) reduces to solving the spectral problem with local stiffness and mass matrices defined on $\omega_i$. We order the eigenvalues as $0 \leq \lambda_{i,1} \leq \lambda_{i,2} \leq \cdots \leq \lambda_{i,N_i}$ and select the first $L_i$ eigenfunctions $\psi_{i,1}, \ldots, \psi_{i,L_i}$ to form a smaller subspace $V^{\text{off}}(\omega_i)$:

$$V^{\text{off}}(\omega_i) = \text{span}\{\psi_{i,j}\}_{j=1}^{L_i}.$$

For each $\omega_i$, we form the local multiscale space $M_H(F)$ by taking the traces of the

functions in $V^{\text{off}}$ on each $F$ and form the set of trace of $\psi_{i,j}$ on the face $F$:

$$\bigcup_{F\in\mathcal{E}_i}\{\psi_{i,j}|_F : \qquad \psi_{i,j}\in V^{\text{off}}(\omega_i),\quad j=1,\ldots,L_i\}.$$

Note that, in general, these functions will not be linearly independent so we need to perform a *Proper Orthogonal Decomposition* (POD) in order to eliminate the linearly dependent modes (e.g., [40]) or to select most important modes in order to further reduce the dimension to $L_F$. In this way, we produce the space $M_H(F)$. Finally, the multiscale space $M_H$ is defined as:

$$M_H := \bigcup_{F\in\mathcal{E}_H} M_H(F).$$

**Remark 4.2.1.** *Notice that in general $M_H$ is nonconforming in the sense that the functions in $M_H$ will have discontinuities on the coarse grid nodes. If it is desired to have a conforming space, in* **Step 1***, we need to ensure that $\{\omega_i\}_{i=1}^N$ is a covering of the domain $\Omega$. Let $\{\chi_i\}_{i=1}^N$ be a set of partition of unity functions associated with the covering $\{\omega_i\}_{i=1}^N$. In* **Step 3***, we modify the definition of $V^{off}$ by multiplying the space with the partition of unity function $\chi_i$ (so the functions are globally continuous and hence $M_H$ is conforming) to get*

$$V^{off}(\omega_i) = span\{\chi_i\psi_{i,j}\}_{j=1}^{L_i}. \tag{4.12}$$

## 4.3 Examples of the multiscale space $M_H$

In this section, we present several examples of the construction of the multiscale space $M_H$. The Multiscale Spaces I (see Section 4.3.1.1 and 4.3.1.2) will use the traces of the multiscale function constructed locally on each coarse block, where

these multiscale functions are a low dimensional representation of the solution in each $\Omega_i$ and thus they provide a low dimensional trace space $M_H$. Furthermore, we remove linearly dependent components.

For the Multiscale space II, defined in Sections 4.3.2.1 and 4.3.2.2, we employ local spectral problem defined on coarse neighborhood that strictly contain the face $F$. Compared to the multiscale space I, this approach uses oversampling technique in computing $M_H$. The space proposed in Section 4.3.2.2 uses a partition of unity and provides a conforming $M_H$.

As the last example, the Multiscale space III will be constructed locally by choosing coarse block in Section 4.3.3. In the Spece I, we select two coarse blocks sharing common face $F$ to generated $M_H(F)$, but in this space, we choose only one coarse block for a face $F$. Thus, it provides the lowest dimensional multiscale space $M_H$.

### *4.3.1 Non-oversampling examples*

Based on the general framework for constructing $M_H$ space, we will generate two non-oversampling spaces which are defined on each coarse block $\Omega_i$. There are two main differences: snapshot space and eigenvalue problem. For generating local snapshot space, in the multiscale space I-a (see Section 4.3.1.1), we use all fine grid functions, but in the space I-b, we use local solutions of some problems as functions of a snapshot space. For the local eigenvalue problem of the first space, we employ the mass matrix defined on a coarse block which is one of the examples used in SIPDG case. On the other hand, we use the mass matrix defined on the coarse face $F$ in the second spectral problem which contains weighted parameter $1/H$.

#### *4.3.1.1 Mutiscale space I-a*

For this choice, $\mathcal{E}_i$ refers to the boundary of a coarse-grid element $\Omega_i$ and $\omega_i = \Omega_i$ (see Figure 7). The snapshot space consists of all fine-grid functions in $\Omega_i$.

We generate $V^{\text{off}}(\omega_i)$ by solving a local spectral problem described below. Let $X_h(\Omega_i)$ be the conforming finite element space of continuous piece-wise linear functions in $\mathcal{T}_h(\Omega_i)$. For any given subdomain $\Omega_i$, we find $\lambda$ and $\psi \in X_h(\Omega_i)$ such that

$$\int_{\Omega_i} \kappa(x)\nabla\psi\nabla z dx = \lambda \int_{\Omega_i} \widetilde{\kappa}(x)\psi z dx \quad \text{for all} \quad z \in X_h(\Omega_i). \tag{4.13}$$

$\widetilde{\kappa}$ is a properly selected weight. For a scalar permeability, we select $\widetilde{\kappa} = \kappa$. For tensor permeability, for the choice of $\widetilde{\kappa}$, we refer to [32].

We order the eigenvalues so that $0 = \lambda_{i,1} \leq \lambda_{i,2} \leq \cdots \leq \lambda_{i,N_i}$, where $N_i$ is the number of vertices of $\mathcal{T}_h(\Omega_i)$. Then $V^{\text{off}}(\Omega_i)$ is the space spanned by the eigenfunctions $\psi_{i,l}$, $l = 1, \cdots, L_i$ corresponding to the first $L_i$ eigenvalues.

As we see from (4.1.1), the space $M_H$ is defined edge-wise (face-wise). Therefore, for a face $F \in \mathcal{E}_H$ common for the coarse blocks $\Omega_i$ and $\Omega_j$ we collect all traces of the constructed above eigenfunctions, namely

$$F \in \mathcal{E}_H(\Omega_i) \cap \mathcal{E}_H(\Omega_j): \quad \psi_{i,l}|_F, \quad l = 1, \cdots, L_i, \quad \psi_{j,l}|_F, \quad l = 1, \cdots, L_j. \tag{4.14}$$

The selected traces are in general linearly dependent, so we need to eliminate the linearly dependent ones. We use POD method and select the first $L_F$ linearly independent functions denoted by $\psi_{j,F},\ j = 1, \ldots, L_F$.

Thus, for any $F \in \mathcal{E}_H$, we define

$$M_H^{I_a}(F) := \text{span}\{\psi_{j,F}, \quad 0 \leq j \leq L_F\}, \quad \text{and} \quad M_H^{I_a} := \bigcup_{F \in \mathcal{E}_H} M_H^{I_a}(F). \tag{4.15}$$

#### *4.3.1.2 Mutiscale space I-b*

The definition of $\omega_i$ and $\mathcal{E}_i$ are the same as in the case of the Multiscale Space I-a. Let $m_{\mathcal{E}_i}$ be the number of nodal basis function corresponding to the fine-grid nodes on $\mathcal{E}_i$. Then the snapshot space is defined by the finite element approximations (we keep the same notation for discrete solution as the continuous solution in (4.10)) $\phi_l$, $l = 1, ..., m_{\mathcal{E}_i}$ of the problem (4.10) on $X_h(\omega_i)$:

$$V^{\text{snap}}(\Omega_i) = \text{span}\{\phi_l, 1 \leq l \leq m_{\mathcal{E}_i}\}. \tag{4.16}$$

For the local spectral problem, we use the matrices

$$A_i^{\text{snap}} = \left[\int_{\Omega_i} \kappa \nabla \phi_l \nabla \phi_{l'} dx\right]_{l,l'=1,}^{m_{\mathcal{E}_i}}, \quad M_i^{\text{snap}} = \left[\frac{1}{H}\int_{\mathcal{E}_i} \kappa \phi_l \phi_{l'} ds\right]_{l,l'=1}^{m_{\mathcal{E}_i}}.$$

Using these matrices, we solve the following algebraic eigenvalue problem:

$$A_i^{\text{snap}} \mathbf{\Sigma}_i = \Lambda_i M_i^{\text{snap}} \mathbf{\Sigma}_i, \tag{4.17}$$

where $\Lambda_i$ is the diagonal matrix with the eigenvalues on the diagonal, $\mathbf{\Sigma}_i$ is a square matrix with columns that are the corresponding eigenvectors. We define the functions along the edge $F \in \mathcal{E}_i$

$$\psi_{j,F} = \psi_{j,\mathcal{E}_i}|_F,$$

where $\psi_{j,\mathcal{E}_i}$ is the linear combination of snapshot vectors with the coefficients being the coordinates of the $j$th eigenvector.

Further, if $F$ is a common face of $\Omega_i$ and $\Omega_j$, we need to apply to POD procedure in order to eliminate linearly dependent functions. After POD process, we get $L_F$

functions $\psi_{1,F}, \cdots, \psi_{L_F,F}$. Then for $F \in \mathcal{E}_H$

$$M_H^{I_b}(F) = \text{span}\{\psi_{j,F} : 0 \leq j \leq L_F\} \quad \text{and} \quad M_H^{I_b} := \bigcup_{F \in \mathcal{E}_H} M_H^{I_b}(F). \tag{4.18}$$

### *4.3.2 Oversampling examples*

In these examples, we apply oversampling techniques. In the first approach, we construct the space based on each coarse face by considering two coarse blocks sharing common face $F$ as a coarse neighborhood. Otherwise, in the Space II-b, we consider four coarse blocks as a coarse neighborhood because the space based on coarse nodes. Also, we apply a partition of unity in order to generate a conforming multiscale space $M_H$.

#### *4.3.2.1 Mutiscale space II-a*

We define $\mathcal{E}_i$ as a single coarse face and $\omega_i$ as the union of two coarse elements, $\Omega_1$ and $\Omega_2$, that share this face $\mathcal{E}_i$, see Figure 9. The snapshot space will consist of all fine-grid functions and thus the local spectral problem is solved directly on a fine grid (locally). In this case, we solve an eigenvalue problem in a coarse neighborhood $\omega_i$.

Let $X_h(\omega_i)$ be the conforming finite element space of continuous piece-wise linear functions in $\mathcal{T}_h(\omega_i)$. For any given coarse neighborhood $\omega_i$ and the common face $\mathcal{E}_i$, we find $\lambda$ and $\psi \in X_h(\omega_i)$ such that

$$\int_{\omega_i} \kappa(x) \nabla\psi \nabla z dx = \frac{\lambda}{H} \int_{\mathcal{E}_i} \overline{\kappa} \psi z ds, \qquad \forall z \in X_h(\omega_i), \tag{4.19}$$

with $\overline{\kappa} = 2\kappa_1\kappa_2/(\kappa_1 + \kappa_2)$ and $\kappa_1 = \kappa|_{\Omega_1}$ and $\kappa_2 = \kappa|_{\Omega_2}$.

We order the eigenvalues so that $0 \leq \lambda_{i,1} \leq \lambda_{i,2} \leq \cdots \leq \lambda_{i,N_i}$, where $N_i$ is

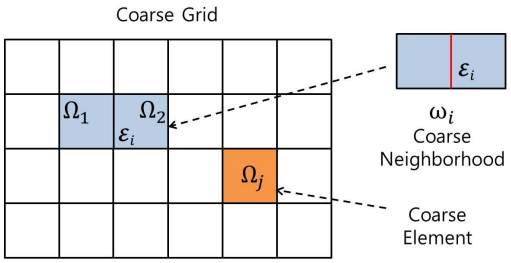


Figure 9: Illustration of a coarse neighborhood and coarse element. Space II-a.

the number of vertices of $\mathcal{T}_h(\omega_i)$ and denote the corresponding eigenfunctions by $\psi_{i,1}, \psi_{i,2}, \ldots, \psi_{i,N_i}$, which form the space $V^{\text{off}}(\omega_i)$.

Since the space $M_H$ is defined face-wise, we take the traces of the constructed above eigenfunctions, denoted by $\psi_{l,F}$, $l = 1, \cdots, N_i$, where $F$ is the common coarse face of $\omega_i$. These functions may be linearly dependent, so we choose only linearly independent functions that correspond to the smallest $L_F$ eigenvalues. Then, for $F \in \mathcal{E}_H$

$$M_H^{II_a}(F) := \text{span}\{\psi_{j,F}, \quad 1 \leq j \leq L_F\} \quad \text{so that} \quad M_H^{II_a} := \bigcup_{F \in \mathcal{E}_H} M_H^{II_a}(F). \tag{4.20}$$

#### *4.3.2.2 Mutiscale space II-b*

For each node $\boldsymbol{x}_i$, we define $\mathcal{E}_i$ as the union of all coarse faces (edges) that share the node $\boldsymbol{x}_i$. Similarly, $\omega_i$ is the union of coarse elements that share a common node $\boldsymbol{x}_i$ (see Figure 10, where the coarse grid elements that form $\omega_i$ are $\Omega_1, \ldots, \Omega_4$).

We choose for the snapshot space the set of all fine-grid functions. Then the local spectral problem (4.11) is a finite element approximation of the following homoge-

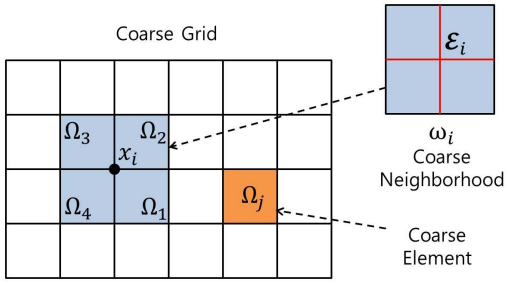


Figure 10: Illustration of a coarse neighborhood and coarse element. Space II-b.

neous Neumann eigenvalue problem: find $\psi^{\text{aux}} \in X_h(\omega_i)$ such that

$$\begin{aligned} \int_{\omega_i} \kappa(x)\nabla\psi^{\text{aux}}\nabla z dx = \lambda \int_{\omega_i} \tilde{\kappa}\psi^{\text{aux}} z dx, \quad \text{for all} \quad \in X_h(\omega_i) \\ \text{with} \quad \tilde{\kappa} := \kappa \sum_{l=1}^{N_v} |\nabla\chi_l|^2, \end{aligned} \tag{4.21}$$

where $\chi_l$ form partition of unity, e.g., piece-wise bilinear functions (see [37]).

Then, we order the eigenvalues as $0 = \lambda_{i,1} \leq \lambda_{i,2} \leq \cdots$ and choose the $L_i$ eigenfunctions $\psi^{\text{aux}}_{i,1}, \ldots, \psi^{\text{aux}}_{i,L_i}$, associated to the smallest eigenvalues and form basis $\psi_{i,j} = \chi_i \psi^{\text{aux}}_{i,j}$. Due to the properties of $\chi_i$, $\psi_{i,j} \in H^1_0(\Omega)$. Thus, we form $V^{\text{off}}(\omega_i) = \text{span}\{\psi_{i,j}\}_{j=1}^{L_i}$.

Finally, we define

$$M_H^{II_b}(F) = \bigcup_{F\in\mathcal{E}_i} V^{\text{off}}(\omega_i)|_F \quad \text{and} \quad M_H^{II_b} := \bigcup_{F\in\mathcal{E}_H} M_H^{II_b}(F),$$

where $V^{\text{off}}(\omega_i)|_F$ denotes the traces on $F$ of the functions in $V^{\text{off}}(\omega_i)$.

### *4.3.3 Chessboard example*

One of benefits for the multiscale space I is a low dimensional space, but for every coarse face, we get two basis functions from two coarse blocks shared coarse face. These basis functions may contain linearly dependent ones and thus we need to apply POD or to choose only linearly independent one. For the multiscale space II, we take oversampling techniques, so dimension of the spaces is high. In order to overcome this issue, we select only one coarse block for a coarse face, use a low dimensional snapshot space, and solve the local spectral problem on a choosing coarse block. Comparing with first two approaches, the local problem will be on the smallest domain and there is no overlap for all coarse faces.

To construct the space, we need to define a set $\mathcal{T}_C$ which satisfies the following properties:

- for any two different subdomain (coarse element) $\Omega_1, \Omega_2 \in \mathcal{T}_C$, they are either disjointed or only sharing one vertex.
- $\mathcal{E}_H \subset \bigcup_{\Omega_i \in \mathcal{T}_C} \partial\Omega_i$.

The example of such kind of subset is that if we use uniform coarse square triangulation, we call $\Omega_{ij}$ be the square located at $i-th$ row and $j-th$ column. Then a choice of $\mathcal{T}_C$ can be

$$\mathcal{T}_C := \{\Omega_{ij} \mid i+j \text{ is even}\}.$$

This is like we select all blue/white blocks of a chessboard. (See Figure 11). We consider the set of blue blocks as $\mathcal{T}_C$.

We define $\omega_i$ as a element of $\mathcal{T}_C$ and $\mathcal{E}_i$ as the boundary of a coarse-grid element $\omega_i$. The snapshot space and the local spectral problem is defined by the same with the definition (4.16) and the problem (4.17) of Section 4.3.1.2. In this example, we

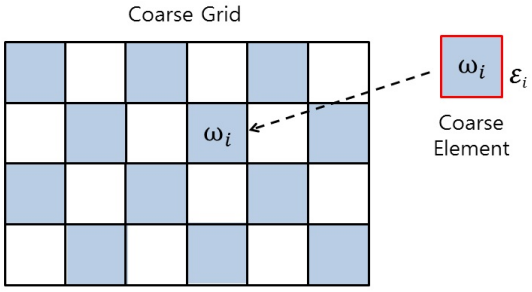


Figure 11: Illustration of a coarse element and the set $\mathcal{T}_C$.

do not need POD procedure in order to remove linear dependent one because we choose only one element $\Omega_i \in \mathcal{T}_C$ for any face $F$.

After solving the local spectral problem, we sort the eigenvalues in an ascending order as $0 = \lambda_1 \leq \lambda_2 \leq \cdots$ and the corresponding eigenvectors are $\{\psi_i\}_{i=1}^n$. Next we select first $L_F$ eigenvectors as the important modes to generate the local multiscale space on the coarse edges $F \subset \partial\omega_i$, namely, it can be written as:

$$M_H^{III}(F) := \text{span}\{\psi_{j,F}, \quad 1 \leq j \leq L_F\} \quad \text{so that} \quad M_H^{III} := \bigcup_{F \in \mathcal{E}_H} M_H^{III}(F). \tag{4.22}$$

Notice here, if we apply the integration by parts on the eigenvalue problem, it is equivalent as

$$\int_{\partial K} \kappa \frac{\partial \psi_i}{\partial \boldsymbol{n}} v ds = \frac{\lambda_i}{H} \int_{\partial K} \psi_i v ds.$$

This means that for these eigenfunctions, we have

$$P_{snap}(\kappa \frac{\partial \psi_i}{\partial \boldsymbol{n}}) = \frac{\lambda_i}{H} \psi_i. \tag{4.23}$$

Here $P_{snap}$ is the $L^2-$projection onto $V^{\text{snap}}(\Omega_i)|_F$, for all $F \in \partial\Omega_i$. We point out that this property is crucial for the analysis of the method.

## 4.4 Numerical experiments

In this section, we discuss the results obtained on a number of representative numerical tests. We compute the coarse-grid solution and study the error with respect to the reference solution (or the fine-grid solution of (4.3)). We note that the solution of (4.3) depends on both fine-scale and coarse-scale parameters, $h$ and $H$. We report the errors of the obtained solution compared with a reference solution when we add more spectral basis functions. We study the error behavior when we add more coarse basis functions for fixed values of $h$ and $H$.

We consider the domain $\Omega = (0,1)^2$ and divide $\Omega$ into $N = M \times M$ square coarse blocks, $\{\Omega_i\}_{i=1}^N$, which are unions of fine elements. In this case $H = 1/M$ is the coarse mesh parameter. Inside each subdomain $\Omega_i$, we generate a structured triangulation with $m$ subintervals in each coordinate direction (and thus $h = 1/(Mm)$ is the fine mesh parameter). We consider the solution of Equation (4.3) with $f = 1$ and the stabilization parameter $\tau = 1$ on each edge (coarse and fine edge). We test our methods on two different distributions of the coefficient $\kappa(x)$ shown in Figure 12. $\kappa(x) = 1$ are for the points in the white background and $\kappa(x) = \eta$ are for the points in the black regions. Topology 1 represents the permeability of a media with highly permeable inclusions and relatively short isolated channels (not interconnected). Topology 2 has one global channel. In our numerical experiments, we consider $\eta$ to be $10^4$.

We consider the following finite element spaces which satisfy the assumptions of Subsection 4.5 in order to apply the mutiscale HDG method. $W_h$ and $\boldsymbol{V}_h$ consist of piece-wise linear, discontinuous functions on $\mathcal{T}_h$, $M_h$ of piece-wise linear, discontinuous functions in $\mathcal{E}_h$, and $M_H$ is the mutiscale finite element space, which has been constructed in the previous section. The error of $\boldsymbol{q}$ is measured in the weighted

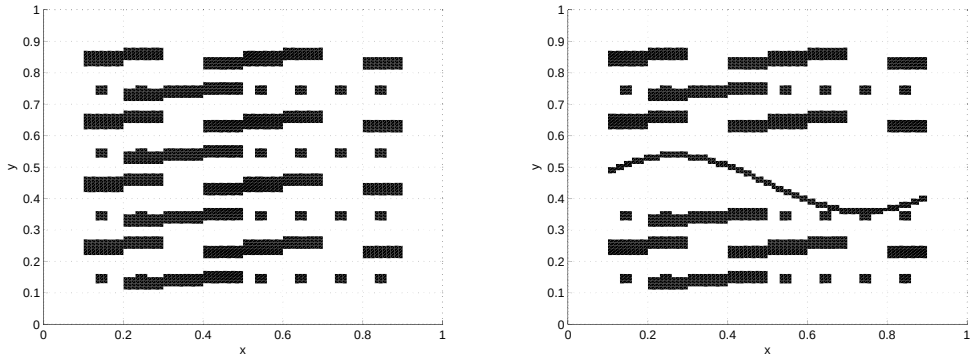

(a) Topology 1 (b) Topology 2

Figure 12: Topology of heterogeneous coefficient $\kappa$.

$L^2$-norm:

$$\|\boldsymbol{q}\|^2_{\alpha,L^2(\Omega)} := \sum_{i=1}^{N} \int_{\Omega_i} \alpha |\boldsymbol{q}|^2 dx.$$

We report the relative $L^2$-error for the pressure $\|u_h^* - u_H\|_{L^2(\Omega)}$ and the relative weighted $L^2$-error for the velocity $\|\boldsymbol{q}_h^* - \boldsymbol{q}_H\|_{\alpha,L^2(\Omega)}$. Here $(u_h^*, \boldsymbol{q}_h^*)$ is a fine-grid solution and the coarse-grid solution $(u_H, \boldsymbol{q}_H)$ is one of the solution: (I) $(u_H^I, \boldsymbol{q}_H^I)$ obtained using the space $I$ introduced in the Subsection 4.3.1.1 and 4.3.1.2, (II) $(u_H^{II}, \boldsymbol{q}_H^{II})$ obtained using the space $II$ introduced in Subsection 4.3.2.1 and 4.3.2.2 or (III) $(u_H^{III}, \boldsymbol{q}_H^{III})$ obtained using the space $III$ introduced in Subsection 4.3.3.

### *4.4.1 Numerical results for non-oversampling examples*

In this subsection, we present the numerical experiments for the spaces introduced in Subsection 4.3.1.1 and 4.3.1.2.

In these numerical experiments, we add multiscale basis functions and study the error decay as the coarse space dimension increases. The coefficient $\kappa(x)$ is shown on Figure12. The results for the errors are presented in Table 7 and 8 for $h = 1/100$ and $H = 1/10$. We report the dimension of the coarse spaces (denoted by "Dim.").

Table 7: Numerical results for Multiscale Space I-a (Subsection 4.3.1.1) applied to permeability field of Topology 1 with increasing dimension of the coarse space, $h = 1/100, H = 1/10, \eta = 10^4$. "Dim." stands for the dimension of the coarse space.

| Dim. | $\|u_h^* - u_H\|_{L^2(\Omega)}$ | $\|\boldsymbol{q}_h^* - \boldsymbol{q}_H\|_{\alpha,L^2(\Omega)}$ |
|---|---|---|
| 180 | 0.6412 | 0.8028 |
| 469 | 0.1208 | 0.3547 |
| 682 | 0.0362 | 0.2181 |
| 888 | 0.0204 | 0.1659 |

Table 8: Numerical results for Multiscale Space I-b (Subsection 4.3.1.1) applied to permeability field of Topology 1 with increasing dimension of the coarse space, $h = 1/100, H = 1/10, \eta = 10^4$. "Dim." stands for the dimension of the coarse space.

| Dim. | $\|u_h^* - u_H\|_{L^2(\Omega)}$ | $\|\boldsymbol{q}_h^* - \boldsymbol{q}_H\|_{\alpha,L^2(\Omega)}$ |
|---|---|---|
| 180 | 0.6412 | 0.8028 |
| 514 | 0.0393 | 0.2321 |
| 738 | 0.0312 | 0.1395 |
| 848 | 0.0266 | 0.1247 |

The results show reduction of the error compared to the reference fine-grid solution computed on a fine grid with mesh-size $h = 1/100$ and dimension (of fine-scale system) $60,000$. We observe a reasonable error decay when adding more coarse basis functions. In particular, for $H = 1/10$, we only have the dimensions of coarse spaces 682 and 738 to get the solution error 3.6% and 3.1% for the MS Space I-a and I-b, respectively. From this table we observe that the MS Space I-b performs slightly better compared to the MS Space I-a.

Next, we consider a permeability field for Topology 2 (see Figure 12) with the contrast $\eta = 10^4$. For this permeability field, a long channel in the middle of the domain is added to introduce a long-range effect in the solution. The numerical results are presented in Figure 13 and 14 where the pressure and velocity errors are depicted. We note that the error behavior of these methods is similar to the previous

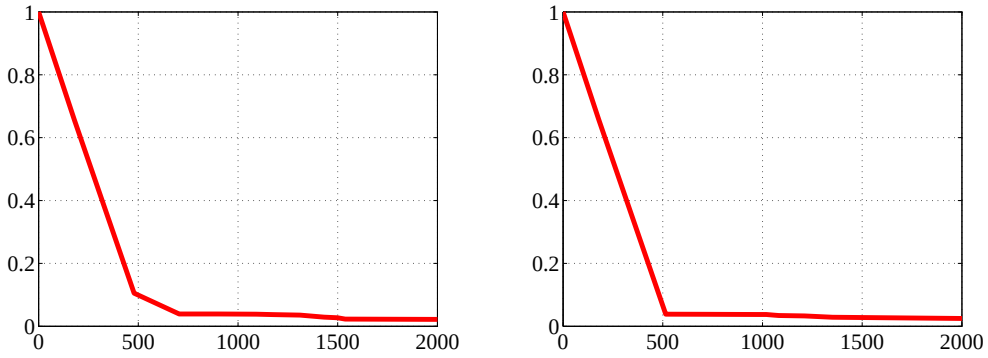


(a) MS space I-a (b) MS space I-b

Figure 13: Numerical results for MS Spaces I applied to permeability field of Topology 2 with $h = 1/100, H = 1/10$, $\eta = 10^4$ and increasing dimension of the coarse space. "Dim." stands for the dimension of the coarse space. The graphs show the relative error $\|u_h^* - u_H\|_{L^2(\Omega)}$ vs. the dimension of the coarse space.

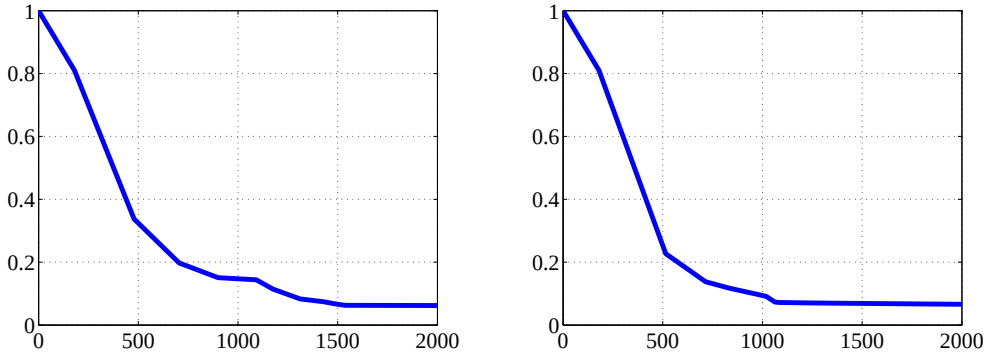


(a) MS space I-a (b) MS space I-b

Figure 14: Numerical results for MS Spaces I applied to permeability field of Topology 2 with $h = 1/100, H = 1/10$, $\eta = 10^4$ and increasing dimension of the coarse space. "Dim." stands for the dimension of the coarse space. The graphs show the relative error $\|\boldsymbol{q}_h^* - \boldsymbol{q}_H\|_{\alpha,L^2(\Omega)}$ vs. the dimension of the coarse space.

case (namely, Topology 1) with slightly smaller errors.

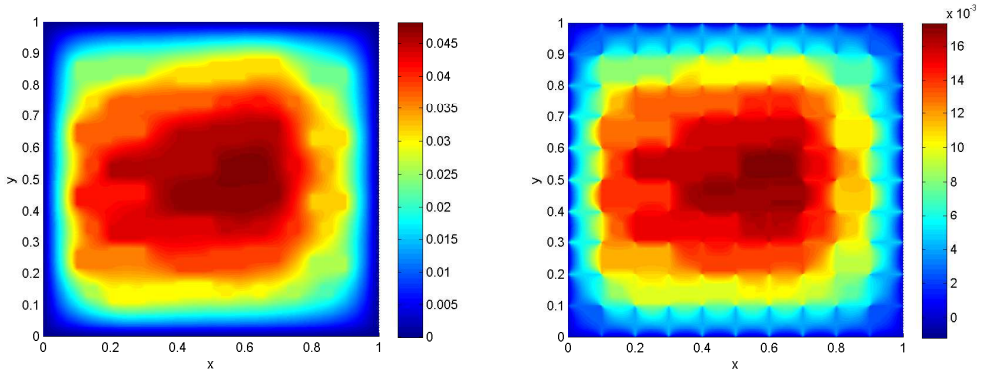

(a) Fine-scale solution (b) Multiscale solution with Dim.= 180

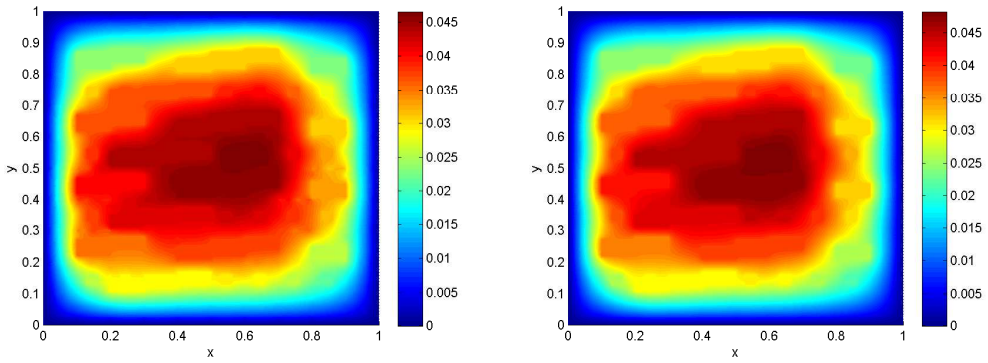

(c) Multiscale solution with Dim.= 720 (d) Multiscale solution with Dim.= 1800

Figure 15: Comparison of the Multiscale solutions for MS Space II-a with the reference (fine-scale) solution.

### *4.4.2 Numerical results for oversampling examples*

Next, we consider the spaces introduced in Section 4.3.2.1 and Section 4.3.2.2. We note that these spaces use an oversampling technique by solving local problems around faces and the numerical results corresponding to the MS Spaces II are better compared to MS Spaces I.

Figure 15 illustrates the effect of increasing the dimension of the coarse space in the MS Space II-a. We show the fine-scale solution and coarse-scale solutions computed with three different coarse space dimensions in Figure 15. We repeat the

Table 9: Numerical results for Multiscale Space II-a (Subsection 4.3.2.1) applied to permeability field of Topology 1 with increasing dimension of the coarse space, $h = 1/100, H = 1/10, \eta = 10^4$. "Dim." stands for the dimension of the coarse space.

| Dim. | $\|u_h^* - u_H\|_{L^2(\Omega)}$ | $\|\boldsymbol{q}_h^* - \boldsymbol{q}_H\|_{\alpha,L^2(\Omega)}$ |
|---|---|---|
| 180 | 0.6412 | 0.8028 |
| 360 | 0.0561 | 0.2843 |
| 540 | 0.0274 | 0.2306 |
| 720 | 0.0251 | 0.1627 |

Table 10: Numerical results for Multiscale Space II-b (Subsection 4.3.2.2) applied to permeability field of Topology 1 with increasing dimension of the coarse space, $h = 1/100, H = 1/10, \eta = 10^4$. "Dim." stands for the dimension of the coarse space.

| Dim. | $\|u_h^* - u_H\|_{L^2(\Omega)}$ | $\|\boldsymbol{q}_h^* - \boldsymbol{q}_H\|_{\alpha,L^2(\Omega)}$ |
|---|---|---|
| 360 | 0.1078 | 0.3290 |
| 720 | 0.0384 | 0.0922 |
| 1080 | 0.0381 | 0.0629 |

detailed numerical study described in Section 4.4.1. The results for the computation of errors with the MS Space II-a and II-b are presented in Table 9 and 10 for $h = 1/100$ and $H = 1/10$, respectively. When we use the coarse space with the dimension of 720, we observe that the solution errors for the MS Space II-a and II-b are 2.5% and 3.8% and the velocity errors are 16.3% and 9.2%, respectively. Here, the dimension of the fine-grid system is $60,000$.

The numerical results for Topology 2 are presented in Figure 16 and 17 where solution and velocity errors for these spaces are depicted. We note that the convergence behavior of these methods is similar to the previous permeability case with the errors that are slightly smaller.

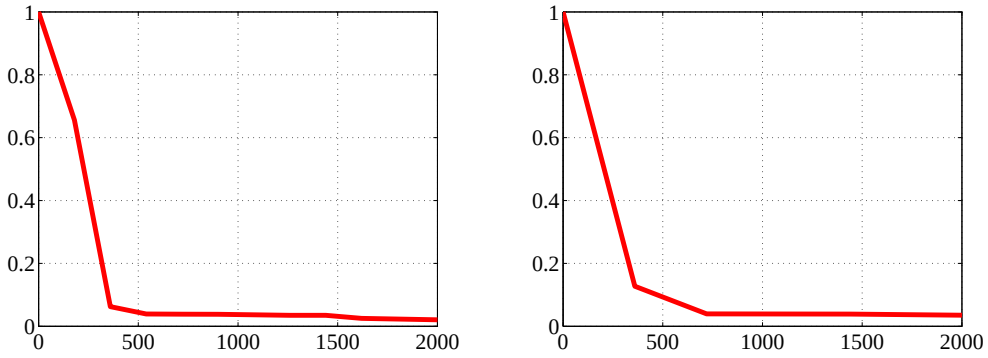


(a) MS space II-a (b) MS space II-b

Figure 16: Numerical results for MS Spaces II applied to permeability field of Topology 2 with $h = 1/100, H = 1/10$, $\eta = 10^4$ and increasing dimension of the coarse space. "Dim." stands for the dimension of the coarse space. The graphs show the relative error $\|u_h^* - u_H\|_{L^2(\Omega)}$ vs. the dimension of the coarse space.

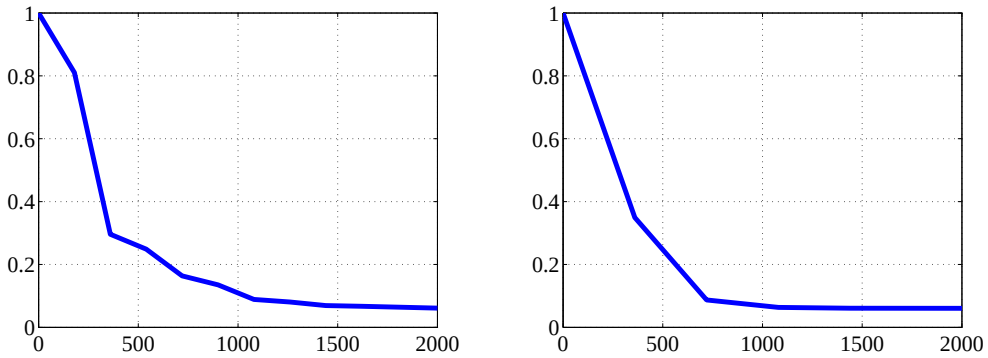


(a) MS space II-a (b) MS space II-b

Figure 17: Numerical results for MS Spaces II applied to permeability field of Topology 2 with $h = 1/100, H = 1/10$, $\eta = 10^4$ and increasing dimension of the coarse space. "Dim." stands for the dimension of the coarse space. The graphs show the relative error $\|\boldsymbol{q}_h^* - \boldsymbol{q}_H\|_{\alpha,L^2(\Omega)}$ vs. the dimension of the coarse space.

### *4.4.3 Numerical results for chessboard example*

In this subsection, we present the numerical experiments for the method introduced in Subsection 4.3.3. Like previous results, the errors decay when adding more

coarse basis functions.

Table 11: Numerical results for Multiscale Space III applied to permeability field of Topology 1 (Subsection 4.3.3) with increasing dimension of the coarse space, $h = 1/100, H = 1/10, \eta = 10^4$ and $\eta = 10^6$(in parentheses). "Dim." stands for the dimension of the coarse space.

| Dim. | $\|u_h^* - u_H\|_{L^2(\Omega)}$ | $\|\boldsymbol{q}_h^* - \boldsymbol{q}_H\|_{\alpha,L^2(\Omega)}$ |
|---|---|---|
| 180 (180) | 0.641 (0.641) | 0.803 (0.803) |
| 360 (360) | 0.111 (0.112) | 0.352 (0.352) |
| 540 (540) | 0.042 (0.044) | 0.235 (0.236) |
| 720 (720) | 0.022 (0.034) | 0.180 (0.212) |
| 900 (900) | 0.022 (0.025) | 0.152 (0.189) |

Table 12: Numerical results for Multiscale Space III applied to permeability field of Topology 2 (Subsection 4.3.3) with increasing dimension of the coarse space, $h = 1/100, H = 1/10, \eta = 10^4$ and $\eta = 10^6$(in parentheses). "Dim." stands for the dimension of the coarse space.

| Dim. | $\|u_h^* - u_H\|_{L^2(\Omega)}$ | $\|\boldsymbol{q}_h^* - \boldsymbol{q}_H\|_{\alpha,L^2(\Omega)}$ |
|---|---|---|
| 180 (180) | 0.656 (0.656) | 0.810 (0.811) |
| 360 (360) | 0.103 (0.116) | 0.342 (0.357) |
| 540 (540) | 0.040 (0.041) | 0.229 (0.231) |
| 720 (720) | 0.022 (0.031) | 0.170 (0.199) |
| 900 (900) | 0.022 (0.024) | 0.142 (0.175) |

We repeat the detailed numerical study described in previous section. Table 11 and 12 show the results for the computation of pressure and velocity error for $h = 1/100$ and $H = 1/10$ and two different contrasts $10^4$ and $10^6$. Similarly, we report the dimension of the coarse spaces. From these results, we observe a reasonable error decay when increasing the coarse dimension. In particular, for $H = 1/10$ and $\eta = 10^4$, we only need Dim = 720 to get the pressure error 2.2% and velocity error

18.0% for Topology 1. The error is computed with respect to the fine-grid solution (that is $h = 1/100$) obtained by solving a system of dimension $60,000$.

We have also tested all the numerical cases with $\eta = 10^6$ and observed similar accuracy. This shows that the above certain threshold the proposed method produces similar results.

## 4.5 Stability analysis

In this section, we discuss the stability of HDG method with multiscale spaces constructed in Section 4.1.1. Due to the *stabilization parameter* $\tau$, the stability estimate of the system is independent of the choice of the multiscale space $M_H$. To proceed, we need the following two assumptions on the local fine element spaces.

**Assumption 4.5.1.** *For any $T \in \mathcal{T}_h$, $F^*$ an arbitrary edge of $T$, and $\mu \in M_h(F), F \in \partial T$, there exists a element $\boldsymbol{Z} \in \boldsymbol{V}_h(T)$ such that*

$$(\boldsymbol{Z}, \nabla w) = 0, \quad \textit{for all } w \in W_h(T), \tag{4.24}$$

$$\boldsymbol{Z} \cdot \boldsymbol{n}|_F = \mu, \quad \textit{for all } F \in \partial T \backslash F^*. \tag{4.25}$$

This assumption is trivially satisfied by all classical mixed finite elements, e.g. **RT, BDM, BDDF**, etc. For these elements one can simply define $\boldsymbol{Z} = \boldsymbol{\Pi}_h \boldsymbol{Q}$, where $\boldsymbol{Q}$ is any solution of the problem:

$$\nabla \cdot \boldsymbol{Q} = 0 \quad \text{in } T \quad \text{and} \quad \boldsymbol{Q} \cdot \boldsymbol{n} = \mu \quad \text{on } \partial T,$$

where $\boldsymbol{\Pi}_h$ is the Fortin projection to the mixed elements (see, e.g. [15]). For the case of simplex triangulations and HDG elements, we refer readers to Lemma 3.2, [19]. The proof for other HDG elements are very similar to the case of simplicial elements considered in [19]. Further, we need an assumption on the stabilization parameter

$\tau$.

**Assumption 4.5.2.** *On each $F_H \in \mathcal{E}_H$, for any $\Omega_i$ adjacent to $F_H$, i.e. $\overline{\Omega}_i \cap F_H \neq \emptyset$, there exists at least one element $T \in \mathcal{T}_h(\Omega_i)$ adjacent to $F_H$, such that the stabilization operator $\tau > 0$ on $F^* = F_H \cap \partial T$.*

Now we state the solvability result of the method that is established by using approach developed in [24].

**Theorem 4.5.3.** *If Assumptions 4.5.1 and 4.5.2 are satisfied, then for any $f$, the system* (4.3) *has unique solution.*

*Proof.* Note that the system (4.3) is a square system. It suffices to show that the homogeneous system has only the trivial solution. From (4.3d) we see that $\widehat{u}_{h,H} = 0$ on $\partial\Omega$. Now assume that $(u_h, \boldsymbol{q}_h, \widehat{u}_{h,H})$ is any solution of (4.3). Setting $(w, \boldsymbol{v}, \mu) = (u_h, \boldsymbol{q}_h, \widehat{u}_{h,H})$ in (4.3a)-(4.3c) and adding all equations, we get after some algebraic manipulation,

$$(\alpha \boldsymbol{q}_h \, , \, \boldsymbol{q}_h)_{\mathcal{T}_h} - \langle \boldsymbol{q}_h \cdot \boldsymbol{n} - \widehat{\boldsymbol{q}}_{h,H} \cdot \boldsymbol{n} \, , \, u_h - \widehat{u}_{h,H} \rangle_{\partial \mathcal{T}_h} = 0.$$

By the definition of the numerical traces (4.3e), we have

$$(\alpha \boldsymbol{q}_h \, , \, \boldsymbol{q}_h)_{\mathcal{T}_h} + \langle \tau (u_h - \widehat{u}_{h,H}) \, , \, u_h - \widehat{u}_{h,H} \rangle_{\partial \mathcal{T}_h} = 0$$

and since $\tau > 0$ we get

$$\boldsymbol{q}_h = 0, \quad \tau (u_h - \widehat{u}_{h,H}) = 0.$$

and (4.3a) becomes

$$-(u_h \, , \, \nabla \cdot \boldsymbol{v})_{\mathcal{T}_h} + \langle \widehat{u}_{h,H} \, , \, \boldsymbol{v} \cdot \boldsymbol{n} \rangle_{\partial \mathcal{T}_h} = 0, \quad \text{for all} \quad \boldsymbol{v} \in \boldsymbol{V}_h.$$

Now we take this over an element $T$ and after integration by parts, we get

$$(\nabla u_h, \boldsymbol{v})_T + \langle \widehat{u}_{h,H} - u_h, \boldsymbol{v} \cdot \boldsymbol{n} \rangle_{\partial T} = 0, \quad \text{for all} \quad \boldsymbol{v} \in \boldsymbol{V}(T). \tag{4.26}$$

Since $\tau > 0$ on $F^* \in \partial T$, we get $u_h - \widehat{u}_{h,H} = 0$ on $F^*$. Next by Assumption 4.5.1, there is $\boldsymbol{v} \in \boldsymbol{V}_h$ such that

$$\begin{aligned} (\boldsymbol{v}\,, \nabla w)_{\mathcal{T}_h} &= 0, \quad \text{for all} \quad w \in W(T), \\ \boldsymbol{v} \cdot \boldsymbol{n}|_F &= P_h^{\partial} \widehat{u}_{h,H} - u_h, \quad \text{for all} \quad F \in \partial T \backslash F^* \end{aligned}$$

where for $T \in \mathcal{T}_h$, $P_h^{\partial} : L^2(F) \to M_h(F)$ is the local $L^2$-projection onto $M_h(F)$, for all $F \in \partial T$. Inserting such $\boldsymbol{v}$ in (4.26), we get

$$0 = (\nabla u_h, \boldsymbol{v})_K + \langle \widehat{u}_{h,H} - u_h, \boldsymbol{v} \cdot \boldsymbol{n} \rangle_{\partial T} = \langle P_h^{\partial} \widehat{u}_{h,H} - u_h, P_h^{\partial} \widehat{u}_{h,H} - u_h \rangle_{\partial T \backslash F^*}.$$

This implies that $P_h^{\partial} \widehat{u}_{h,H} - u_h = 0$ on $\partial T \backslash F^*$.

Since on $F^*$, $P_h^{\partial} \widehat{u}_{h,H} - u_h = P_h^{\partial}(\widehat{u}_{h,H} - u_h) = 0$, we have

$$P_h^{\partial} \widehat{u}_{h,H} - u_h = 0 \quad \text{on} \quad \partial T, \quad \text{for all} \quad T \in \mathcal{T}_h.$$

Moreover, this means that $(\nabla u_h, \boldsymbol{v})_T = 0$ for all $\boldsymbol{v} \in \boldsymbol{V}(T)$. Taking $\boldsymbol{v} = \nabla u_h$, we have $u_h$ is piecewise constant on each $T \in \mathcal{T}_h$. The above equation shows that $u_h = P_h^{\partial} \widehat{u}_{h,H}$ on $\partial T$. On each $\Omega_i$, $\mathcal{T}_h(\Omega_i)$ is a conforming triangulation, so this implies that for any interior face $F \in \mathcal{E}_h^0$ shared by two neighboring element $T^+, T^-$, the local spaces satisfy $M_h(F^+) = M_h(F^-)$ and hence $P_h^{\partial} \widehat{u}_{h,H}$ coincides from both sides. This implies that in fact $u_h = C_i$ in each subdomain $\Omega_i$ and $\widehat{u}_{h,H}|_{\mathcal{E}_h^0 \cap \Omega_i} = C_i$.

Next, on each $F_H \in \mathcal{E}_H$, we assume that $F_H \subset \overline{\Omega}_1 \cap \overline{\Omega}_2$, if $F_H \subset \partial\Omega$ then

$F_H \subset \partial\Omega_1$. By Assumption 4.5.2, there exists $T_1 \in \mathcal{T}_h(\Omega_1), T_2 \in \mathcal{T}_h(\Omega_2)$ adjacent to $F_H$ such that $\tau > 0$ on $F_j = \partial T_j \cap F_H$, $j = 1, 2$. Then, we have

$$\widehat{u}_{h,H} - u_h = 0 \quad \text{on} \quad F_j, \quad j = 1, 2.$$

This implies that $\widehat{u}_{h,H}|_{F_H} = C_1 = C_2$. Hence we have $C_i = C$ for all $i$, which means that $u_h = C$ over the domain $\Omega$ and $\widehat{u}_{h,H} = C$. Finally, by the fact that $\widehat{u}_{h,H} = 0$ on $\partial\Omega$, we must have $u_h = \widehat{u}_{h,H} = 0$ and this completes the proof. □

In [9], in order to ensure the solvability of the mortar methods, the key assumption (roughly speaking) is that on $\mathcal{E}$ the fine scale space $M_h$ should be rich enough comparing with the coarse scale space $M_H$. Since the stabilization is achieved by the parameter $\tau$, we prove stability under the assumption that on each $F_H \in \mathcal{E}_H$ the parameter $\tau$ is strictly positive on some portion of $F_H$. We do not need any conditions between the local spaces $M_h(F_h)$ and $M_H(F_H)$.

## 4.6 Error analysis

In this section, we derive error estimates for the specific examples which are proposed Section 4.3. We would like stress on important point of this estimates. Upon different choices of the multiscale spaces, we can get different convergence rates. The reason is that the error estimates reflect the local spectral problems. For the sake of simplicity, we assume that the nonzero stabilization parameter $\tau$ is a positive constant on all fine-scale element $T \in \mathcal{T}_h$.

### *4.6.1 Preliminary results*

In this section, we present some necessary preliminary results. In order to carry out the a priori error estimates, we need some assumptions on the proposed scheme. The assumption is identical to *Assumption A* in [24], but in order to be self-consistent,

we will give it below:

**Assumption 4.6.1.** *The local spaces satisfy the following inclusion property:*

$$W(T)|_F \subset M_h(F) \quad \textit{for all } F \in \partial T, \tag{4.27a}$$

$$\boldsymbol{V}(T) \cdot \boldsymbol{n}|_F \subset M_h(F) \quad \textit{for all } F \in \partial T. \tag{4.27b}$$

*On each element $T \in \mathcal{T}_h$, there exist local projection operators*

$$\Pi_W : \ H^1(T) \to W(T) \quad \textit{and} \quad \boldsymbol{\Pi}_V : \ \boldsymbol{H}_{div}(T) \to \boldsymbol{V}(T)$$

*associated with the spaces $W(T)$, $\boldsymbol{V}(T)$, $M_h(F)$ defined by:*

$$(u, w)_T = (\Pi_W u, w)_T \qquad \textit{for all } w \in \nabla \cdot \boldsymbol{V}(T), \tag{4.28a}$$

$$(\boldsymbol{q}, \boldsymbol{v})_T = (\boldsymbol{\Pi}_V \boldsymbol{q}, \boldsymbol{v})_T \qquad \textit{for all } \boldsymbol{v} \in \nabla W(T), \tag{4.28b}$$

$$\langle \boldsymbol{q} \cdot \boldsymbol{n} + \tau u \, , \, \mu \rangle_F = \langle \boldsymbol{\Pi}_V \boldsymbol{q} \cdot \boldsymbol{n} + \tau \Pi_W u \, , \, \mu \rangle_F \quad \textit{for all } \mu \in M_h(F), F \in \partial T. \tag{4.28c}$$

The above suggested local spaces $W(T) \times \boldsymbol{V}(T) \times M_h(F)$ or any set of local spaces presented in [24] satisfy Assumption 4.6.1. In [24] it has been shown that for any $(u, \boldsymbol{q}) \in H^1(T) \times \boldsymbol{H}_{div}(T)$, the projection $(\Pi_W u, \boldsymbol{\Pi}_V \boldsymbol{q}) \in W(T) \times \boldsymbol{V}(T)$ exists and is unique. Moreover, for all elements listed in Table 1, the projection has the following approximation property:

**Lemma 4.6.2.** *If the local spaces $\boldsymbol{V}(T), W(T)$ are mixed element spaces $\mathbf{RT}_k$ or $\mathbf{BDFM}_{k+1}$, then*

$$\|\boldsymbol{q} - \boldsymbol{\Pi}_V \boldsymbol{q}\|_T \leq C h^s (\|\boldsymbol{q}\|_{s,T} + \tau \|u\|_{s,T}) \quad \textit{and} \quad \|u - \Pi_W u\|_T \leq C h^s \|u\|_{s,T}$$

*and if the local spaces* $\boldsymbol{V}(T), W(T)$ *are* $\mathbf{HDG}_k$ *spaces, then*

$$\|\boldsymbol{q} - \boldsymbol{\Pi}_V \boldsymbol{q}\|_T \leq Ch^s(\|\boldsymbol{q}\|_{s,T}) \quad \textit{and} \quad \|u - \Pi_W u\|_T \leq Ch^s(\|u\|_{s,T} + \tau^{-1}\|\boldsymbol{q}\|_{s,T})$$

*for all* $1 \leq s \leq k+1$.

Further in our analysis we shall need some auxiliary local projections and their properties:

$$\begin{aligned}
&P_H^\partial : L^2(F) \to M_H(F), \qquad \langle P_H^\partial u, \mu\rangle_F = \langle u, \mu\rangle_F \quad \forall F \in \mathcal{E}_H,\ \mu \in M_H(F),\\
&P_h^\partial : L^2(F) \to M_h(F), \qquad \langle P_h^\partial u, \mu\rangle_F = \langle u, \mu\rangle_F \quad \forall F \in \mathcal{E}_h,\ \mu \in M_h(F),\\
&P_M : L^2(\mathcal{E}_{h,H}) \to M_{h,H}, \qquad \text{with} \quad P_M = \begin{cases} P_H^\partial & \text{on} \quad \mathcal{E}_H, \\ P_h^\partial & \text{on} \quad \mathcal{E}_h^0. \end{cases}
\end{aligned} \tag{4.29}$$

From the last equation (4.28c) and the definitions (4.29) of the projection operators, we immediately have

$$P_h^\partial(\boldsymbol{q}\cdot\boldsymbol{n}) + \tau P_h^\partial u = \boldsymbol{\Pi}_V \boldsymbol{q}\cdot\boldsymbol{n} + \tau \Pi_W u, \quad \text{for all} \quad F \in \partial\mathcal{T}_h. \tag{4.30}$$

In the analysis, we will need the following standard approximation properties of the projections $P_h^\partial$:

**Lemma 4.6.3.** *For any coarse-scale element* $\Omega_i \in \mathcal{T}_h$ *with mesh size* $H$ *and any smooth enough function* $u$*, we have*

$$\begin{aligned}
\|u - P_h^\partial u\|_{\partial\Omega_i} &\leq CH^{-\frac{1}{2}} h^s \|u\|_{s+1,\Omega_i} \quad 0 \leq s \leq k+1\\
\|\boldsymbol{q}\cdot\boldsymbol{n} - P_h^\partial(\boldsymbol{q}\cdot\boldsymbol{n})\|_{\partial\Omega_i} &\leq CH^{-\frac{1}{2}} h^s \|\boldsymbol{q}\|_{s+1,\Omega_i} \quad 0 \leq s \leq k+1.
\end{aligned} \tag{4.31}$$

*Here, constants* $C$ *solely depends on the shape of the subdomain* $\Omega_i$ *but not its mesh*

*size $H$.*

*Proof.* We note that the following standard estimates for the error on any edgy/face $F\partial\Omega_i$, see [18]:

$$\begin{aligned}\|u - P_h^{\partial} u\|_F &\leq Ch^s |u|_{s+1,F} \\ \|\boldsymbol{q}\cdot\boldsymbol{n} - P_h^{\partial}(\boldsymbol{q}\cdot\boldsymbol{n})\|_F &\leq Ch^s |\boldsymbol{q}\cdot\boldsymbol{n}|_{s+1,F},\end{aligned}$$

for all integer $0 \leq s \leq k+1$. All two inequalities can be obtained by a similar scaling argument. Here we only present the proof of the first one of them. Assume $F$ is one of the faces of a subdomain $\Omega_i$. By the above notice, we have

$$\begin{aligned}\|u - P_h^{\partial} u\|_{\partial\Omega_i} &\leq Ch^s |u|_{s,\partial\Omega_i} \\ &\leq Ch^s (H^{-\frac{1}{2}} |u|_{s,\Omega_i} + H^{\frac{1}{2}} |u|_{s+1,\Omega_i}) \quad \text{by the trace inequality in (4.4)} \\ &\leq CH^{-\frac{1}{2}} h^s \|u\|_{s+1,\Omega_i},\end{aligned}$$

for all integer $0 \leq s \leq k+1$. The case of $s$ non integer follows by interpolation and the another is proven in a similar way. This complete the proof. □

### *4.6.2 Error equations*

In this section, we derive the error equations that are needed in the analysis. The idea is to work with the following projection errors:

$$\begin{aligned}\boldsymbol{e}_q &:= \boldsymbol{\Pi}_V \boldsymbol{q} - \boldsymbol{q}_h, \\ e_u &:= \Pi_W u - u_h, \\ \boldsymbol{e}_{\widehat{q}}\cdot\boldsymbol{n} &:= P_M(\boldsymbol{q}\cdot\boldsymbol{n}) - \widehat{\boldsymbol{q}}_{h,H}\cdot\boldsymbol{n}, \\ e_{\widehat{u}} &:= P_M u - \widehat{u}_{h,H}\end{aligned}$$

and further introduce

$$\delta_u := u - \Pi_W u,$$

$$\boldsymbol{\delta}_q := \boldsymbol{q} - \boldsymbol{\Pi}_V \boldsymbol{q}.$$

**Lemma 4.6.4.** *Let the Assumption 4.6.1 be valid. Then we have*

$$(\alpha \boldsymbol{e}_q\,,\,\boldsymbol{v})_{\mathcal{T}_h} - (e_u\,,\,\nabla\cdot\boldsymbol{v})_{\mathcal{T}_h} + \langle e_{\widehat{u}}\,,\,\boldsymbol{v}\cdot\boldsymbol{n}\rangle_{\partial\mathcal{T}_h} = -(\alpha\boldsymbol{\delta}_q\,,\,\boldsymbol{v})_{\mathcal{T}_h} - \langle (I-P_M)u\,,\,\boldsymbol{v}\cdot\boldsymbol{n}\rangle_{\partial\mathcal{T}_h} \tag{4.32a}$$

$$-(\boldsymbol{e}_q\,,\,\nabla w)_{\mathcal{T}_h} + \langle \boldsymbol{e}_{\widehat{q}}\cdot\boldsymbol{n}\,,\,w\rangle_{\partial\mathcal{T}_h} = -\langle (I-P_M)(\boldsymbol{q}\cdot\boldsymbol{n})\,,\,w\rangle_{\partial\mathcal{T}_h}, \tag{4.32b}$$

$$\langle \boldsymbol{e}_{\widehat{q}}\cdot\boldsymbol{n}\,,\,\mu\rangle_{\partial\mathcal{T}_h} = 0, \tag{4.32c}$$

$$e_{\widehat{u}}|_{\partial\Omega} = 0, \tag{4.32d}$$

*for all* $(w,\boldsymbol{v},\mu)\in W_h\times\boldsymbol{V}_h\times M_{h,H}$. *Here* $I$ *is the identity operator and*

$$\boldsymbol{e}_{\widehat{q}}\cdot\boldsymbol{n} = \boldsymbol{e}_q\cdot\boldsymbol{n} + \tau(e_u - e_{\widehat{u}}) - (P_h^{\partial} - P_M)(\boldsymbol{q}\cdot\boldsymbol{n} + \tau u) \quad on \quad \partial\mathcal{T}_h. \tag{4.33}$$

*Proof.* We first note that the exact solution $(u,\boldsymbol{q})$ obviously satisfies

$$\begin{aligned}
(\alpha\boldsymbol{q}\,,\,\boldsymbol{v})_{\mathcal{T}_h} - (u\,,\,\nabla\cdot\boldsymbol{v})_{\mathcal{T}_h} + \langle u\,,\,\boldsymbol{v}\cdot\boldsymbol{n}\rangle_{\partial\mathcal{T}_h} &= 0,\\
-(\boldsymbol{q}\,,\,\nabla w)_{\mathcal{T}_h} + \langle \boldsymbol{q}\cdot\boldsymbol{n}\,,\,w\rangle_{\partial\mathcal{T}_h} &= (f\,,\,w)_{\mathcal{T}_h},\\
\langle \boldsymbol{q}\cdot\boldsymbol{n}\,,\,\mu\rangle_{\partial\mathcal{T}_h} &= 0,
\end{aligned}$$

for all $(w,\boldsymbol{v},\mu)\in W_h\times\boldsymbol{V}_h\times M_{h,H}$. By the properties of the projections $\boldsymbol{\Pi}_V$ and $\Pi_W$, defined by (4.28) we obtain

$$\begin{aligned}
(\alpha\boldsymbol{q}\,,\,\boldsymbol{v})_{\mathcal{T}_h} - (\Pi_W u\,,\,\nabla\cdot\boldsymbol{v})_{\mathcal{T}_h} + \langle u\,,\,\boldsymbol{v}\cdot\boldsymbol{n}\rangle_{\partial\mathcal{T}_h} &= 0,\\
-(\boldsymbol{\Pi}_V\boldsymbol{q}\,,\,\nabla w)_{\mathcal{T}_h} + \langle \boldsymbol{q}\cdot\boldsymbol{n}\,,\,w\rangle_{\partial\mathcal{T}_h} &= (f\,,\,w)_{\mathcal{T}_h},\\
\langle \boldsymbol{q}\cdot\boldsymbol{n}\,,\,\mu\rangle_{\partial\mathcal{T}_h} &= 0,
\end{aligned}$$

for all $(w, \boldsymbol{v}, \mu) \in W_h \times \boldsymbol{V}_h \times M_{h,H}$. Moreover, since $P_M$ is the $L^2$-projection into $M_{h,H}$, we get

$$\begin{aligned}
(\alpha \boldsymbol{q}\,,\, \boldsymbol{v})_{\mathcal{T}_h} - (\Pi_W u\,,\, \nabla\cdot\boldsymbol{v})_{\mathcal{T}_h} + \langle P_M u\,,\, \boldsymbol{v}\cdot\boldsymbol{n}\rangle_{\partial\mathcal{T}_h} &= -\langle (I-P_M)u\,,\, \boldsymbol{v}\cdot\boldsymbol{n}\rangle_{\partial\mathcal{T}_h}, \\
-(\boldsymbol{\Pi}_V \boldsymbol{q}\,,\, \nabla w)_{\mathcal{T}_h} + \langle P_M(\boldsymbol{q}\cdot\boldsymbol{n})\,,\, w\rangle_{\partial\mathcal{T}_h} &= (f\,,\, w)_{\mathcal{T}_h} \\
&\quad -\langle (I-P_M)(\boldsymbol{q}\cdot\boldsymbol{n})\,,\, w\rangle_{\partial\mathcal{T}_h}, \\
\langle P_M(\boldsymbol{q}\cdot\boldsymbol{n})\,,\, \mu\rangle_{\partial\mathcal{T}_h} &= 0,
\end{aligned}$$

for all $(w, \boldsymbol{v}, \mu) \in W_h \times \boldsymbol{V}_h \times M_{h,H}$. Subtracting the four equations defining the weak formulation of the upscale HDG method (4.3) from the above equations, respectively, we obtain the equations for the projection of the errors. The last error equation (4.32d) is due to the definition of $\widehat{u}_{h,H}$ on $\partial\Omega$.

It remains to prove the identity (4.33) for $\boldsymbol{e}_{\widehat{q}}\cdot\boldsymbol{n}$. On each face $F \in \partial T$, $T \in \mathcal{T}_h$ after using the definition of numerical traces (4.3e), we have

$$\begin{aligned}
\boldsymbol{e}_{\widehat{q}}\cdot\boldsymbol{n} - \boldsymbol{e}_q\cdot\boldsymbol{n} &= P_M(\boldsymbol{q}\cdot\boldsymbol{n}) - \widehat{\boldsymbol{q}}_{h,H}\cdot\boldsymbol{n} - (\boldsymbol{\Pi}_V\boldsymbol{q}\cdot\boldsymbol{n} - \boldsymbol{q}_h\cdot\boldsymbol{n}) \\
&= P_M(\boldsymbol{q}\cdot\boldsymbol{n}) - \boldsymbol{\Pi}_V\boldsymbol{q}\cdot\boldsymbol{n} - (\widehat{\boldsymbol{q}}_{h,H}\cdot\boldsymbol{n} - \boldsymbol{q}_h\cdot\boldsymbol{n}) \\
&= P_h^{\partial}(\boldsymbol{q}\cdot\boldsymbol{n}) - \boldsymbol{\Pi}_V\boldsymbol{q}\cdot\boldsymbol{n} - \tau(u_h - \widehat{u}_{h,H}) + (P_M - P_h^{\partial})(\boldsymbol{q}\cdot\boldsymbol{n}).
\end{aligned}$$

Then using the property (4.30) of the projections $\Pi_W$ the equality reduces to

$$\begin{aligned}
\boldsymbol{e}_{\widehat{q}}\cdot\boldsymbol{n} - \boldsymbol{e}_q\cdot\boldsymbol{n} &= \tau(-P_h^{\partial}u + \Pi_W u) - \tau(u_h - \widehat{u}_{h,H}) + (P_M - P_h^{\partial})(\boldsymbol{q}\cdot\boldsymbol{n}) \\
&= \tau(-P_M u + \Pi_W u) - \tau(u_h - \widehat{u}_{h,H}) + (P_M - P_h^{\partial})(\boldsymbol{q}\cdot\boldsymbol{n} + \tau u) \\
&= \tau(e_u - e_{\widehat{u}}) + (P_M - P_h^{\partial})(\boldsymbol{q}\cdot\boldsymbol{n} + \tau u).
\end{aligned}$$

This complete the proof. □

### *4.6.3 General error estimates*

In this section, we propose the error estimates which are independent of the choice of multiscale spaces in order to get the error estimates for various multiscale spaces. Especially, for the error estimate of $e_u$, we consider the standard dual problem without a high contrast coefficient.

First, in order to get an error estimate for $\boldsymbol{e}_q$, we need the following identity:

**Lemma 4.6.5.** *Let the Assumption 4.6.1 be satisfied. Then for any $w \in M_H$ we have*

$$\|\boldsymbol{e}_q\|_\alpha^2 + \|e_u - e_{\widehat{u}}\|_\tau^2 = \sum_{i=1} \mathbb{T}_i,$$

*where*

$$\mathbb{T}_1 = -(\alpha\boldsymbol{\delta}_q\,,\,\boldsymbol{e}_q)_{\mathcal{T}_h}, \qquad \mathbb{T}_2 = -\langle u - w\,,\,\boldsymbol{e}_q\cdot\boldsymbol{n}\rangle_{\partial\mathcal{T}_H},$$

$$\mathbb{T}_3 = -\langle \boldsymbol{q}\cdot\boldsymbol{n} - P_h^\partial(\boldsymbol{q}\cdot\boldsymbol{n})\,,\,e_u - e_{\widehat{u}}\rangle_{\partial\mathcal{T}_H}, \qquad \mathbb{T}_4 = \langle P_h^\partial u - P_H^\partial u\,,\,\tau(e_u - e_{\widehat{u}})\rangle_{\partial\mathcal{T}_H},$$

$$\mathbb{T}_5 = \langle w - P_H^\partial u\,,\,\tau(e_u - e_{\widehat{u}})\rangle_{\partial\mathcal{T}_H}, \qquad \mathbb{T}_6 = \langle w - P_H^\partial u\,,\,\tau(P_h^\partial u - u)\rangle_{\partial\mathcal{T}_H}.$$

*Proof.* The error equation (4.32d) ensures that $e_{\widehat{u}} \in M_{h,H}$. Then take $(\boldsymbol{v}, w, \mu) = (\boldsymbol{e}_q, e_u, e_{\widehat{u}})$ in the error equations (4.32a)-(4.32c) and ddd all equations, to get after some algebraic manipulation,

$$\begin{aligned}\|\boldsymbol{e}_q\|_\alpha^2 + \langle \boldsymbol{e}_{\widehat{q}}\cdot\boldsymbol{n} - \boldsymbol{e}_q\cdot\boldsymbol{n}\,,\,e_u - e_{\widehat{u}}\rangle_{\partial\mathcal{T}_h} =& -(\alpha\boldsymbol{\delta}_q\,,\,\boldsymbol{e}_q)_{\mathcal{T}_h} - \langle (I - P_M)u\,,\,\boldsymbol{e}_q\cdot\boldsymbol{n}\rangle_{\partial\mathcal{T}_h} \\ & - \langle (I - P_M)(\boldsymbol{q}\cdot\boldsymbol{n})\,,\,e_u\rangle_{\partial\mathcal{T}_h}.\end{aligned}$$

Inserting the identity (4.33) in the above equation, we get

$$\begin{aligned}
\|\boldsymbol{e}_q\|_\alpha^2+\|e_u-e_{\widehat{u}}\|_\tau^2 &= -(\alpha\boldsymbol{\delta}_q\,,\,\boldsymbol{e}_q)_{\mathcal{T}_h} - \langle (I-P_M)u\,,\,\boldsymbol{e}_q\cdot\boldsymbol{n}\rangle_{\partial\mathcal{T}_h} \\
&\quad - \langle (I-P_M)(\boldsymbol{q}\cdot\boldsymbol{n})\,,\,e_u\rangle_{\partial\mathcal{T}_h} + \langle (P_h^\partial - P_M)(\boldsymbol{q}\cdot\boldsymbol{n}+\tau u)\,,\,e_u-e_{\widehat{u}}\rangle_{\partial\mathcal{T}_h} \\
&= -(\alpha\boldsymbol{\delta}_q\,,\,\boldsymbol{e}_q)_{\mathcal{T}_h} - \langle (I-P_M)u\,,\,\boldsymbol{e}_q\cdot\boldsymbol{n}\rangle_{\partial\mathcal{T}_h} \\
&\quad - \langle (I-P_M)(\boldsymbol{q}\cdot\boldsymbol{n})\,,\,e_u-e_{\widehat{u}}\rangle_{\partial\mathcal{T}_h} + \langle (P_h^\partial - P_M)(\boldsymbol{q}\cdot\boldsymbol{n})\,,\,e_u-e_{\widehat{u}}\rangle_{\partial\mathcal{T}_h} \\
&\quad + \langle (P_h^\partial - P_M)(\tau u)\,,\,e_u-e_{\widehat{u}}\rangle_{\partial\mathcal{T}_h} \\
&= -(\alpha\boldsymbol{\delta}_q\,,\,\boldsymbol{e}_q)_{\mathcal{T}_h} - \langle (I-P_M)u\,,\,\boldsymbol{e}_q\cdot\boldsymbol{n}\rangle_{\partial\mathcal{T}_h} \\
&\quad - \langle (I-P_h^\partial)(\boldsymbol{q}\cdot\boldsymbol{n})\,,\,e_u-e_{\widehat{u}}\rangle_{\partial\mathcal{T}_h} + \langle (P_h^\partial - P_M)u\,,\,\tau(e_u-e_{\widehat{u}})\rangle_{\partial\mathcal{T}_h}.
\end{aligned}$$

We used the fact that $e_{\widehat{u}}$ is single valued on $\mathcal{E}_h$ and $e_{\widehat{u}}=0$ on $\partial\Omega$. Noticing that on each $F\in\mathcal{E}_h^0$

$$P_M = P_h^\partial, \quad e_u|_F,\ e_{\widehat{u}}|_F,\ \boldsymbol{e}_q\cdot\boldsymbol{n}|F\in M_h(F),$$

we get the following equalities:

$$\begin{aligned}
\langle (I-P_M)u\,,\,\boldsymbol{e}_q\cdot\boldsymbol{n}\rangle_{\partial\mathcal{T}_h} &= \langle (I-P_H^\partial)u\,,\,\boldsymbol{e}_q\cdot\boldsymbol{n}\rangle_{\partial\mathcal{T}_H}, \\
\langle (I-P_h^\partial)(\boldsymbol{q}\cdot\boldsymbol{n})\,,\,e_u-e_{\widehat{u}}\rangle_{\partial\mathcal{T}_h} &= \langle (I-P_h^\partial)(\boldsymbol{q}\cdot\boldsymbol{n})\,,\,e_u-e_{\widehat{u}}\rangle_{\partial\mathcal{T}_H}, \\
\langle (P_h^\partial-P_M)u\,,\,\tau(e_u-e_{\widehat{u}})\rangle_{\partial\mathcal{T}_h} &= \langle (P_h^\partial-P_H^\partial)u\,,\,\tau(e_u-e_{\widehat{u}})\rangle_{\partial\mathcal{T}_H}.
\end{aligned}$$

Now we rewrite $\langle (I - P_H^\partial)\,,\, \boldsymbol{e}_q \cdot \boldsymbol{n} \rangle_{\partial \mathcal{T}_H}$. For any $w \in M_H$, we have

$$\begin{aligned}
\langle (I - P_H^\partial)u\,,\, \boldsymbol{e}_q \cdot \boldsymbol{n} \rangle_{\partial \mathcal{T}_H} =& \langle u - w\,,\, \boldsymbol{e}_q \cdot \boldsymbol{n} \rangle_{\partial \mathcal{T}_h} + \langle w - P_H^\partial u\,,\, \boldsymbol{e}_q \cdot \boldsymbol{n} \rangle_{\partial \mathcal{T}_H} \\
=& \langle u - w\,,\, \boldsymbol{e}_q \cdot \boldsymbol{n} \rangle_{\partial \mathcal{T}_H} + \langle w - P_H^\partial u\,,\, \boldsymbol{e}_{\widehat{q}} \cdot \boldsymbol{n} \rangle_{\partial \mathcal{T}_H} \\
& - \langle w - P_H^\partial u\,,\, \tau(e_u - e_{\widehat{u}}) \rangle_{\partial \mathcal{T}_H} \\
& + \langle w - P_H^\partial u\,,\, (P_h^\partial - P_M)(\boldsymbol{q} \cdot \boldsymbol{n} - \tau u) \rangle_{\partial \mathcal{T}_H} \\
=& \langle u - w\,,\, \boldsymbol{e}_q \cdot \boldsymbol{n} \rangle_{\partial \mathcal{T}_H} - \langle w - P_H^\partial u\,,\, \tau(e_u - e_{\widehat{u}}) \rangle_{\partial \mathcal{T}_H} \\
& + \langle w - P_H^\partial u\,,\, \tau(P_h^\partial u - P_M u) \rangle_{\partial \mathcal{T}_H} \\
& + \langle w - P_H^\partial u\,,\, (P_h^\partial - P_H^\partial)(\boldsymbol{q} \cdot \boldsymbol{n}) \rangle_{\partial \mathcal{T}_H} \\
=& \langle u - w\,,\, \boldsymbol{e}_q \cdot \boldsymbol{n} \rangle_{\partial \mathcal{T}_H} - \langle w - P_H^\partial u\,,\, \tau(e_u - e_{\widehat{u}}) \rangle_{\partial \mathcal{T}_H} \\
& + \langle w - P_H^\partial u\,,\, \tau(P_h^\partial u - u) \rangle_{\partial \mathcal{T}_H}.
\end{aligned}$$

Here we used the fact that $w - P_H^\partial u \in M_H$ and $w - P_H^\partial u|_{\partial\Omega} = 0$. This completes the proof. □

Now we derive an error bound for $\boldsymbol{e}_q$ that is independent of the choice of multiscale spaces. For $\mathbb{T}_2$, we provide two types of error estimates based on applying integration by parts with using multiscale space II-b. Our analysis is based on $\mathbf{HDG}_k$ as the local spaces of HDG method.

**Theorem 4.6.6.** *Let Assumption 4.6.1 be satisfied and the local space be the type of* $\mathbf{HDG}_k$*. Then, we have*

$$\begin{aligned}
\|\boldsymbol{e}_q\|_\alpha + \|e_u - e_{\widehat{u}}\|_\tau \le Ch^s \|\boldsymbol{q}\|_s + Ch^s H^{-\frac{1}{2}} \|\boldsymbol{q}\|_{s+1} + Ch^s H^{-\frac{1}{2}} \|u\|_{s+1} \\
+ Ch^{-\frac{1}{2}} \inf_{w \in M_H} \|\kappa^{\frac{1}{2}}(u - w)\|_{\partial \mathcal{T}_H}
\end{aligned} \tag{4.34}$$

*Moreover, if* $\boldsymbol{e}_q \in \mathbf{H}(div, \Omega_i)$ *for all* $i = 1, \cdots, N$*, then we have*

$$\begin{aligned} \|\boldsymbol{e}_q\|_\alpha + \|e_u - e_{\widehat{u}}\|_\tau \leq & Ch^s \|\boldsymbol{q}\|_s + Ch^s H^{\frac{1}{2}} \|\boldsymbol{q}\|_{s+1} + Ch^s H^{\frac{1}{2}} \|u\|_{s+1} \\ & + C \inf_{w \in M_H} \left( \|\kappa^{\frac{1}{2}} \nabla (u - \tilde{w})\| + \|u - w\|_{\partial \mathcal{T}_H} \right), \end{aligned} \tag{4.35}$$

*where* $\tilde{w}$ *is any extension such that* $\tilde{w}|_{\mathcal{E}_H} = w$*. In order to drive the specific error estimates, we choose* $\tilde{w} = I_0 u$ *(see Lemma 4.6.21).*

*Proof.* We estimate each term in the right hand side in Lemma 4.6.5 separately.

$$|\mathbb{T}_1| = |(\alpha \boldsymbol{\delta}_q \,,\, \boldsymbol{e}_q)_{\mathcal{T}_h}| \leq \|\alpha^{\frac{1}{2}} \boldsymbol{\delta}_q\| \|\boldsymbol{e}_q\|_\alpha \leq Ch^s \|\boldsymbol{q}\|_s \|\boldsymbol{e}_q\|_\alpha,$$

for all $1 \leq s \leq k+1$. For $\mathbb{T}_2$, we apply the trace inequality to obtain :

$$\begin{aligned} |\mathbb{T}_2| &= |\langle u - w \,,\, \boldsymbol{e}_q \cdot \boldsymbol{n} \rangle_{\partial \mathcal{T}_H}| \\ &\leq \|\kappa^{\frac{1}{2}} (u - w)\|_{\partial \mathcal{T}_H} \|\alpha^{\frac{1}{2}} \boldsymbol{e}_q \cdot \boldsymbol{n}\|_{\partial \mathcal{T}_H} \leq Ch^{-\frac{1}{2}} \|\kappa^{\frac{1}{2}} (u - w)\|_{\partial \mathcal{T}_H} \|\boldsymbol{e}_q\|_\alpha \end{aligned}$$

By the estimate (4.31) established in Lemma 4.6.3, we have

$$\begin{aligned} |\mathbb{T}_3| &= |\langle \boldsymbol{q} \cdot \boldsymbol{n} - P_h^\partial (\boldsymbol{q} \cdot \boldsymbol{n}) \,,\, e_u - e_{\widehat{u}} \rangle_{\partial \mathcal{T}_H}| \\ &\leq \tau^{-\frac{1}{2}} \|\boldsymbol{q} \cdot \boldsymbol{n} - P_h^\partial (\boldsymbol{q} \cdot \boldsymbol{n})\|_{\partial \mathcal{T}_H} \|e_u - e_{\widehat{u}}\|_\tau \leq Ch^s \tau^{-\frac{1}{2}} H^{-\frac{1}{2}} \|\boldsymbol{q}\|_{s+1} \|e_u - e_{\widehat{u}}\|_\tau. \end{aligned}$$

The terms $\mathbb{T}_4$ and $\mathbb{T}_5$ can be estimated similarly as $\mathbb{T}_3$, so we have

$$\begin{aligned} |\mathbb{T}_4| &= |\langle P_h^\partial u - P_H^\partial u \,,\, \tau (e_u - e_{\widehat{u}}) \rangle_{\partial \mathcal{T}_H}| \\ &\leq \tau^{\frac{1}{2}} \left( \|u - P_h^\partial u\|_{\partial \mathcal{T}_H} + \|u - P_H^\partial u\|_{\partial \mathcal{T}_H} \right) \|e_u - e_{\widehat{u}}\|_\tau \\ &\leq Ch^s H^{-\frac{1}{2}} \tau^{\frac{1}{2}} \|u\|_{s+1} \|e_u - e_{\widehat{u}}\|_\tau + \tau^{\frac{1}{2}} \|u - w\|_{\partial \mathcal{T}_H} \|e_u - e_{\widehat{u}}\|_\tau \\ &\leq Ch^s H^{-\frac{1}{2}} \tau^{\frac{1}{2}} \|u\|_{s+1} \|e_u - e_{\widehat{u}}\|_\tau + (\tau \alpha)^{\frac{1}{2}} \|\kappa^{\frac{1}{2}} (u - w)\|_{\partial \mathcal{T}_H} \|e_u - e_{\widehat{u}}\|_\tau, \end{aligned}$$

and

$$
\begin{aligned}
|\mathbb{T}_5| &= |\langle w - P_H^{\partial} u \,,\, \tau(e_u - e_{\widehat{u}})\rangle_{\partial\mathcal{T}_H}| \\
&\le \tau^{\frac{1}{2}} \left( \|w-u\|_{\partial\mathcal{T}_H} + \|u - P_H^{\partial} u\|_{\partial\mathcal{T}_H} \right) \|e_u - e_{\widehat{u}}\|_{\tau} \\
&\le 2\tau^{\frac{1}{2}} \|u-w\|_{\partial\mathcal{T}_H} \|e_u - e_{\widehat{u}}\|_{\tau} \le 2(\tau\alpha)^{\frac{1}{2}} \|\kappa^{\frac{1}{2}}(u-w)\|_{\partial\mathcal{T}_H} \|e_u - e_{\widehat{u}}\|_{\tau},
\end{aligned}
$$

For the last term, $\mathbb{T}_6$, we have

$$
\begin{aligned}
|\mathbb{T}_6| &= |\langle w - P_H^{\partial} u \,,\, \tau(P_h^{\partial} u - u)\rangle_{\partial\mathcal{T}_H}| \le 2\tau \|u-w\|_{\partial\mathcal{T}_H} \|P_h^{\partial} u - u\|_{\partial\mathcal{T}_H} \\
&\le 2C\tau h^s H^{-\frac{1}{2}} \|u\|_{s+1} \|u-w\|_{\partial\mathcal{T}_H} \le 2C\tau h^s H^{-\frac{1}{2}} \alpha^{\frac{1}{2}} \|u\|_{s+1} \|\kappa^{\frac{1}{2}}(u-w)\|_{\partial\mathcal{T}_H}.
\end{aligned}
$$

Finally, we obtain the first estimate in the lemma by a simply Young's inequality for each term and arrange the terms.

To get the second estimates (4.35), we need to bound four terms $\mathbb{T}_2$, $\mathbb{T}_4$, $\mathbb{T}_5$, and $\mathbb{T}_6$. For $\mathbb{T}_4$ – $\mathbb{T}_6$, we already derived in terms of $\|u-w\|_{\partial\mathcal{T}_H}$. The main difference is in bounding the term $\mathbb{T}_2$. Since $\boldsymbol{e}_q \in \mathbf{H}(div, \Omega_i)$ we can use the Green's identity to get

$$
\begin{aligned}
\langle u - w \,,\, \boldsymbol{e}_q \cdot \boldsymbol{n}\rangle_{\partial\mathcal{T}_h(\Omega_i)} &= (u - \tilde{w} \,,\, \nabla\cdot \boldsymbol{e}_q)_{\mathcal{T}_h(\Omega_i)} + (\nabla(u-\tilde{w}) \,,\, \boldsymbol{e}_q)_{\mathcal{T}_h(\Omega_i)} \\
&= (\nabla(u-\tilde{w}) \,,\, \boldsymbol{e}_q)_{\mathcal{T}_h(\Omega_i)}, \quad \text{where} \quad \tilde{w}|_{\mathcal{E}_H} = w,
\end{aligned}
$$

so that

$$
\begin{aligned}
|\mathbb{T}_2| = |\langle u - w \,,\, \boldsymbol{e}_q \cdot \boldsymbol{n}\rangle_{\partial\mathcal{T}_H}| &= |(\kappa^{\frac{1}{2}} \nabla(u-\tilde{w}) \,,\, \alpha^{\frac{1}{2}} \boldsymbol{e}_q)_{\mathcal{T}_h(\Omega_i)}| \\
&\le \|\kappa^{\frac{1}{2}} \nabla(u-\tilde{w})\|_0 \|\boldsymbol{e}_q\|_{\alpha}.
\end{aligned}
$$

Applying Young's inequality for each term and arranging them we complete the proof. □

To get an error estimate for $e_u$ we consider the dual problem: let $(\boldsymbol{\theta}, \phi)$ be the

solution of

$$\boldsymbol{\theta} + \nabla\phi = 0 \quad \text{in } \Omega, \tag{4.36a}$$

$$\nabla \cdot \boldsymbol{\theta} = e_u \quad \text{in } \Omega, \tag{4.36b}$$

$$\phi = 0 \quad \text{on } \partial\Omega. \tag{4.36c}$$

in a weak form: find $\boldsymbol{\theta} \in \mathbf{H}(div, \Omega)$ and $\phi \in L^2(\Omega)$ such that

$$(\boldsymbol{\theta}, \boldsymbol{\psi}) - (\phi, \nabla \cdot \boldsymbol{\psi}) = 0 \qquad \text{for all } \boldsymbol{\psi} \in \mathbf{H}(div, \Omega), \tag{4.37a}$$

$$(\nabla \cdot \boldsymbol{\theta}, w) = (e_u, w) \text{ for all } \quad w \in L^2(\Omega). \tag{4.37b}$$

We assume that the solution of this problem has full $H^2$ regularity and satisfies the a priori estimate

$$\|\phi\|_2 + \|\boldsymbol{\theta}\|_1 \leq C\|e_u\|_0, \tag{4.38}$$

where $C$ only depends on the domain $\Omega$. Notice here the permeability coefficient $\kappa$ is not in the equation, so the regularity assumption is quite reasonable.

Using the standard elliptic duality argument, we can establish the following result:

**Lemma 4.6.7.** *Let $(\boldsymbol{\theta}, \phi)$ be the solution of the dual problem* (4.36) *and Assumption 4.6.1 hold. Then we have*

$$\begin{aligned} \|e_u\|^2 =& (\alpha(\boldsymbol{q} - \boldsymbol{q}_h)\,,\, \boldsymbol{\Pi}_V\boldsymbol{\theta})_{\mathcal{T}_h} - \langle (I - P_H^{\partial})u\,,\, (\boldsymbol{\theta} - \boldsymbol{\Pi}_V\boldsymbol{\theta}) \cdot \boldsymbol{n}\rangle_{\partial\mathcal{T}_H} \\ &+ \langle e_u - e_{\widehat{u}}\,,\, (\boldsymbol{\theta} - \boldsymbol{\Pi}_V\boldsymbol{\theta}) \cdot \boldsymbol{n}\rangle_{\partial\mathcal{T}_H}, \end{aligned} \tag{4.39}$$

*Proof.* We begin by taking $w = e_u$ in the equation (4.37b) we get

$$\begin{aligned}\|e_u\|^2 = (e_u\,,\, e_u)_{\mathcal{T}_h} &= (e_u\,,\, \nabla\cdot\boldsymbol{\theta})_{\mathcal{T}_h} \\ &= (e_u\,,\, \nabla\cdot\boldsymbol{\Pi}_V\boldsymbol{\theta})_{\mathcal{T}_h} + (e_u\,,\, \nabla\cdot(\boldsymbol{\theta}-\boldsymbol{\Pi}_V\boldsymbol{\theta}))_{\mathcal{T}_h}.\end{aligned}$$

Integrating by parts in the second term, we have

$$\begin{aligned}\|e_u\|^2 &= (e_u\,,\, \nabla\cdot\boldsymbol{\Pi}_V\boldsymbol{\theta})_{\mathcal{T}_h} - (\nabla e_u\,,\, \boldsymbol{\theta}-\boldsymbol{\Pi}_V\boldsymbol{\theta})_{\mathcal{T}_h} + \langle e_u\,,\, (\boldsymbol{\theta}-\boldsymbol{\Pi}_V\boldsymbol{\theta})\cdot\boldsymbol{n}\rangle_{\partial\mathcal{T}_h} \\ &= (e_u\,,\, \nabla\cdot\boldsymbol{\Pi}_V\boldsymbol{\theta})_{\mathcal{T}_h} + \langle e_u\,,\, (\boldsymbol{\theta}-\boldsymbol{\Pi}_V\boldsymbol{\theta})\cdot\boldsymbol{n}\rangle_{\partial\mathcal{T}_h}\end{aligned}$$

where we used the property of the projection $\boldsymbol{\Pi}_V$, see equation (4.28b), and noting that $e_u \in \nabla\cdot\mathbf{V}_h$.

Taking $\boldsymbol{v} = \boldsymbol{\Pi}_V\boldsymbol{\theta}$ in the first error equation (4.32a), we observe that

$$\begin{aligned}(e_u\,,\, \nabla\cdot\boldsymbol{\Pi}_V\boldsymbol{\theta})_{\mathcal{T}_h} =& (\alpha(\boldsymbol{q}-\boldsymbol{q}_h)\,,\, \boldsymbol{\Pi}_V\boldsymbol{\theta})_{\mathcal{T}_h} + \langle (I-P_M)u\,,\, \boldsymbol{\Pi}_V\boldsymbol{\theta}\cdot\boldsymbol{n}\rangle_{\partial\mathcal{T}_h} \\ &+ \langle e_{\widehat{u}}\,,\, \boldsymbol{\Pi}_V\boldsymbol{\theta}\cdot\boldsymbol{n}\rangle_{\partial\mathcal{T}_h}.\end{aligned}$$

Now using the fact that $e_{\widehat{u}}$ and $(I-P_M)u$ are single valued on $\partial\mathcal{T}_h$ we get that

$$\langle e_{\widehat{u}}\,,\, \boldsymbol{\theta}\cdot\boldsymbol{n}\rangle_{\partial\mathcal{T}_h} = \langle (I-P_M)u\,,\, \boldsymbol{\theta}\cdot\boldsymbol{n}\rangle_{\partial\mathcal{T}_h} = 0$$

and after some algebraic manipulation we obtain

$$\begin{aligned}\|e_u\|^2 =& (\alpha(\boldsymbol{q}-\boldsymbol{q}_h)\,,\, \boldsymbol{\Pi}_V\boldsymbol{\theta})_{\mathcal{T}_h} + \langle (I-P_M)u\,,\, \boldsymbol{\Pi}_V\boldsymbol{\theta}\cdot\boldsymbol{n}\rangle_{\partial\mathcal{T}_h} \\ &+ \langle e_{\widehat{u}}\,,\, \boldsymbol{\Pi}_V\boldsymbol{\theta}\cdot\boldsymbol{n}\rangle_{\partial\mathcal{T}_h} + \langle e_u\,,\, (\boldsymbol{\theta}-\boldsymbol{\Pi}_V\boldsymbol{\theta})\cdot\boldsymbol{n}\rangle_{\partial\mathcal{T}_h} \\ &(\alpha(\boldsymbol{q}-\boldsymbol{q}_h)\,,\, \boldsymbol{\Pi}_V\boldsymbol{\theta})_{\mathcal{T}_h} - \langle (I-P_M)u\,,\, (\boldsymbol{\theta}-\boldsymbol{\Pi}_V\boldsymbol{\theta})\cdot\boldsymbol{n}\rangle_{\partial\mathcal{T}_h} \\ &+ \langle e_u - e_{\widehat{u}}\,,\, (\boldsymbol{\theta}-\boldsymbol{\Pi}_V\boldsymbol{\theta})\cdot\boldsymbol{n}\rangle_{\partial\mathcal{T}_h}.\end{aligned}$$

Then since for any $F \in \mathcal{E}_h^0$, $P_M = P_h^\partial$ and $\mathbf{\Pi}_V \boldsymbol{\theta} \cdot \boldsymbol{n}|_F \in M_h(F)$, we have

$$\langle (I - P_M)u \,,\, (\boldsymbol{\theta} - \mathbf{\Pi}_V \boldsymbol{\theta}) \cdot \boldsymbol{n} \rangle_{\partial \mathcal{T}_h} = \langle (I - P_H^\partial)u \,,\, (\boldsymbol{\theta} - \mathbf{\Pi}_V \boldsymbol{\theta}) \cdot \boldsymbol{n} \rangle_{\partial \mathcal{T}_H}.$$

and

$$\langle e_u - e_{\widehat{u}} \,,\, (\boldsymbol{\theta} - \mathbf{\Pi}_V \boldsymbol{\theta}) \cdot \boldsymbol{n} \rangle_{\partial \mathcal{T}_h} = \langle e_u - e_{\widehat{u}} \,,\, (\boldsymbol{\theta} - \mathbf{\Pi}_V \boldsymbol{\theta}) \cdot \boldsymbol{n} \rangle_{\partial \mathcal{T}_H}$$

In the last step we used that $\boldsymbol{e}_{\widehat{q}} \cdot \boldsymbol{n} = \boldsymbol{e}_q \cdot \boldsymbol{n} + \tau(e_u - e_{\widehat{u}})$ for all $F \in \mathcal{E}_h^0$. Therefore

$$\begin{aligned} \|e_u\|^2 = (\alpha(\boldsymbol{q} - \boldsymbol{q}_h) \,,\, \mathbf{\Pi}_V \boldsymbol{\theta})_{\mathcal{T}_h} &- \langle (I - P_H^\partial)u \,,\, (\boldsymbol{\theta} - \mathbf{\Pi}_V \boldsymbol{\theta}) \cdot \boldsymbol{n} \rangle_{\partial \mathcal{T}_H} \\ &+ \langle e_u - e_{\widehat{u}} \,,\, (\boldsymbol{\theta} - \mathbf{\Pi}_V \boldsymbol{\theta}) \cdot \boldsymbol{n} \rangle_{\partial \mathcal{T}_H} \end{aligned}$$

and this completes the proof. □

We are ready to state the estimate for $e_u$.

**Theorem 4.6.8.** *Suppose that $(\boldsymbol{\theta}, \phi)$ is the solution of the dual problem* (4.36) *and Assumption 4.6.1 holds. In addition, we also assume the H-regularity* (4.38) *holds. Then, we have*

$$\|e_u\| \leq C\|\boldsymbol{q} - \boldsymbol{q}_h\|_\alpha + C\left(\frac{h}{H}\right)^{\frac{1}{2}} \|e_u - e_{\widehat{u}}\|_\tau + C\left(\frac{h}{H}\right)^{\frac{1}{2}} \|u - P_H^\partial u\|_{\partial \mathcal{T}_H} \tag{4.40}$$

*Proof.* We shall use the identity of Lemma 4.6.7 and shall estimate the three terms separately. First, we note

$$\begin{aligned} (\alpha(\boldsymbol{q} - \boldsymbol{q}_h) \,,\, \mathbf{\Pi}_V \boldsymbol{\theta})_{\mathcal{T}_h} &= (\alpha(\boldsymbol{q} - \boldsymbol{q}_h) \,,\, \boldsymbol{\theta})_{\mathcal{T}_h} - (\alpha(\boldsymbol{q} - \boldsymbol{q}_h) \,,\, \boldsymbol{\theta} - \mathbf{\Pi}_V \boldsymbol{\theta})_{\mathcal{T}_h} \\ &\leq C\left(\|\boldsymbol{q} - \boldsymbol{q}_h\|_\alpha \|\boldsymbol{\theta}\|_0 + \|\boldsymbol{q} - \boldsymbol{q}_h\|_\alpha \|\boldsymbol{\theta} - \mathbf{\Pi}_V \boldsymbol{\theta}\|_0\right) \\ &\leq C\left(\|\boldsymbol{q} - \boldsymbol{q}_h\|_\alpha \|\boldsymbol{\theta}\|_0 + h\|\boldsymbol{q} - \boldsymbol{q}_h\|_\alpha \|\boldsymbol{\theta}\|_1\right) \end{aligned}$$

so that after using the full regularity assumption (4.38) and Lemma 4.6.2, we get

$$(\alpha(\boldsymbol{q}-\boldsymbol{q}_h)\,,\,\boldsymbol{\Pi}_V\boldsymbol{\theta})_{\mathcal{T}_h} \leq C\|\boldsymbol{q}-\boldsymbol{q}_h\|_\alpha\|e_u\|.$$

In order to bound the other two terms, we use the following estimate of Lemma 4.6.3:

$$\|(\boldsymbol{\theta}-\boldsymbol{\Pi}_V\boldsymbol{\theta})\cdot\boldsymbol{n}\|_{\partial\mathcal{T}_H} \leq Ch^{\frac{1}{2}}H^{-\frac{1}{2}}\|\boldsymbol{\theta}\|_1 \leq Ch^{\frac{1}{2}}H^{-\frac{1}{2}}\|e_u\|$$

and apply Cauchy-Schwarz inequality to obtain :

$$\langle(I-P_H^\partial)u\,,\,(\boldsymbol{\theta}-\boldsymbol{\Pi}_V\boldsymbol{\theta})\cdot\boldsymbol{n}\rangle_{\partial\mathcal{T}_H} \leq Ch^{\frac{1}{2}}H^{-\frac{1}{2}}\|u-P_H^\partial u\|_{\partial\mathcal{T}_H}\|e_u\|.$$

Thus

$$\begin{aligned}\langle e_u-e_{\widehat{u}}\,,\,(\boldsymbol{\theta}-\boldsymbol{\Pi}_V\boldsymbol{\theta})\cdot\boldsymbol{n}\rangle_{\partial\mathcal{T}_h} &\leq \tau^{-\frac{1}{2}}\|e_u-e_{\widehat{u}}\|_\tau\|(\boldsymbol{\theta}-\boldsymbol{\Pi}_V\boldsymbol{\theta})\cdot\boldsymbol{n}\|_{\partial\mathcal{T}_H}\\ &\leq C\tau^{-\frac{1}{2}}h^{\frac{1}{2}}H^{-\frac{1}{2}}\|e_u-e_{\widehat{u}}\|_\tau\|e_u\|.\end{aligned}$$

and the proof is completed by combining the above three estimates. □

### *4.6.4 Error estimates for specific examples*

The goal of this section is to derive the error estimate for a specific example introduced in Section 4.3. Since the error estimates depend on a local spectral problem, we present the error estimates for three different multiscale spaces.

#### *4.6.4.1 Error estimates for multiscale space II-a*

Now we present the error analysis of the multiscale space II-a introduced in Section 4.3.2.1. The main tolls are the estimates established in Theorem 4.6.6 and 4.6.8 which are independent of the choice of the multiscale space $M_H$. Thus, we

only need to estimate $\inf_{w\in M_H} \|\kappa^{\frac{1}{2}}(u-w)\|_{\partial\mathcal{T}_H}$. For this estimate, we shall use the properties of the local spectral problem (4.19).

For the estimate, we need the following assumption:

**Assumption 4.6.9.** *On each coarse neighborbood $\omega_i$ the exact solution on the common coarse face $\mathcal{E}_i$ has the following spectral expansion:*

$$u|_{\mathcal{E}_i} = \sum_j u_{ij}\psi_j^i, \tag{4.41}$$

*where $\psi_j^i$ is the $j$-th eigenfunction of the spectral problem (4.19) on $\omega_i$.*

**Remark 4.6.10.** *Strictly speaking, this assumption does not hold in general. What we can ensure in the general case is that there is a function $\widetilde{u}$ which differs from $u$ by higher order terms and that satisfies the above assumption. For example, such a function could be the solution of a standard Galerkin FEM on a fine mesh.*

**Lemma 4.6.11.** *Let the Assumption 4.6.9 be satisfied. Then we have*

$$\inf_{w\in M_h} \|\kappa^{\frac{1}{2}}(u-w)\|_{\partial\mathcal{T}_H} \leq C\left(\frac{H}{\Lambda_1^*}\right)^{\frac{1}{2}} \|\kappa^{\frac{1}{2}}\nabla u\|_{\Omega}. \tag{4.42}$$

*where $\Lambda_1^* = \min_{\omega_i} \lambda_{i,L_i+1}$.*

*Proof.* On each $F = \mathcal{E}_i \in \mathcal{E}_H$, we may write $u|_F$ as $u = \sum_{j=1}^n u_{ij}\psi_j^i$, and choose

$w \in M_H$ such as $w = \sum_{j=1}^{L_i} u_{ij}\psi_j^i$. Then, we have

$$
\begin{aligned}
\leq \|\kappa^{\frac{1}{2}}(u-w)\|_F &= \left\| \kappa^{\frac{1}{2}} \left( \sum_{j=L_i+1}^{n} u_{ij}\psi_j^i \right) \right\|_F \\
&\leq \sum_{j=L_i+1}^{n} u_{ij} \|\kappa^{\frac{1}{2}}\psi_j^i\|_F \quad (\text{by} \quad \alpha \leq 1) \\
&\leq \sum_{j=L_i+1}^{n} u_{ij} \left(\frac{H}{\lambda_{i,j}}\right)^{\frac{1}{2}} \|\kappa^{\frac{1}{2}}\nabla\psi_j^i\|_{\omega_i} \\
&\leq \left(\frac{H}{\lambda_{i,L_i+1}}\right)^{\frac{1}{2}} \left\| \kappa^{\frac{1}{2}}\nabla \left( \sum_{j=L_i+1}^{n} u_{ij}\psi_j^i \right) \right\|_{\omega_i} \\
&\leq \left(\frac{H}{\lambda_{i,L_i+1}}\right)^{\frac{1}{2}} \left\| \kappa^{\frac{1}{2}}\nabla \left( \sum_{j=1}^{n} u_{ij}\psi_j^i \right) \right\|_{\omega_i} \\
&= \left(\frac{H}{\lambda_{i,L_i+1}}\right)^{\frac{1}{2}} \|\kappa^{\frac{1}{2}}\nabla u\|_{\omega_i}
\end{aligned}
$$

Here we used the fact that for fixed $i$, $\{\psi_j^i\}$ are orthogonal in the inner products $(\kappa\cdot,\cdot)_F$, $F \subset \partial\omega_i$, and $(\kappa\cdot,\cdot)_{\omega_i}$. Finally, we obtain the estimate in the lemma by summing all coarse face $F$ and taking minimum of $\lambda_{i,L_i+1}$. □

**Theorem 4.6.12.** *Let Assumptions 4.6.1 and 4.6.9 hold and the local space be the type of* $\mathbf{HDG}_k$. *Then, we have*

$$
\|\boldsymbol{q} - \boldsymbol{q}_h\|_\alpha \leq Ch^s\|\boldsymbol{q}\|_s + Ch^s H^{-\frac{1}{2}} \left(\|\boldsymbol{q}\|_{s+1} + \|u\|_{s+1}\right) + C\left(\frac{H}{h\Lambda_1^*}\right)^{\frac{1}{2}} \|\kappa^{\frac{1}{2}}\nabla u\|_0,
$$

*for all* $1 \leq s \leq k+1$.

*Proof.* The first estimate of Theorem 4.6.6 and Lemma 4.6.11 gives directly the

following estimate for $\boldsymbol{e}_q$:

$$\begin{aligned}\|\boldsymbol{e}_q\|_\alpha + \|e_u - e_{\widehat{u}}\|_\tau \leq & Ch^s\|\boldsymbol{q}\|_s + Ch^s H^{-\frac{1}{2}}\|\boldsymbol{q}\|_{s+1} + Ch^s H^{-\frac{1}{2}}\|u\|_{s+1} \\ & + C\left(\frac{H}{h\Lambda_1^*}\right)^{\frac{1}{2}} \|\kappa^{\frac{1}{2}}\nabla u\|_0.\end{aligned}$$

The estimate of $\boldsymbol{q} - \boldsymbol{q}_h$ can be directly obtained by the triangle inequality by using local projection $\boldsymbol{\Pi}_V\boldsymbol{q}$ and its approximation properties:

$$\begin{aligned}\|\boldsymbol{q} - \boldsymbol{q}_h\|_\alpha \leq & \|\boldsymbol{q} - \boldsymbol{\Pi}_V\boldsymbol{q}\|_\alpha + \|\boldsymbol{\Pi}_V\boldsymbol{q} - \boldsymbol{q}_h\|_\alpha \\ \leq & Ch^s\|\boldsymbol{q}\|_s + Ch^s H^{-\frac{1}{2}}\left(\|\boldsymbol{q}\|_{s+1} + \|u\|_{s+1}\right) + C\left(\frac{H}{h\Lambda_1^*}\right)^{\frac{1}{2}} \|\kappa^{\frac{1}{2}}\nabla u\|_0.\end{aligned}$$

This completes the proof. □

Using Lemma 4.6.11 and Theorem 4.6.8, we get the following estimate for $u$:

**Theorem 4.6.13.** *Let Assumptions 4.6.1 and 4.6.9 hold and the local space be the type of* $\mathbf{HDG}_k$. *In addition, suppose that the* $H^2$*-regularity* (4.38) *holds. Then, we have*

$$\begin{aligned}\|u - u_h\| \leq & Ch^s\left(\|\boldsymbol{q}\|_s + \|u\|_s\right) + Ch^s H^{-\frac{1}{2}}\left(\|\boldsymbol{q}\|_{s+1} + \|u\|_{s+1}\right) \\ & + C\left(\frac{H}{h\Lambda_1^*}\right)^{\frac{1}{2}} \|\kappa^{\frac{1}{2}}\nabla u\|_0,\end{aligned}$$

*for all* $1 \leq s \leq k+1$.

*Proof.* By the theorem 4.6.8, we have

$$\|e_u\| \leq C\|\boldsymbol{q} - \boldsymbol{q}_h\|_\alpha + C\left(\frac{h}{H}\right)^{\frac{1}{2}} \|e_u - e_{\widehat{u}}\|_\tau + C\left(\frac{h}{H}\right)^{\frac{1}{2}} \|u - P_H^\partial u\|_{\partial\mathcal{T}_H}.$$

By the fact $h < H$, so the above bound can be obtained in the same manner as the

bound for $\|\boldsymbol{q}-\boldsymbol{q}_h\|_\alpha$. Therefore,

$$\begin{aligned}\|u-u_h\| \leq & \|u-\Pi_W u\|+\|\Pi_W u-u_h\| \\ \leq & Ch^s\Big(\|\boldsymbol{q}\|_s+\|u\|_s\Big)+Ch^s H^{-\frac{1}{2}}\Big(\|\boldsymbol{q}\|_{s+1}+\|u\|_{s+1}\Big) \\ & +C\left(\frac{H}{h\Lambda_1^*}\right)^{\frac{1}{2}}\|\kappa^{\frac{1}{2}}\nabla u\|_0.\end{aligned}$$

This completes the proof. □

**Corollary 4.6.14.** *Let Assumptions 4.6.1 and 4.6.9 hold and the local space be the type of* $\mathbf{HDG}_k$. *In addition, suppose that the* $H^2$ *regularity* (4.38) *holds. Then, we have*

$$\begin{aligned}\|\boldsymbol{q}-\boldsymbol{q}_h\|_\alpha+\|u-u_h\| \leq & Ch^s\left(\|\boldsymbol{q}\|_s+\|u\|_s\right)+Ch^s H^{-\frac{1}{2}}\left(\|\boldsymbol{q}\|_{s+1}+\|u\|_{s+1}\right) \\ & +C\left(\frac{H}{h\Lambda_1^*}\right)^{\frac{1}{2}}\|\kappa^{\frac{1}{2}}\nabla u\|_0,\end{aligned}$$

*for all* $1\leq s\leq k+1$.

**Remark 4.6.15.** *We note that due to the discontinuity of the permeability field* $\kappa$ *the solution* $u$ *(and also* $\boldsymbol{q}$*) have limited regularity. So in general,* $s\leq 1$.

#### *4.6.4.2 Error estimates for multiscale space II-b*

In this case, by the construction of the space $M_H$ in Section 4.3.2.2, we can see that for each $w\in M_H$ there is a function $\tilde{w}\in H^1(\Omega)$ such that $\tilde{w}|_{\mathcal{E}_H}=w$. In order to carry out the estimates for the case, we need some additional assumptions on the scheme.

**Assumption 4.6.16.** *On each fine grid element* $T$, *the stabilization operator* $\tau$ *is positive on only one face* $F\in\partial T$.

**Assumption 4.6.17.** *For any fine grid element $T$ adjacent to some subdomain $\partial\Omega_i$ on a face $F$, shared by $K$ and $\partial\Omega_i$, $\tau$ is strictly positive, i.e. $\tau|_F > 0$.*

Assumptions 4.6.16 and 4.6.17 are the key to obtain optimal approximation results with this space. In fact, without these two assumptions, we can still get some error estimates. However, the result will have a term with negative power of $h$ which is not desirable since $h$ is the finest scale.

As a consequence of Assumptions 4.6.16 and 4.6.17, the triangulation of each subdomain has to satisfy the requirement that each fine scale finite element $T \in \mathcal{T}_h$ can share at most one face with the coarse skeleton $\mathcal{E}_H$. This requirement impies that we need to put at least two fine elements to fill a corner of any subdomain. This suggests that we should use triangular (2D) or tetrahedral (3D) elements. In what follows, we restrict the choice of local spaces to be in Table 1. Notice that here we exclude the famous $\mathbf{BDM}_k$ space from the table. Roughly speaking, the reason is that in the case of $\mathbf{BDM}_k$ element, the local space $W(T) = P^{k-1}(T)$ is too small to provide a key property for the optimality of the error bound, see the following Lemma 4.6.18.

**Lemma 4.6.18.** *Let Assumptions 4.6.16 and 4.6.17 hold. Then*

*(a) on each subdomain $\Omega_i$, $\boldsymbol{e}_q \in \mathbf{H}(div, \Omega_i)$, $i = 1, \cdots, N$;*

*(b) $\|\nabla \cdot \boldsymbol{e}_q\|_{\Omega_i} = 0$, $i = 1, \cdots, N$;*

*(c) $\boldsymbol{e}_q \cdot \boldsymbol{n}|_F = \boldsymbol{e}_{\widehat{q}} \cdot \boldsymbol{n}|_F$, for all $F \in \mathcal{E}_h^0(\Omega_i)$, $i = 1, \cdots, N$.*

*Proof.* Now take any $\Omega_i$. To prove that $\boldsymbol{e}_q$ is $\mathbf{H}(div)$-conforming in $\Omega_i$, we need to show that $\boldsymbol{e}_q \cdot \boldsymbol{n}$ is continuous across all interior interfaces $F \in \mathcal{E}_h^0(\Omega_i)$. By the error equation (4.32c), we know that $\boldsymbol{e}_{\widehat{q}} \cdot \boldsymbol{n}$ is single valued on all interior interfaces due to the fact that $\boldsymbol{e}_{\widehat{q}} \cdot \boldsymbol{n}$ and the test function $\mu$ are in the same space $M_h(F)$. Hence, it

is suffices to show that

$$\boldsymbol{e}_q \cdot \boldsymbol{n}|_F = \boldsymbol{e}_{\widehat{q}} \cdot \boldsymbol{n}|_F, \quad \text{for all} \quad F \in \mathcal{E}_h^0(\Omega_i).$$

First of all, on each interior face $P_h^\partial = P_M$, together with the numerical trace (4.33), we have

$$\boldsymbol{e}_{\widehat{q}} \cdot \boldsymbol{n} = \boldsymbol{e}_q \cdot \boldsymbol{n} + \tau(e_u - e_{\widehat{u}}), \quad \text{for all} \quad F \in \mathcal{E}_h^0(\Omega_i).$$

From here we can see that $\boldsymbol{e}_q \cdot \boldsymbol{n}|_F = \boldsymbol{e}_{\widehat{q}} \cdot \boldsymbol{n}|_F$ if $\tau|_F = 0$. We only need to show that

$$\tau(e_u - e_{\widehat{u}})|_{F^*} = 0, \quad \text{for all} \quad F^* \in \partial T, \quad F^* \cap \mathcal{E}_H = \emptyset.$$

On any $T$ adjacent with $\mathcal{E}_H$, by our assumptions, $\tau > 0$ on $F^*$ where $F^*$ is on the boundary of $\Omega_i$. So, on the other faces $\tau = 0$ and hence $\boldsymbol{e}_{\widehat{q}} \cdot \boldsymbol{n} = \boldsymbol{e}_q \cdot \boldsymbol{n}$.

Let us consider an arbitrary interior element $T$ with $\tau > 0$ on $F^*$. We restrict the error equation (4.32b) on $T$, integrating by parts, we get

$$(\nabla \cdot \boldsymbol{e}_q, w)_T + \langle \boldsymbol{e}_{\widehat{q}} \cdot \boldsymbol{n} - \boldsymbol{e}_q \cdot \boldsymbol{n}, w \rangle_{\partial T} = -\langle (I - P_M)(\boldsymbol{q} \cdot \boldsymbol{n}), w \rangle_{\partial T}.$$

By (4.33) and the fact that $P_M = P_h^\partial$ on $\partial T$, we have

$$(\nabla \cdot \boldsymbol{e}_q, w)_T + \langle \tau(e_u - e_{\widehat{u}}), w \rangle_{\partial T} = 0.$$

Since $\tau > 0$ only on $F^*$, we have

$$(\nabla \cdot \boldsymbol{e}_q, w)_T + \langle \tau(e_u - e_{\widehat{u}}), w \rangle_{F^*} = 0.$$

Now let $w \in P^k(T)$ be such that

$$\begin{aligned} (w, r)_T &= (\nabla \cdot \boldsymbol{e}_q, r)_T, \quad \text{for all} \;\; r \in P^{k-1}(T), \\ \langle w, \mu \rangle_{F^*} &= \langle w, e_u - e_{\widehat{u}} \rangle_{F^*}, \quad \text{for all} \;\; \mu \in P^k(F^*). \end{aligned} \tag{4.43}$$

One can easily see that such $w \in P^k(T)$ exists and is unique. Indeed, this is a square system for the coefficients of the polynomial $w$ and it is sufficient to show that the homogeneous system has only a trivial solution. On $F^*$ the equation $\langle w, \mu \rangle_{F^*} = 0$ represents a square homogeneous system for the trace $w|_{F^*} \in P^k(F^*)$. This ensures that the trace is identically zero on $F^*$. Without loss of generality, we can assume that $F^*$ is in the hyperplane $x_1 = 0$. Then obviously $w = x_1 \tilde{w}$ with $\tilde{w} \in P^{k-1}(T)$ and now $(x_1 \tilde{w}, r)_T = 0$ for all $r \in P^{k-1}(T)$ implies $\tilde{w} = 0$. Then we plug $w$ into the above error equation and notice that $\nabla \cdot \boldsymbol{e}_q \in P^{k-1}(T)$, $e_u - e_{\widehat{u}} \in P^k(F^*)$ to get

$$(\nabla \cdot \boldsymbol{e}_q, \nabla \cdot \boldsymbol{e}_q)_T + \langle \tau(e_u - e_{\widehat{u}}), e_u - e_{\widehat{u}} \rangle_{F^*} = 0.$$

This implies

$$\nabla \cdot \boldsymbol{e}_q|_T = 0, \quad e_u - e_{\widehat{u}}|_{F^*} = 0$$

and hence $\boldsymbol{e}_q \cdot \boldsymbol{n}|_F = \boldsymbol{e}_{\widehat{q}} \cdot \boldsymbol{n}|_F$ for all $F \in \mathcal{E}_h^0(\Omega_i)$. Consequently, $\boldsymbol{e}_q \in \mathbf{H}(div, \Omega_i)$, $i = 1, \cdots, N$.

To finish, we still need to show that $\nabla \cdot \boldsymbol{e}_q|_T = 0$ when $T$ is adjacent with the boundary of $\Omega_i$. Similarly as interior element $T$, error equation (4.32b) gives

$$(\nabla \cdot \boldsymbol{e}_q, w)_T + \langle \tau(e_u - e_{\widehat{u}}), w \rangle_{F^*} = 0.$$

Take $w$ to be again the unique element in $P^k(T)$ such as

$$(w, r)_T = (\nabla \cdot \boldsymbol{e}_q, r)_T, \quad \text{for all} \ \ r \in P^{k-1}(T),$$
$$\langle w, \mu \rangle_{F^*} = 0, \quad \text{for all} \ \ \mu \in P^k(F^*).$$

The second equation implies that $w = 0$ on $F^*$, we have

$$(\nabla \cdot \boldsymbol{e}_q, w)_T + \langle \tau(e_u - e_{\widehat{u}}), w \rangle_{F^*} = (\nabla \cdot \boldsymbol{e}_q, \nabla \cdot \boldsymbol{e}_q)_T = 0$$

and hence $\nabla \cdot \boldsymbol{e}_q = 0$. This completes the proof. □

**Remark 4.6.19.** *The above proof cannot be applied for* $\mathbf{BDM}_k$*. Namely, a key step is the special choice of* $w$ *which satisfies* (4.43)*. In the case of* $\mathbf{BDM}_k$*,* $w$ *is in a smaller space* $P^{k-1}(T)$*, hence the existence of* $w$ *is no longer valid.*

By Lemma 4.6.18, we can use the second estimate of Theorem 4.6.6. As we can see in the estimate, we only need to estimate two terms $\|\kappa^{\frac{1}{2}} \nabla(u - \tilde{w})\|_\Omega$ and $\|u - w\|_{\partial \mathcal{T}_H}$. For these estimates, we recall the local spectral problem :

Find $\psi^{\text{aux},i} \in X_h(\omega_i)$ such that

$$\begin{aligned} \int_{\omega_i} \kappa(x) \nabla \psi^{\text{aux},i} \nabla z dx = \lambda \int_{\omega_i} \tilde{\kappa} \psi^{\text{aux},i} z dx, \quad \text{for all} \quad \in X_h(\omega_i) \\ \text{with} \quad \tilde{\kappa} := \kappa \sum_{l=1}^{N_v} |\nabla \chi_l|^2, \end{aligned} \tag{4.44}$$

where $\chi_l$ form partition of unity. See Figure 10 for the coarse neighborhood $\omega_i$.

We need the following assumption about the exact solution regarding the space spanned by the spectral functions $\psi_j^{\text{aux},i}$, $j = 1, \ldots, N_i$.

**Assumption 4.6.20.** *On each coarse neighborhood* $\omega_i$ *the exact solution has the*

*following spectral expansion* $u(x) = \sum_{j=1}^{N_i} u_{ij}\psi_j^{aux,i}(x) \quad x \in \omega_i$.

Next we define the local interpolant $I_0u$ to be the first $L_i$ terms in the expansion:

$$I_0u = \sum_{j=1}^{L_i} u_{ij}\psi_j^{\text{aux},i}. \tag{4.45}$$

For estimating the error for the multiscale method we shall need a bound for the "interpolation" error $\|\kappa^{\frac{1}{2}}\nabla(u - I_0u)\|_{L^2(\Omega)}$. Such a bound was provided in [34] under a condition similar to the Assumption 4.6.20. Although the method in [34] is based on the continuous multiscale methods, we can easily modify the error estimates due to the same local spectral problems and coarse neighborhoods. Now we state the estimate for the term $\|\kappa^{\frac{1}{2}}\nabla(u - I_0u)\|_{L^2(\Omega)}$.

**Lemma 4.6.21.** *Under Assumption 4.6.20, we have*

$$\|\kappa^{\frac{1}{2}}\nabla(u - I_0u)\|_{L^2(\Omega)} \leq C\left(\frac{1}{\Lambda_2^*}\right)^{\frac{1}{2}} \|\kappa^{\frac{1}{2}}\nabla u\|_{L^2(\Omega)} + CH\|g\|_{L^2_\alpha(\Omega)}, \tag{4.46}$$

*where* $\Lambda_2^* = \min_{\omega_i} \lambda_{i,L_i+1}$ *and* $g$ *is the following residual associated with the interplant* $I_0u$ *defined by* (4.45)*:*

$$-\nabla \cdot (\kappa\nabla(u - I_0u)) = g. \tag{4.47}$$

*Proof.* Let $N_v$ be the total number of coarse vertices and let $I_0u$ be the local interpolant and depends on $\omega_i$. Then, we have

$$\begin{aligned}\|\kappa^{\frac{1}{2}}\nabla(u - I_0u)\|^2_{L^2(\Omega)} &\leq \sum_{i=1}^{N_v}\int_{\omega_i} \kappa|\nabla(\chi_i(u - I_0u))|^2 \\ &\leq \sum_{i=1}^{N_v}\int_{\omega_i} \kappa|\nabla\chi_i|^2(u - I_0u)^2 + \sum_{i=1}^{N_v}\int_{\omega_i} \kappa\chi_i^2|\nabla(u - I_0u)|^2.\end{aligned}$$

Multiplying both sides of the equation (4.47) by $\chi_i^2(u - I_0u)$ and taking integration by parts, we have

$$\int_{\omega_i} \kappa\chi_i^2|\nabla(u - I_0u)|^2 + 2\int_{\omega_i} \kappa\chi_i\nabla\chi_i(\nabla(u - I_0u))(u - I_0u) = \int_{\omega_i} g\chi_i^2(u - I_0u).$$

From here, we easily deduce

$$\begin{aligned}\int_{\omega_i} \kappa\chi_i^2|\nabla(u - I_0u)|^2 &\leq \int_{\omega_i} \kappa|\nabla\chi_i|^2(u - I_0u)^2 + \int_{\omega_i} g\chi_i^2(u - I_0u) \\ &\leq \int_{\omega_i} \kappa|\nabla\chi_i|^2(u - I_0u)^2 + \int_{\omega_i} |\nabla\chi_i|^{-2}\alpha g^2.\end{aligned}$$

Consequently,

$$\int_{\omega_i} \kappa|\nabla(\chi_i(u - I_0u))|^2 \leq 2\int_{\omega_i} \kappa|\nabla\chi_i|^2(u - I_0u)^2 + \int_{\omega_i} |\nabla\chi_i|^{-2}\alpha g^2.$$

By Assumption 4.6.20, we obtain

$$\begin{aligned}\int_{\omega_i} \kappa|\nabla\chi_i|^2(u - I_0u)^2 &\leq \int_{\omega_i} \kappa\sum_j |\nabla\chi_j|^2(u - I_0u)^2 = \int_{\omega_i} \tilde{\kappa}(u - I_0u)^2 \\ &\leq \frac{1}{\lambda_{i,L_i+1}}\int_{\omega_i} \kappa|\nabla(u - I_0u)|^2 \leq \frac{1}{\lambda_{i,L_i+1}}\|\kappa^{\frac{1}{2}}\nabla u\|^2_{L^2(\omega_i)}.\end{aligned}$$

Also, since $|\nabla\chi_i| \leq CH^{-1}$, we get

$$\int_{\omega_i} |\nabla\chi_i|^{-2}\alpha g^2 \leq CH^2\|g\|^2_{L^2_\alpha(\omega_i)}.$$

Finally, we obtain the estimates in the lemma by summing to $N_v$ with minimum of $\lambda_{i,L_i+1}$. □

The following lemma show the estimate of the only term left, namely, $\|u-w\|_{\partial\mathcal{T}_H}$.

**Lemma 4.6.22.** *We have*

$$\|u-w\|_{\partial\mathcal{T}_H} \leq CH^{\frac{1}{2}} \sum_{i=1}^{N_v} \|\nabla(\chi_i u - \tilde{w}_i)\|_{\omega_i},$$

*where* $\tilde{w} = \sum_{i=1}^{N_v} \tilde{w}_i$ *and* $\tilde{w}_i|_F = w \in M_H(F)$.

*Proof.* Let $N_v$ be the total number of coarse vertices. Then, we have

$$\begin{aligned}
\|u-w\|_{\partial\mathcal{T}_H} &= \left\| \sum_{i=1}^{N_v} \chi_i u - \tilde{w} \right\|_{\partial\mathcal{T}_H} = \left\| \sum_{i=1}^{N_v} \chi_i u - \sum_{i=1}^{N_v} \tilde{w}_i \right\|_{\partial\mathcal{T}_H} \\
&\leq \sum_{i=1}^{N_v} \sum_{j=1}^{4} \|\chi_i u - \tilde{w}_i\|_{\partial\Omega_j} \\
&\leq \sum_{i=1}^{N_v} \sum_{j=1}^{4} \left( H^{\frac{1}{2}} \|\nabla(\chi_i u - \tilde{w}_i)\|_{\Omega_j} + H^{-\frac{1}{2}} \|\chi_i u - \tilde{w}_i\|_{\Omega_j} \right) \\
&\leq 4 \sum_{i=1}^{N_v} \left( H^{\frac{1}{2}} \|\nabla(\chi_i u - \tilde{w}_i)\|_{\omega_i} + H^{-\frac{1}{2}} \|\chi_i u - \tilde{w}_i\|_{\omega_i} \right).
\end{aligned}$$

Note that $\chi_i u - \tilde{w}_i = 0$ on $\partial\omega_i$. By Poincaré inequality, we have

$$\|\chi_i u - \tilde{w}_i\|_{\omega_i} \leq CH \|\nabla(\chi_i u - \tilde{w}_i)\|_{\omega_i}.$$

Inserting this inequality into the estimate above, we complete the proof. □

As a consequence from the second estimate of Theorem 4.6.6 and Lemma 4.6.18 and 4.6.21, we have the following error estimate for $\boldsymbol{q}$:

**Theorem 4.6.23.** *Let Assumptions 4.6.1, 4.6.16, 4.6.17, and 4.6.20 hold and the*

*local space be the type of* $\mathbf{HDG}_k$*. Then,*

$$\begin{aligned}\|\boldsymbol{q}-\boldsymbol{q}_h\|_\alpha \leq & Ch^s\|\boldsymbol{q}\|_s + Ch^s H^{-\frac{1}{2}}\left(\|\boldsymbol{q}\|_{s+1}+\|u\|_{s+1}\right)\\ & + C\left(\frac{1}{\Lambda_2^*}\right)^{\frac{1}{2}}\|\kappa^{\frac{1}{2}}\nabla u\|_0 + CH\|g\|_{L^2_\alpha(\Omega)},\end{aligned}$$

*for all* $1 \leq s \leq k+1$*.*

Similarly, with the above results and Theorem 4.6.8, we have the error estimate for $u$ as following :

**Theorem 4.6.24.** *Let Assumptions 4.6.1, 4.6.16, 4.6.17, and 4.6.20 hold and the local space be the type of* $\mathbf{HDG}_k$*. We also assume the* $H^2$*-regularity* (4.38) *holds. Then, we have*

$$\begin{aligned}\|u-u_h\| \leq & Ch^s\left(\|\boldsymbol{q}\|_s+\|u\|_s\right) + Ch^s H^{-\frac{1}{2}}\left(\|\boldsymbol{q}\|_{s+1}+\|u\|_{s+1}\right)\\ & + C\left(\frac{1}{\Lambda_2^*}\right)^{\frac{1}{2}}\|\kappa^{\frac{1}{2}}\nabla u\|_0 + CH\|g\|_{L^2_\alpha(\Omega)},\end{aligned}$$

*for all* $1 \leq s \leq k+1$*.*

#### *4.6.4.3 Error estimates for multiscale space III*

In this section, we will present the error analysis of the multiscale space III in Section 4.3.3. In this case, we assume that the permeability coefficient is bounded, that is, there exists some positive constant $\kappa_0, \kappa_1$ such that $0 < \kappa_0 \leq \kappa(x) \leq \kappa_1$. Similarly, we will use Theorems 4.6.6 and 4.6.8. Like multiscale space II-a, we need only the estimates of $\|\kappa^{\frac{1}{2}}(u-w)\|_{\partial\mathcal{T}_H}$. Now, we recall the equivalent version of the local spectral problem and the $L^2-$projection onto $V^{\text{snap}}(\Omega_i)|_F$:

$$\int_{\partial K}\kappa\frac{\partial\psi_i}{\partial\boldsymbol{n}}v ds = \frac{\lambda_i}{H}\int_{\partial K}\psi_i v ds,$$

and

$$P_{snap}(\kappa\frac{\partial\psi_i}{\partial\boldsymbol{n}}) = \frac{\lambda_i}{H}\psi_i.$$

Here $P_{snap}$ is the $L^2-$projection onto $V^{\text{snap}}(\Omega_i)|_F$, for all $F \in \partial\Omega_i$.

For the estimate, we consider consider the following assumption:

**Assumption 4.6.25.** *On each coarse neighborbood $\omega_i$, we assume that the exact solution on the a coarse face $\mathcal{E}_i$ has the spectral expansion as:*

$$u|_{\mathcal{E}_i} = \sum_j u_{ij}\psi_j^i, \tag{4.48}$$

*where $\psi_j^i$ is the $j$-th eigenfunction of the above spectral problem on chess board type $\omega_i$. See Figure 11 for $\omega_i$ and $\mathcal{E}_i$.*

**Lemma 4.6.26.** *Under Assumption 4.6.25, for any coarse face $F$, we have*

$$\inf_{w\in M_H} \|\kappa^{\frac{1}{2}}(u-w)\|_{\partial\mathcal{T}_H} \leq C\kappa_1^{\frac{1}{2}}\frac{H}{\Lambda_3^*}\left\|\kappa\frac{\partial u}{\partial\boldsymbol{n}}\right\|_{\partial\mathcal{T}_H}. \tag{4.49}$$

*where $\Lambda_3^* = \min_{\omega_i}\lambda_{i,L_i+1}$.*

*Proof.* On each coarse boundary$\partial\Omega_i \in \mathcal{E}_H$, we may write $u$ as $u = \sum_{j=1}^n u_{ij}\psi_j^i$, and choose $w \in M_H$ such as $w = \sum_{j=1}^{L_i} u_{ij}\psi_j^i$. Then, we have

$$\kappa_1^{\frac{1}{2}}\|(u-w)\|_{\partial\Omega_i} = \kappa_1^{\frac{1}{2}}\left\|\left(\sum_{j=L_i+1}^n u_{ij}\psi_j^i\right)\right\|_{\partial\Omega_i} = \kappa_1^{\frac{1}{2}}\sum_{j=L_i+1}^n u_{ij}\|\psi_j^i\|_{\partial\Omega_i}$$

Using the fact that the eigenfunctions are orthogonal on $\partial\Omega_i$. By the property of

$P_{snap}$, we have

$$\begin{aligned}
\|\kappa^{\frac{1}{2}}(u-w)\|_{\partial\Omega_i} &\leq \kappa_1^{\frac{1}{2}} \sum_{j=L_i+1}^{n} u_{ij} \frac{H}{\lambda_{i,j}} \left\| P_{\text{snap}} \left( \kappa \frac{\partial \psi_j^i}{\partial \boldsymbol{n}} \right) \right\|_{\partial\Omega_i} \\
&\leq \kappa_1^{\frac{1}{2}} \frac{H}{\lambda_{i,L_i+1}} \sum_{j=L_i+1}^{n} \left\| P_{\text{snap}} \left( \kappa u_{ij} \frac{\partial \psi_j^i}{\partial \boldsymbol{n}} \right) \right\|_{\partial\Omega_i} \\
&\leq \kappa_1^{\frac{1}{2}} \frac{H}{\lambda_{i,L_i+1}} \sum_{j=1}^{n} \left\| P_{\text{snap}} \left( \kappa u_{ij} \frac{\partial \psi_j^i}{\partial \boldsymbol{n}} \right) \right\|_{\partial\Omega_i} \\
&= \kappa_1^{\frac{1}{2}} \frac{H}{\lambda_{i,L_i+1}} \left\| \kappa \frac{\partial u}{\partial \boldsymbol{n}} \right\|_{\partial\Omega_i}
\end{aligned}$$

Here we used the fact that $\{\psi_j^i\}$ is an orthogonal basis set in terms of $\|\kappa^{\frac{1}{2}} \cdot\|_F$ and $\|\kappa^{\frac{1}{2}} \cdot\|_{\omega_i}$. Finally, we obtain the estimate in the lemma by summing all coarse boundary $\partial\Omega_i$ and taking minimum of $\lambda_{i,L_i+1}$. □

Now we are ready to state our main error estimate for $\boldsymbol{q}$:

**Theorem 4.6.27.** *Let Assumptions 4.6.1 and 4.6.25 hold and the local space be the type of* $\mathbf{HDG}_k$*. Then, we have*

$$\begin{aligned}
\|\boldsymbol{q} - \boldsymbol{q}_h\|_\alpha \leq Ch^s \|\boldsymbol{q}\|_s + Ch^s H^{-\frac{1}{2}} \left( \|\boldsymbol{q}\|_{s+1} + \|u\|_{s+1} \right) \\
+ C \left( \frac{\kappa_1}{h} \right)^{\frac{1}{2}} \left( \frac{H}{\Lambda_3^*} \right) \left\| \kappa \frac{\partial u}{\partial \boldsymbol{n}} \right\|_{\partial \mathcal{T}_H},
\end{aligned}$$

*for all* $1 \leq s \leq k+1$.

In a similar way, using a standard duality argument and Theorem 4.6.8, we can show that $L^2-$ error for $u$.

**Theorem 4.6.28.** *Let Assumptions 4.6.1 and 4.6.25 hold and the local space be the type of* $\mathbf{HDG}_k$*. In addition, Suppose that the* $H^2$*-regularity* (4.38) *holds. Then, we*

*have*

$$\|u - u_h\| \leq Ch^s \left(\|\boldsymbol{q}\|_s + \|u\|_s\right) + Ch^s H^{-\frac{1}{2}} \left(\|\boldsymbol{q}\|_{s+1} + \|u\|_{s+1}\right) + C\left(\frac{\kappa_1}{h}\right)^{\frac{1}{2}} \left(\frac{H}{\Lambda_3^*}\right) \left\|\kappa \frac{\partial u}{\partial \boldsymbol{n}}\right\|_{\partial \mathcal{T}_H},$$

*for all* $1 \leq s \leq k+1$.

# 5. EXTENSION OF GENERALIZED MULTISCALE HDG METHODS

In many applications, time dependent problems with nonlinear permeability fields are required for flow simulations through heterogeneous porous media. In this chapter, we extend generalized multiscale hybridizable discontinuous Galerkin (GMsHDG) methods to nonlinear and time dependent problems. This extension, as the GMsHDG methods for linear elliptic equations, has two main ingredients: deriving upscaling structure and generating multiscale spaces. As a model we consider the following initial value problem for nonlinear parabolic differential equation

$$u_t(x,t) - \nabla \cdot (\kappa(x,u)\nabla u(x,t)) = f(x,t), \quad \text{in} \quad \Omega \times (0,t_F], \tag{5.1a}$$

$$u(x,t) = 0, \quad \text{on} \quad \partial\Omega \times (0,t_F], \tag{5.1b}$$

$$u(x,0) = 0, \quad \text{on} \quad \Omega. \tag{5.1c}$$

Here, $\kappa(x,u) \geq \kappa_0 > 0$ is a heterogeneous coefficient, $\Omega$ is a bounded polyhedral domain in $\mathbb{R}^n, n = 2, 3$, and $t_F$ is a final time. Non-homogeneous initial and boundary conditions are handled in the same way.

To extend GMsHDG methods to nonlinear time dependent problems, we modify the general framework for constructing the multiscale space proposed in Chapter 4 and provide a specific example of this. Within this space, we present a number of representative numerical experiments for linear and nonlinear parabolic problems. The numerical results demonstrate that the errors for both of them decay as increasing the dimension of the coarse space, which is similar to linear elliptic problems. In the analysis, we investigate the stability which is independent the choice of multiscale spaces with space discretization. We also derive error estimates for the linear

parabolic equation based on space discretization (semi-discretization). We note that as a product of our considerations in the section we also get the case of nonlinear steady-state problem. This is the case when the right-hand side $f$ does not depend on time $t$ and the process reaches gets to the asymptotic state, when the solution does not change in time.

## 5.1 GMsHDG method for nonlinear parabolic equation

The purpose of this section is to design the GMsHDG method to approximate the model problem (5.1). As before we rewrite (5.1) as

$$\alpha(x,u)\boldsymbol{q}(x,t) + \nabla u(x,t) = 0 \qquad \text{in} \quad \Omega \times (0,t_F], \tag{5.2a}$$

$$u_t(x,t) + \nabla \cdot \boldsymbol{q}(x,t) = f(x,t) \quad \text{in} \quad \Omega \times (0,t_F], \tag{5.2b}$$

$$u(x,t) = 0 \qquad \text{on} \quad \partial\Omega \times (0,t_F], \tag{5.2c}$$

$$u(x,0) = 0 \qquad \text{on} \quad \Omega, \tag{5.2d}$$

where $\alpha(x,u) = \kappa^{-1}(x,u)$.

Similarly, we utilize the concept of two-grid approximation, i.e., fine and coarse grids, introduced in Chapter 3 and 4, in order to present the multiscale finite element approximation. We use notation from Sobolev spaces and norms in used in Chapter 4. Additionally, we denote $\|\cdot\|_{X(0,t_F;Y(\Omega))}$ by $\|\cdot\|_{X(Y)}$. For instance, we will use $L^\infty(L^2)$ and $L^2(H^s), s \geq 0$ for numerical experiments and error estimates.

### *5.1.1 Multiscale finite element spaces*

In Chapter 4, we introduce the multiscale finite element spaces, $W_h, \boldsymbol{V}_h$, and $M_{h,H}$ for the linear elliptic equation. Similar to the elliptic equation, we focus on construction of the multiscale space $M_H$. The multiscale space $M_H$ generated in the elliptic problem can be used in a linear time-dependent problem, but not nonlinear

one. So, we further will focus on construction of the multiscale space $M_H$ for nonlinear problems. To construct the multiscale space $M_H$ for nonlinear problems, we slightly modify general framework of linear $M_H$ spaces proposed in Section 4.3.2.1. The framework in elliptic problems consists of the following three steps: (1) Define partitions $\mathcal{E}_i$ and $\omega_i$, (2) Generate the local snapshot space, and (3) Form the multiscale space. Similar to this process, we construct the framework for building the nonlinear multiscale space $M_H$. The main idea of this construction is linearization, so we can use the framework of linear problems. To linearize the nonlinear term, we deal with a nonlinear coefficient as a parameter dependent one, that is $\kappa(u_h) = \kappa(\eta)$. This approach will be used to present upscaling structure for nonlinear problems in the next section.

Now we construct the $M_H$ space for nonlinear problems. First, we define a set of a coarse face $\mathcal{E}_i$ and the coresponding coarse neighborhood $\omega_i$ with the same process of the linear case. The remaining steps are slightly modified the comparing to linear ones. To generate the local snapshot space in the linear framework, we introduce two cases: (1) all fine-grid functions and (2) local solutions of the snapshot problem as basis functions for the snapshot space. We also use all fine-grid basis functions as basis functions of the snapshot space in nonlinear problems. However, to generate the snapshot space by using local solutions, we need to propose the following local problems depending on the input parameters. For each coarse neighborhood $\omega_i$, we consider the local solution $\phi_l$ such that

$$\nabla \cdot (\kappa(\eta)\nabla\phi_l) = 0 \quad \text{in} \quad \omega_i, \quad \phi_l = \delta_l \quad \text{on} \quad \partial\omega_i, \tag{5.3}$$

where $\delta_l$ is a continuous piecewise linear function defined on $\partial\omega_i$ such that $\delta(x_l) = 1$ and vanished on all other boundary nodes.

The last step for the nonlinear frame is to find basis functions of $M_H$ space by solving a local spectral problems. Within the choice of snapshot spaces, we solve a spectral problems such as

$$\boldsymbol{A}(\overline{\eta})\psi = \lambda \boldsymbol{M}(\overline{\eta})\psi.$$

Here $\boldsymbol{A}(\overline{\eta})$ and $\boldsymbol{M}(\overline{\eta})$ are modified matrices of $\boldsymbol{A}$ and $\boldsymbol{M}$ introduced in Section 4.2 by using a parameter dependent coefficient $\kappa(x, \eta)$.

Finally, we define the multiscale space $M_H$ after arranging and choosing of eigenfunctions according to the order of eigenvalues and restricting the functions to coarse face $\mathcal{E}_i$ with the same procedure.

Now we give a specific example of $M_H$ which is similar to one introduced in Section 4.3.2.1. We define $\mathcal{E}_i$ as a single coarse face and $\omega_i$ as the union of two coarse element sharing the face $\mathcal{E}_i$, referring to Figure 9. The snapshot space consist of all fine-grid functions and thus the local spectral problem is solved directly on a fine grid. Now we solve the local spectral problem in a coarse neighborhood $\omega_i$. Let $X_h(\Omega_i)$ be the conforming finite element space of continuous piece-wise linear function in $\mathcal{T}_h(\omega_i)$. For each coarse neighborhood $\omega_i$ and the common face $\mathcal{E}_i$, we find $\lambda$ and $\psi \in X_h(\Omega_i)$ such that

$$\int_{\omega_i} \kappa(x, \overline{\eta}) \nabla\psi \nabla z dx = \frac{\lambda}{H} \int_{\mathcal{E}_i} \tilde{\kappa}(x, \overline{\eta}), \quad \text{for all} \quad z \in X_h(\omega_i),$$

where $\kappa(x, \overline{\eta})$ and $\tilde{\kappa}(x, \overline{\eta})$ are domain-based averaged coefficients with $\overline{\eta}$ chosen as the average of $\eta$. Also, $\tilde{\kappa}(x, \overline{\eta})$ is the harmonic average of coefficients $\kappa_1(x, \overline{\eta})$ and $\kappa_2(x, \overline{\eta})$ of two coarse blocks sharing the common face $\mathcal{E}_i$. We define the multiscale space $M_H$ with arrangement and restriction in the framework.

We note that this example of $M_H$ will be only used in Numerical tests and analysis

because we are able to extend to another multiscale spaces with the similar steps.

### *5.1.2 Upscale structure of GMsHDG methods*

The multiscale HDG method is: Find $(u_h(t), \boldsymbol{q}_h(t), \widehat{u}_{h,H}(t)) \in W_h \times \boldsymbol{V}_h \times M_{h,H}$, $t \in (0, t_F]$, such that

$$(\alpha(u_h)\boldsymbol{q}_h(t)\,,\,\boldsymbol{v})_{\mathcal{T}_h} - (u_h(t)\,,\,\nabla\cdot\boldsymbol{v})_{\mathcal{T}_h} + \langle\widehat{u}_{h,H}(t)\,,\,\boldsymbol{v}\cdot\boldsymbol{n}\rangle_{\partial\mathcal{T}_h} = 0, \tag{5.4a}$$

$$(\partial_t u_h(t)\,,\,w)_{\mathcal{T}_h} - (\boldsymbol{q}_h(t)\,,\,\nabla w)_{\mathcal{T}_h} + \langle\widehat{\boldsymbol{q}}_{h,H}(t)\cdot\boldsymbol{n}\,,\,w\rangle_{\partial\mathcal{T}_h} = (f(t)\,,\,w)_{\mathcal{T}_h}, \tag{5.4b}$$

$$\langle\widehat{\boldsymbol{q}}_{h,H}(t)\cdot\boldsymbol{n}\,,\,\mu\rangle_{\partial\mathcal{T}_h} = 0, \tag{5.4c}$$

$$\widehat{u}_{h,H}(t) = 0,\ x \in \partial\Omega, \tag{5.4d}$$

$$u_h(0) = 0,\ x \in \Omega, \tag{5.4e}$$

for all $(w, \boldsymbol{v}, \mu) \in W_h \times \boldsymbol{V}_h \times M_h$, with a numerical flux defined

$$\widehat{\boldsymbol{q}}_{h,H}(t)\cdot\boldsymbol{n} = \boldsymbol{q}_h(t)\cdot\boldsymbol{n} + \tau(u_h(t) - \widehat{u}_{h,H}(t)) \quad \text{on} \quad \partial\mathcal{T}_h. \tag{5.4f}$$

**Remark 5.1.1.** *Since $u_h$ and $\boldsymbol{q}_h$ are functions defined on the the space-time $\Omega \times (0, t_F]$. Then, it is convenient to consider $u_h$ and $\boldsymbol{q}_h$ as functions of the only time variable with values in a HDG spaces $W_h$ and $\boldsymbol{V}_h$, respectively. For any time $t \in (0, t_F]$, we consider $u_h$ and $\boldsymbol{q}_h$ in such a way that*

$$u_h(t) \equiv u_h(\cdot, t) \in W_h, \quad \boldsymbol{q}_h(t) \equiv \boldsymbol{q}_h(\cdot, t) \in \boldsymbol{V}_h.$$

Let $\Delta t$ be the time step, taken to be constant for simplicity and such that $t_F = N \times \Delta t$ where $N$ is an integer. For $n \in \{0, \cdots, N\}$, we define the discrete time $t^n := n \times \Delta t$.

The multiscale HDG method with backward-Euler scheme is:

Find $(u_h(t^n), \boldsymbol{q}_h(t^n), \widehat{u}_{h,H}(t^n)) \in W_h \times \boldsymbol{V}_h \times M_{h,H}$, $n \in \{1, \cdots, N\}$, such that

$$(\alpha(u_h(t^n))\boldsymbol{q}_h(t^n)\,,\,\boldsymbol{v})_{\mathcal{T}_h} - (u_h(t^n)\,,\,\nabla\cdot\boldsymbol{v})_{\mathcal{T}_h} + \langle\widehat{u}_{h,H}(t^n)\,,\,\boldsymbol{v}\cdot\boldsymbol{n}\rangle_{\partial\mathcal{T}_h} = 0, \tag{5.5a}$$

$$\left(\frac{u_h(t^n) - u_h(t^{n-1})}{\Delta t}, w\right)_{\mathcal{T}_h} - (\boldsymbol{q}_h(t^n)\,,\,\nabla w)_{\mathcal{T}_h} + \langle\widehat{\boldsymbol{q}}_{h,H}(t^n)\cdot\boldsymbol{n}\,,\,w\rangle_{\partial\mathcal{T}_h} = (f(t^n)\,,\,w)_{\mathcal{T}_h}, \tag{5.5b}$$

$$\langle\widehat{\boldsymbol{q}}_{h,H}(t^n)\cdot\boldsymbol{n}\,,\,\mu\rangle_{\partial\mathcal{T}_h} = 0, \tag{5.5c}$$

$$\widehat{u}_{h,H}(t^n)|_{x\in\partial\Omega} = 0, \tag{5.5d}$$

$$u_h(t^0)|_{x\in\Omega} = 0, \tag{5.5e}$$

for all $(w, \boldsymbol{v}, \mu) \in W_h \times \boldsymbol{V}_h \times M_h$, with a numerical flux defined

$$\widehat{\boldsymbol{q}}_{h,H}(t^n)\cdot\boldsymbol{n} = \boldsymbol{q}_h(t^n)\cdot\boldsymbol{n} + \tau(u_h(t^n) - \widehat{u}_{h,H}(t^n)) \quad \text{on} \quad \partial\mathcal{T}_h. \tag{5.5f}$$

First, we propose the upscale structure for the linear parabolic problem, i.e., $\alpha(u_h(t^n)) = \alpha$. With the same procedure in elliptic problems, we split (5.5c) into two equations by testing separately with $\mu \in M_h^0$ and $\mu \in M_H$ so that

$$\langle\widehat{\boldsymbol{q}}_{h,H}(t^n)\cdot\boldsymbol{n}\,,\,\mu\rangle_{\partial\mathcal{T}_h} = 0 \quad \text{for all} \quad \mu \in M_h^0, \tag{5.6a}$$

$$\langle\widehat{\boldsymbol{q}}_{h,H}(t^n)\cdot\boldsymbol{n}\,,\,\mu\rangle_{\partial\mathcal{T}_H} = 0 \quad \text{for all} \quad \mu \in M_H. \tag{5.6b}$$

On any subdomain $\Omega_i$, given the boundary data of $\widehat{u}_{h,H}(t^n) = \xi_H$ for $\xi_H|_F \in M_H(F)$, $F \in \mathcal{E}_H(\Omega_i)$, we can solve for $(\boldsymbol{q}_h(t^n), u_h(t^n), \widehat{u}_{h,H}(t^n))|_{\Omega_i}$ by restricting the

equations (5.5a)-(5.5e):

$$
\begin{aligned}
(\alpha \boldsymbol{q}_h(t^n)\,,\, v)_{\mathcal{T}_h(\Omega_i)} - (u_h(t^n)\,,\, \nabla\cdot v)_{\mathcal{T}_h(\Omega_i)} + \langle \widehat{u}_{h,H}(t^n)\,,\, \boldsymbol{v}\cdot\boldsymbol{n}\rangle_{\partial\mathcal{T}_h(\Omega_i)} &= 0,\\
\frac{1}{\Delta t}(u_h(t^n)\,,\, w)_{\mathcal{T}_h(\Omega_i)} - (\boldsymbol{q}_h(t^n)\,,\, \nabla w)_{\mathcal{T}_h(\Omega_i)} + \langle \widehat{\boldsymbol{q}}_{h,H}(t^n)\cdot\boldsymbol{n}\,,\, w\rangle_{\partial\mathcal{T}_h(\Omega_i)} &= (\tilde{f}(t^n)\,,\, w)_{\mathcal{T}_h(\Omega_i)},\\
\langle \widehat{\boldsymbol{q}}_{h,H}(t^n)\cdot\boldsymbol{n}\,,\, \mu\rangle_{\partial\mathcal{T}_h(\Omega_i)} &= 0,\\
\widehat{u}_{h,H}(t^n) &= \xi_H,\ x\in\partial\Omega_i,\\
u_h(0) &= 0,\ x\in\Omega_i,
\end{aligned}
$$

for all $(w,\boldsymbol{v},\mu)\in W_h\times\boldsymbol{V}_h\times M_h^0|_{\mathcal{E}_h^0(\Omega_i)}$ with numerical flux $\widehat{\boldsymbol{q}}_{h,H}(t)$ in (5.5f). Here, $\tilde{f}(t^n) := f(t^n) + \frac{1}{\Delta t}u_h(t^{n-1})$. By superposition principle, the solution of the system (5.5) can be split into two parts, namely,

$$
\begin{aligned}
&(\boldsymbol{q}_h(t^n), u_h(t^n), \widehat{u}_{h,H}(t^n))\\
&\qquad = (\boldsymbol{q}_h(t^n;\tilde{f}), u_h(t^n;\tilde{f}), \widehat{u}_{h,H}(t^n;\tilde{f})) + (\boldsymbol{q}_h(t^n;\xi_H), u_h(t^n;\xi_H), \widehat{u}_{h,H}(t^n;\xi_H))
\end{aligned}
$$

where $(\boldsymbol{q}_h(t^n;\tilde{f})), u_h(t^n;\tilde{f})), \widehat{u}_{h,H}(t^n;\tilde{f})))$ is a solution of the above system with $\xi_H = 0$ and $(\boldsymbol{q}_h(t^n;\xi_H), u_h(t^n;\xi_H), \widehat{u}_{h,H}(t^n;\xi_H))$ is a solution with $\tilde{f}(t^n) = 0$.

Then, the equation of (5.6b) reduces to finding $\xi_H(t^n)\in M_H$ such that

$$
a(\xi_H(t^n),\mu) = l(\mu) \quad \text{for all} \quad \mu\in M_H, \quad n\in\{1,\cdots,N\} \tag{5.7}
$$

where

$$
a(\xi_H(t^n),\mu) := \langle \widehat{\boldsymbol{q}}_{h,H}(t^n;\xi_H)\,,\, \mu\rangle_{\partial\mathcal{T}_H} \quad \text{and} \quad l(\mu) := -\langle \widehat{\boldsymbol{q}}_{h,H}(t^n;\tilde{f})\,,\, \mu\rangle_{\partial\mathcal{T}_H}.
$$

We note that the choice of discretization techniques for time dependent problems is not unique, and we could choose any of the popular time discretization techniques

such as forward or backward Euler methods, Crank-Nicolson method or a multistep methods. However, since the problem (5.1) has high contrast, any explicit method will be a subject to a unreasonably restrictive Courant time step condition.

Now we present upscale structure for nonlinear problems. In this case, we cannot use the above structure immediately due to absence of the superposition principle. To figure out this shortcoming, we consider linearizing of the problem and use an iterative technique for obtaining the solution. To linearize the problems, we consider a nonlinear permeability coefficient as a parameter dependent one, that is, $\alpha(u_h) = \alpha(\eta)$.

Then, we can apply the structure derived for linear problems. However, we need to use an iterative method to find the solution of nonlinear problems with linear structure. An example of iterative techniques is Picard iteration which is considered in this chapter. In this method, we use a previous solution to update the solution at the current iteration step. To find a final solution, we use a suitable tolerance between the current and previous iteration.

We note that the same procedure can be applied for non-homogeneous boundary condition $u(x,t) = g$ and initial condition $u(x,0) = u_0$.

Considering parameter dependent coefficient and Picard iterative method, the equation (5.7) reduces to find $\xi_H^{k+1}$ such that

$$a^k(\xi_H^{k+1}, \mu) = l^k(\mu) \quad \text{for all} \quad \mu \in M_H, \tag{5.8}$$

where

$$a^k(\xi_H(t^n), \mu) := \langle \widehat{\boldsymbol{q}}_{h,H}^k(t^n; \xi_H)\,,\, \mu\rangle_{\partial\mathcal{T}_H} \quad \text{and} \quad l^k(\mu) := -\langle \widehat{\boldsymbol{q}}_{h,H}^k(t^n; \tilde{f})\,,\, \mu\rangle_{\partial\mathcal{T}_H}.$$

Here, $n$ is an iteration steps, $\widehat{\boldsymbol{q}}_{h,H}^{k}(t^n;\xi_H)$ and $\widehat{\boldsymbol{q}}_{h,H}^{k}(t^n;\tilde{f})$ are numerical traces computed in $k$-th iterative step.

## 5.2 Numerical experiments

In this section, we discuss the results obtained on a number of representative numerical tests. Similarly, we compute the coarse-grid solution and study the error with respect to the reference solution on the domain $\Omega = (0,1)^2$ with the same partitions. In order to apply the GMsHDG method, we consider the local finite element space $(W_h, \boldsymbol{V}_h, M_h)$ of the type of $\mathbf{HDG}_1$ and the multiscale space $M_H$ constructed in the previous section. to apply the GMsHDG method.

### *5.2.1 Linear time-dependent problem*

In this section is to present some numerical results for linear parabolic equations. We consider the solution of equation (5.1) with $f = 1$ and linear coefficient $\kappa(x,u) = \kappa(x)$. We also use the stabilization parameter $\tau_f = 1$ and $\tau_c = h$ on each fine and coarse edges, respectively. We test the methods on two different permeability fields in Figure 12 with $\eta = 10^4$.

We report the relative $L^\infty(L^2)$-error for the pressure $\|u_h^* - u_H\|_{L^\infty(L^2)}$ and the relative weighted $L^\infty(L^2)$-error for the velocity $\|\boldsymbol{q}_h^* - \boldsymbol{q}_H\|_{L^\infty(L^2_a)}$. Here $(u_h^*, \boldsymbol{q}_h^*)$ is a reference solution and $(u_H, \boldsymbol{q}_H)$ is a coarse solution obtained using the multiscale space proposed in the Section 4.3.2.1. For a time-discretization, we consider backward Euler methods with the finial time $t_F = 1$ and the time step size $dt = 1/100$.

The result for the errors with Topology 1 is presented in Table 13 for $h = 1/100$ and $H = 1/10$. We report the dimension of the coarse spaces for each time $t$ denoted by "Dim" because the solutions for time steps $t_n$ and $t_{n+1}$ are computed in coarse spaces of the same dimension. We observe that the errors decay when the dimension of the coarse spaces increase. When we use a coarse space with the dimension of

720, we observe that the errors of the solution and the velocity are 1.1% and 11.1%, respectively.

Table 13: Numerical results for linear parabolic equation applied to permeability field of Topology 1 with increasing dimension of the coarse space, $h = 1/100, H = 1/10, \eta = 10^4$. "Dim." stands for the dimension of the coarse space at time $t$.

| Dim. | $\|u_h^* - u_H\|_{L^\infty(L^2)}$ | $\|\boldsymbol{q}_h^* - \boldsymbol{q}_H\|_{L^\infty(L^2_\alpha)}$ |
|---|---|---|
| 180 | 0.6456 | 0.9526 |
| 360 | 0.1159 | 0.3164 |
| 540 | 0.0376 | 0.1996 |
| 720 | 0.0109 | 0.1105 |
| 900 | 0.0084 | 0.0963 |
| 1080 | 0.0049 | 0.0689 |

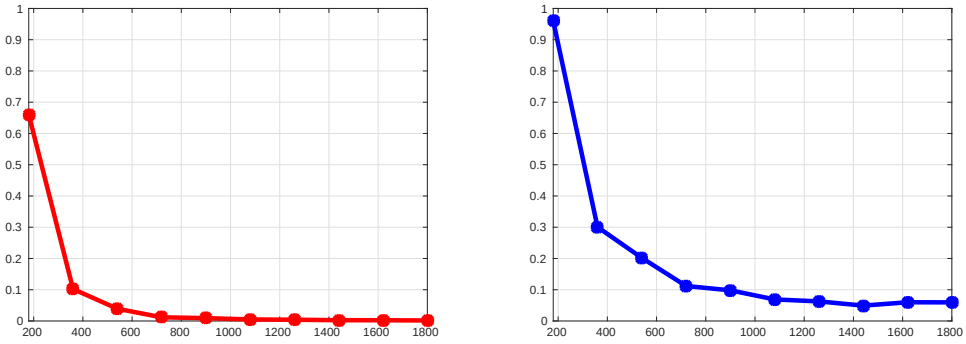


(a) Solution error (b) Velocity error

Figure 18: Numerical results for the linear parabolic equation applied to permeability field of Topology 2, $h = 1/100, H = 1/10$, $\eta = 10^4$ and increasing dimension of the coarse space. "Dim." stands for the dimension of the coarse space for each time $t$. The graphs show the relative solution error $\|u_h^* - u_H\|_{L^\infty(L^2)}$ and the relative velocity error $\|\boldsymbol{q}_h^* - \boldsymbol{q}_H\|_{L^\infty(L^2_\alpha)}$ vs. the dimension of the coarse space.

The numerical results for Topology 2 are presented in Figure 18 where solution

and velocity errors are depicted. We note that the convergence behavior is similar to Topology 1 case.

### *5.2.2 Nonlinear problem*

In this section, we solve nonlinear problems using GMsHDG formulations described in Section 5.1. We first consider the following nonlinear elliptic equation

$$-\nabla \cdot (\kappa(x,u)\nabla u(x)) = f, \quad \text{in} \quad \Omega, \tag{5.9a}$$

$$u(x,t) = 0, \quad \text{on} \quad \partial\Omega. \tag{5.9b}$$

with $f = 1$. For the nonlinear coefficient $\kappa(x,u)$, we consider two different cases: (1) $\kappa(x,u) = \kappa_1(x)\exp(u(x))$ – nonlinear separable coefficient; (2) $\kappa(x,u) = \exp(\kappa_2(x)u(x))$ – non-separable coefficient . For the coefficients $\kappa_1(x)$ and $\kappa_2(x)$, we use high contrast permeability field of Topology 1 as illustrated Figure 12 with $\eta = 10^4$ and $\eta = 10$, respectively. Further, we use $f = 1$ and the stabilization parameter $\tau_f = 1$ and $\tau_c = h$ on each fine and coarse edges, respectively.

To solve nonlinear equation (5.9), we use a Picard iterative technique. In particular, we take the initial guess $u^0 = 0$ and terminate the iterative loop when $\|a^{n+1}(\xi_H^{n+1}) - l^n\| \leq \delta\|l^n\|$, where $a^{n+1}$ and $l^n$ are defined in the previous section. Also, $\delta$ is the tolerance for the iteration and we select $\delta = 10^{-3}$.

The results for the computation of errors with the separable and nonseparable coefficients are presented in Table 14 and 15. Similar to the linear case, we observe that the errors decay when increasing the coarse dimension. For example, when we use the coarse space with the dimension of 720, we see that the solution errors for the separable and nonseparable coefficients are 3.7% and 5.2%, and the velocity

Table 14: Numerical results for nonlinear elliptic equation with separable coefficient $\kappa(x,u) = \kappa_1(x)\exp(u(x))$, $h = 1/100, H = 1/10, \eta = 10^4$ and increasing dimension of the coarse space. "Dim." stands for the dimension of the coarse space.

| Dim. | $\|u_h^* - u_H\|_{L^2(\Omega)}$ | $\|\boldsymbol{q}_h^* - \boldsymbol{q}_H\|_{L^2_{\mathcal{A}}(\Omega)}$ |
|---|---|---|
| 180 | 0.6417 | 0.8027 |
| 360 | 0.0744 | 0.2435 |
| 540 | 0.0651 | 0.2199 |
| 720 | 0.0368 | 0.1616 |
| 900 | 0.0198 | 0.1196 |
| 1080 | 0.0113 | 0.0918 |

Table 15: Numerical results for nonlinear elliptic equation with nonseparable coefficient $\kappa(x,u) = \exp(\kappa_1(x)\exp(u(x))$, $h = 1/100, H = 1/10, \eta = 10$ and increasing dimension of the coarse space. "Dim." stands for the dimension of the coarse space.

| Dim. | $\|u_h^* - u_H\|_{L^2(\Omega)}$ | $\|\boldsymbol{q}_h^* - \boldsymbol{q}_H\|_{L^2_{\mathcal{A}}(\Omega)}$ |
|---|---|---|
| 180 | 0.7195 | 0.8492 |
| 360 | 0.1235 | 0.3231 |
| 540 | 0.0776 | 0.2513 |
| 720 | 0.0516 | 0.2018 |
| 900 | 0.0282 | 0.1500 |
| 1080 | 0.0208 | 0.1259 |

errors are 16.2% and 20.2%, respectively. The errors are computed with respect to the fine-grid solution obtained by solving a system of dimension $60,000$. We note that the errors with nonseparable coefficient are slightly bigger than the errors with separable one. Also, the Picard iteration converges in 4 or 5 steps for all cases.

Figure 19 illustrates the effect of increasing the dimension of the coarse space for nonlinear elliptic equation with nonseparable coefficient $\exp(\kappa_1(x)u(x))$. We report the fine-scale solution and multiscale solution computed with three different coarse dimension.

Now we consider the nonlinear parabolic equation (5.1). We also consider the non-

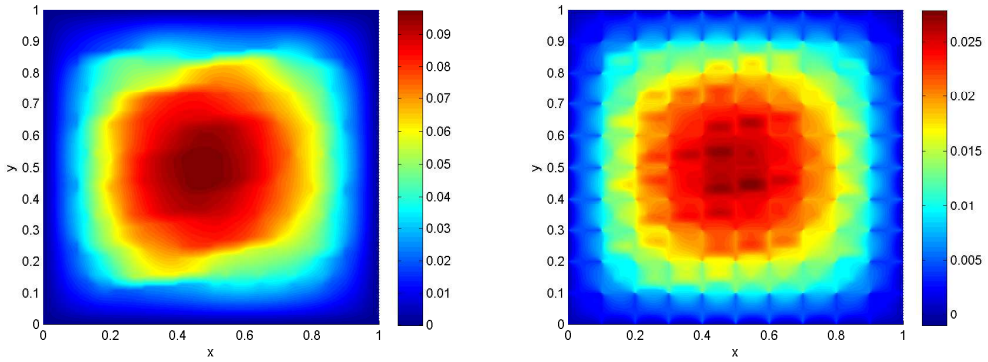

(a) Fine-scale solution (b) Multiscale solution with Dim.= 180

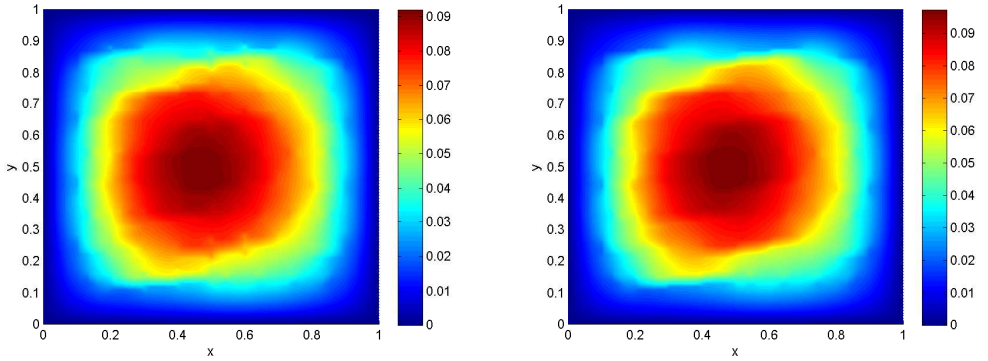

(c) Multiscale solution with Dim.= 720 (d) Multiscale solution with Dim.= 1800

Figure 19: Comparison of the multiscale solutions with the reference (fine-scale) solution for nonseparable elliptic problem.

Table 16: Numerical results for the nonlinear parabolic equation with nonseparable coefficient $\kappa(x,u) = \exp(\kappa_1(x)\exp(u(x))$, $h = 1/100, H = 1/10, \eta = 10$ and increasing dimension of the coarse space. "Dim." stands for the dimension of the coarse space at time $t$.

| Dim. | $\|u_h^* - u_H\|_{L^\infty(L^2)}$ | $\|\boldsymbol{q}_h^* - \boldsymbol{q}_H\|_{L^\infty(L^2_\alpha)}$ |
|---|---|---|
| 180 | 0.7157 | 0.8655 |
| 360 | 0.0750 | 0.3537 |
| 540 | 0.0350 | 0.2902 |
| 720 | 0.0320 | 0.2460 |

linear nonseparable coefficient used in the previous test, i.e., $\kappa(x,u) = \exp(\kappa_2(x)u(x))$ and $f = 1$. We repeat the detailed numerical study described in previous section. Table 16 show the results for computation of the pressure and the velocity error for $h = 1/100$ and $H = 1/10$. Similarly, we report the dimension of the coarse spaces for each time step. Similar to the linear case, we observe a reasonable error decay when increasing the coarse dimension.

## 5.3 Stability analysis for the semi-discretization

The goal of this section is to ensure the solvability of the system (5.4). To do this, we need Assumptions 4.5.1 and 4.5.2 on the stability parameter $\tau$ introduced in Section 4.5. The following theorem holds in both of linear and nonlinear cases on the condition of $\alpha > 0$. Also, the stability is independent of the choice of multiscale spaces.

**Theorem 5.3.1.** *Let Assumptions 4.5.1 and 4.5.2 be satisfied. Then for any $t \in (0, t_F]$ and $f$, the system* (5.4) *has a unique solution.*

*Proof.* Note that the system (5.4) is a square system for any time $t$. It is enough to show that the homogeneous system has only the trivial solution for any time $t$. Now we assume that $(u_h(t), \boldsymbol{q}_h(t), \widehat{u}_{h,H}(t))$ is the solution of (5.4). Taking $(w, \boldsymbol{v}, \mu) = (u_h(t), \boldsymbol{q}_h(t), \widehat{u}_{h,H}(t))$ in (5.4a)-(5.4c) and adding all equations, we get after some algebraic manipulation,

$$(\alpha(u_h)\boldsymbol{q}_h(t)\,,\,\boldsymbol{q}_h(t))_{\mathcal{T}_h} + (\partial_t u_h(t)\,,\,u_h(t))_{\mathcal{T}_h} + \langle \widehat{\boldsymbol{q}}_{h,H}(t)\cdot\boldsymbol{n} - \boldsymbol{q}_h(t)\cdot\boldsymbol{n}\,,\,u_h(t) - \widehat{u}_{h,H}(t)\rangle_{\partial\mathcal{T}_h} = 0.$$

By the definition of the numerical traces (5.4f), we have

$$(\alpha(u_h)\boldsymbol{q}_h(t)\,,\,\boldsymbol{q}_h(t))_{\mathcal{T}_h} + \frac{1}{2}\frac{d}{dt}\|u_h(t)\|^2 + \langle \tau(u_h(t) - \widehat{u}_{h,H}(t))\,,\,u_h(t) - \widehat{u}_{h,H}(t)\rangle_{\partial\mathcal{T}_h} = 0$$

and since $\alpha(u_h) > 0$, $\tau \geq 0$, and $u_h(0) = 0$, we get

$$\boldsymbol{q}_h(t) = \mathbf{0}, \quad u_h(t) = 0, \quad \text{and} \quad \tau(u_h(t) - \widehat{u}_{h,H}(t)) = 0,$$

for any time $t \in (0, t_F]$.

For any $F^* \in \partial T$, we have $\widehat{u}_{h,H}(t) = 0$ on $F^*$. For $F \in \partial T \backslash F^*$, we consider the equation (5.4a)

$$\langle \widehat{u}_{h,H}(t)\,,\, \boldsymbol{v} \cdot \boldsymbol{n} \rangle_{\partial \mathcal{T}_h} = 0, \quad \text{for all} \quad \boldsymbol{v} \in \boldsymbol{V}_h$$

since $u_h(t) = 0$ and $\boldsymbol{q}_h(t) = 0$. Now we take this over an element $T$, we get

$$\langle \widehat{u}_{h,H}(t), \boldsymbol{v} \cdot \boldsymbol{n} \rangle_{\partial T} = 0, \quad \text{for all} \quad \boldsymbol{v} \in \boldsymbol{V}(T).$$

By Assumption 4.5.1, there is $\boldsymbol{v} \in \boldsymbol{V}_h$ such that

$$\boldsymbol{v} \cdot \boldsymbol{n}|_F = \widehat{u}_{h,H}(t), \quad \text{for all} \quad F \in \partial T \backslash F^*.$$

This implies that for any time $t$, $\widehat{u}_{h,H}(t) = 0$ on $\partial T \backslash F^*$.

Next, on each $F_H \in \mathcal{E}_h$, we assume that $F_H \subset \overline{\Omega}_1 \cap \overline{\Omega}_2$, if $F_H \subset \partial\Omega$ then $F_H \subset \partial\Omega_1$. By Assumption 4.5.2, there exists $T_1 \in \mathcal{T}_h(\Omega_1), T_2 \in \mathcal{T}_h(\Omega_2)$ adjacent to $F_H$ such that $\tau > 0$ on $F_j = \partial T_j \cap F_H, j = 1, 2$. Then, we have

$$\widehat{u}_{h,H}(t) - u_h(t) = 0 \quad \text{on} \quad F_j, \quad j = 1, 2.$$

This implies that $\widehat{u}_{h,H}(t)|_{F_H} = 0$ and this completes the proof. □

**Theorem 5.3.2.** *Let $u_h(t)$ be the solution of* (5.4) *and let the Assumptions 4.5.1*

*and 4.5.2 be satisfied. Then we have*

$$\|u_h\|_{L^\infty(L^2)} \leq C\left(\int_0^{t_F} \|f(t)\|^2 dt\right)^{\frac{1}{2}} \quad \textit{and} \quad \|\boldsymbol{q}_h\|_{L^2(L^2_\alpha)} \leq C\left(\int_0^{t_F} \|f(t)\|^2 dt\right)^{\frac{1}{2}}.$$

*Proof.* Taking $(w, \boldsymbol{v}, \mu) = (u_h(t), \boldsymbol{q}_h(t), \widehat{u}_{h,H}(t))$ in (5.4a)-(5.4c) and adding all equations, we get after some algebraic manipulation,

$$\begin{aligned}(\alpha(u_h)\boldsymbol{q}_h(t)\,,\,\boldsymbol{q}_h(t))_{\mathcal{T}_h} + (\partial_t u_h(t)\,,\,u_h(t))_{\mathcal{T}_h} \\ + \langle \widehat{\boldsymbol{q}}_{h,H}(t)\cdot\boldsymbol{n} - \boldsymbol{q}_h(t)\cdot\boldsymbol{n}\,,\,u_h(t) - \widehat{u}_{h,H}(t)\rangle_{\partial\mathcal{T}_h} = (f(t)\,,\,u_h(t))_{\mathcal{T}_h}.\end{aligned}$$

By the definition of the numerical traces (5.4f), we have

$$\begin{aligned}(\alpha(u_h)\boldsymbol{q}_h(t)\,,\,\boldsymbol{q}_h(t))_{\mathcal{T}_h} + \frac{1}{2}\frac{d}{dt}\|u_h(t)\|^2_{L^2} \\ + \langle \tau(u_h(t) - \widehat{u}_{h,H}(t))\,,\,u_h(t) - \widehat{u}_{h,H}(t)\rangle_{\partial\mathcal{T}_h} = (f(t)\,,\,u_h(t))_{\mathcal{T}_h}.\end{aligned}$$

Using Cauchy-Schwarz and Young's inequality, we observe that

$$|(f(t)\,,\,u_h(t))_{\mathcal{T}_h}| \leq \frac{1}{2}\left(\|f(t)\|^2 + \|u_h(t)\|^2\right).$$

Integrating in time over the interval $(0,t)$ and using $u_h(0) = 0$ and the above results, we get

$$\begin{aligned}\|u_h(t)\|^2_{L^2} + 2\int_0^t \|\boldsymbol{q}_h(s)\|^2_{L^2_\alpha} ds + 2\int_0^t \|u_h(s) - \widehat{u}_{h,H}(s)\|^2_\tau ds \\ \leq \int_0^t \|f(s)\|^2_{L^2} ds + \int_0^t \|u_h(s)\|^2_{L^2} ds.\end{aligned}$$

Using Gronwall's lemma,

$$\|u_h(t)\|^2_{L^2} \leq C\int_0^t \|f(s)\|^2 ds \quad \text{for all} \quad t \in (0, t_F]$$

and

$$\int_0^t \|\boldsymbol{q}_h(s)\|_{L^2_\alpha}^2 ds \leq C \int_0^t \|f(s)\|^2 ds \quad \text{for all} \quad t \in (0, t_F].$$

Taking the maximum, we get the inequalities of the Lemma and this completes the proof. □

## 5.4 Error analysis of the HDG for linear parabolic equations

The purpose of this section is to analyze an approximation of the linear parabolic problem (5.1) using GMsHDG method for space semi-discretization. From the developed earlier schemes for elliptic problem, we know that different choices of multiscale spaces results in different convergent rates. So, we derive the error estimates for a specific example of multiscale spaces introduced in Section 4.3.2.1. This procedure can be used also for other constructions of multiscale spaces.

### *5.4.1 Error equations*

We begin by obtaining the error equations we shall use in the analysis. The main idea is to work with the following projection errors:

$$\begin{aligned}
\boldsymbol{e}_q(t) &:= \boldsymbol{\Pi}_V \boldsymbol{q}(t) - \boldsymbol{q}_h(t), \\
e_u(t) &:= \Pi_W u(t) - u_h(t), \\
\boldsymbol{e}_{\widehat{q}}(t) \cdot \boldsymbol{n} &:= P_M(\boldsymbol{q}(t) \cdot \boldsymbol{n}) - \widehat{\boldsymbol{q}}_{h,H}(t) \cdot \boldsymbol{n}, \\
e_{\widehat{u}}(t) &:= P_M u(t) - \widehat{u}_{h,H}(t).
\end{aligned}$$

Further, we define

$$\delta_u(t) := u(t) - \Pi_W u(t), \quad \boldsymbol{\delta}_q(t) := \boldsymbol{q}(t) - \boldsymbol{\Pi}_V \boldsymbol{q}(t).$$

**Remark 5.4.1.** *The errors defined in the above are functions of time variable $t$.*

*However, There are no values of the variable t which affect the proof of error estimates except initial time $t = 0$. In order to simplify the notations and to make short equations, we will omit the variable $t$.*

**Remark 5.4.2.** *Here we present error analysis for the semidiscrete case just to simplify the presentation. We feel the fully discrete method will be handled in the similar manner.*

**Lemma 5.4.3.** *Let Assumption 4.6.1 be satisfied. Then, for a linear coefficient $\alpha$, we have*

$$\begin{aligned}
(\alpha \boldsymbol{e}_q\,,\,\boldsymbol{v})_{\mathcal{T}_h} - (e_u\,,\,\nabla\cdot\boldsymbol{v})_{\mathcal{T}_h} + \langle e_{\widehat{u}}\,,\,\boldsymbol{v}\cdot\boldsymbol{n}\rangle_{\partial\mathcal{T}_h} =\ & -(\alpha\boldsymbol{\delta}_q\,,\,\boldsymbol{v})_{\mathcal{T}_h} \\
& -\langle (I-P_M)u\,,\,\boldsymbol{v}\cdot\boldsymbol{n}\rangle_{\partial\mathcal{T}_h} && \text{(5.10a)}\\
(\partial_t e_u\,,\,w)_{\mathcal{T}_h} - (\boldsymbol{e}_q\,,\,\nabla w)_{\mathcal{T}_h} + \langle \boldsymbol{e}_{\widehat{q}}\cdot\boldsymbol{n}\,,\,w\rangle_{\partial\mathcal{T}_h} =\ & -(\partial_t\delta_u\,,\,w)_{\mathcal{T}_h} \\
& -\langle (I-P_M)(\boldsymbol{q}\cdot\boldsymbol{n})\,,\,w\rangle_{\partial\mathcal{T}_h}, && \text{(5.10b)}\\
\langle \boldsymbol{e}_{\widehat{q}}\cdot\boldsymbol{n}\,,\,\mu\rangle_{\partial\mathcal{T}_h} =\ & 0, && \text{(5.10c)}\\
e_{\widehat{u}}|_{\partial\Omega} =\ & 0, && \text{(5.10d)}\\
e_u|_{t=0} =\ & 0, && \text{(5.10e)}
\end{aligned}$$

*for all $(w,\boldsymbol{v},\mu)\in W_h\times\boldsymbol{V}_h\times M_{h,H}$. Here $I$ is the identity operator. Moreover,*

$$\boldsymbol{e}_{\widehat{q}}\cdot\boldsymbol{n} = \boldsymbol{e}_q\cdot\boldsymbol{n} + \tau(e_u - e_{\widehat{u}}) - (P_h^{\partial} - P_M)(\boldsymbol{q}\cdot\boldsymbol{n} + \tau u) \quad \text{on} \quad \partial\mathcal{T}_h. \tag{5.10f}$$

*Proof.* Let us begin by noting that the exact solution $(u, \boldsymbol{q})$ obviously satisfies

$$\begin{aligned}(\alpha\boldsymbol{q}\,,\,\boldsymbol{v})_{\mathcal{T}_h} - (u\,,\,\nabla\cdot\boldsymbol{v})_{\mathcal{T}_h} + \langle u\,,\,\boldsymbol{v}\cdot\boldsymbol{n}\rangle_{\partial\mathcal{T}_h} &= 0,\\ (\partial_t u\,,\,w)_{\mathcal{T}_h} - (\boldsymbol{q}\,,\,\nabla w)_{\mathcal{T}_h} + \langle \boldsymbol{q}\cdot\boldsymbol{n}\,,\,w\rangle_{\partial\mathcal{T}_h} &= (f\,,\,w)_{\mathcal{T}_h},\\ \langle \boldsymbol{q}\cdot\boldsymbol{n}\,,\,\mu\rangle_{\partial\mathcal{T}_h} &= 0,\end{aligned}$$

for all $(w, \boldsymbol{v}, \mu) \in W_h \times \boldsymbol{V}_h \times M_{h,H}$. By the properties of the projections $\boldsymbol{\Pi}_V$ and $\Pi_W$, we obtain that

$$\begin{aligned}(\alpha\boldsymbol{q}\,,\,\boldsymbol{v})_{\mathcal{T}_h} - (\Pi_W u\,,\,\nabla\cdot\boldsymbol{v})_{\mathcal{T}_h} + \langle u\,,\,\boldsymbol{v}\cdot\boldsymbol{n}\rangle_{\partial\mathcal{T}_h} &= 0,\\ (\partial_t u\,,\,w)_{\mathcal{T}_h} - (\boldsymbol{\Pi}_V\boldsymbol{q}\,,\,\nabla w)_{\mathcal{T}_h} + \langle \boldsymbol{q}\cdot\boldsymbol{n}\,,\,w\rangle_{\partial\mathcal{T}_h} &= (f\,,\,w)_{\mathcal{T}_h},\\ \langle \boldsymbol{q}\cdot\boldsymbol{n}\,,\,\mu\rangle_{\partial\mathcal{T}_h} &= 0,\end{aligned}$$

for all $(w, \boldsymbol{v}, \mu) \in W_h \times \boldsymbol{V}_h \times M_{h,H}$. Moreover, since $P_M$ is the $L^2$-projection into $M_{h,H}$, we get

$$\begin{aligned}(\alpha\boldsymbol{q}\,,\,\boldsymbol{v})_{\mathcal{T}_h} - (\Pi_W u\,,\,\nabla\cdot\boldsymbol{v})_{\mathcal{T}_h} + \langle P_M u\,,\,\boldsymbol{v}\cdot\boldsymbol{n}\rangle_{\partial\mathcal{T}_h} &= -\langle (I-P_M)u\,,\,\boldsymbol{v}\cdot\boldsymbol{n}\rangle_{\partial\mathcal{T}_h},\\ (\partial_t u\,,\,w)_{\mathcal{T}_h} - (\boldsymbol{\Pi}_V\boldsymbol{q}\,,\,\nabla w)_{\mathcal{T}_h} + \langle P_M(\boldsymbol{q}\cdot\boldsymbol{n})\,,\,w\rangle_{\partial\mathcal{T}_h} &= (f\,,\,w)_{\mathcal{T}_h}\\ &\quad -\langle (I-P_M)(\boldsymbol{q}\cdot\boldsymbol{n})\,,\,w\rangle_{\partial\mathcal{T}_h},\\ \langle P_M(\boldsymbol{q}\cdot\boldsymbol{n})\,,\,\mu\rangle_{\partial\mathcal{T}_h\setminus\partial\Omega} &= 0,\end{aligned}$$

for all $(w, \boldsymbol{v}, \mu) \in W_h \times \boldsymbol{V}_h \times M_{h,H}$. Subtracting the five equations defining the weak formulation of the upscaling HDG method (5.4) from the above equations, respectively, we obtain the equations for the projection of the errors. The equation (5.10d) is due to the definition of $\widehat{u}_{h,H}$ on $\partial\Omega$. The last error equation (5.10e) due to $u_h(0) = \Pi_W 0$.

It remains to prove the identity (5.10f) for $\boldsymbol{e}_{\widehat{q}}\cdot\boldsymbol{n}$. On each face $F \in \partial T$, $T \in \mathcal{T}_h$

after using the definition of numerical traces (5.4f), we have

$$\begin{aligned}
\boldsymbol{e}_{\widehat{q}} \cdot \boldsymbol{n} - \boldsymbol{e}_q \cdot \boldsymbol{n} &= P_M(\boldsymbol{q} \cdot \boldsymbol{n}) - \widehat{\boldsymbol{q}}_{h,H} \cdot \boldsymbol{n} - (\boldsymbol{\Pi}_V \boldsymbol{q} \cdot \boldsymbol{n} - \boldsymbol{q}_h \cdot \boldsymbol{n}) \\
&= P_M(\boldsymbol{q} \cdot \boldsymbol{n}) - \boldsymbol{\Pi}_V \boldsymbol{q} \cdot \boldsymbol{n} - (\widehat{\boldsymbol{q}}_{h,H} \cdot \boldsymbol{n} - \boldsymbol{q}_h \cdot \boldsymbol{n}) \\
&= P_h^{\partial}(\boldsymbol{q} \cdot \boldsymbol{n}) - \boldsymbol{\Pi}_V \boldsymbol{q} \cdot \boldsymbol{n} - \tau(u_h - \widehat{u}_{h,H}) + (P_M - P_h^{\partial})(\boldsymbol{q} \cdot \boldsymbol{n}).
\end{aligned}$$

Then using the property (4.30) of the projections $\Pi_W$ the equality reduces to

$$\begin{aligned}
\boldsymbol{e}_{\widehat{q}} \cdot \boldsymbol{n} - \boldsymbol{e}_q \cdot \boldsymbol{n} &= \tau(-P_h^{\partial} u + \Pi_W u) - \tau(u_h - \widehat{u}_{h,H}) + (P_M - P_h^{\partial})(\boldsymbol{q} \cdot \boldsymbol{n}) \\
&= \tau(-P_M u + \Pi_W u) - \tau(u_h - \widehat{u}_{h,H}) + (P_M - P_h^{\partial})(\boldsymbol{q} \cdot \boldsymbol{n} + \tau u) \\
&= \tau(e_u - e_{\widehat{u}}) + (P_M - P_h^{\partial})(\boldsymbol{q} \cdot \boldsymbol{n} + \tau u).
\end{aligned}$$

This complete the proof. □

### *5.4.2 Estimate of $e_u$ in $L^\infty(L^2)$*

In this section, we obtain an upper bound of the $L^\infty(L^2)$-norm of $e_u$. We first prove the following identity of linear case. Especially, the identities are independent of choices of multiscale spaces.

**Lemma 5.4.4.** *Let Assumption 4.6.1 be satisfied. Then, for any time $t \in (0, t_F]$, we have*

$$\frac{1}{2}\|e_u(t)\|^2 + \int_0^t \|\boldsymbol{e}_q(s)\|_\alpha^2 ds + \int_0^t \|e_u(s) - e_{\widehat{u}}(s)\|_\tau^2 ds = \sum_{i=1}^{7} \mathbb{S}_i,$$

*where*

$$\mathbb{S}_1 = -\int_0^t (\alpha \boldsymbol{\delta}_q \,,\, \boldsymbol{e}_q)_{\mathcal{T}_h}, \qquad \mathbb{S}_2 = -\int_0^t (\partial_t \delta_u \,,\, e_u)_{\mathcal{T}_h},$$
$$\mathbb{S}_3 = -\int_0^t \langle u - w \,,\, \boldsymbol{e}_q \cdot \boldsymbol{n} \rangle_{\partial \mathcal{T}_H}, \qquad \mathbb{S}_4 = -\int_0^t \langle \boldsymbol{q} \cdot \boldsymbol{n} - P_h^{\partial}(\boldsymbol{q} \cdot \boldsymbol{n}) \,,\, e_u - e_{\widehat{u}} \rangle_{\partial \mathcal{T}_H},$$
$$\mathbb{S}_5 = \int_0^t \langle P_h^{\partial} u - P_H^{\partial} u \,,\, \tau(e_u - e_{\widehat{u}}) \rangle_{\partial \mathcal{T}_H}, \qquad \mathbb{S}_6 = \int_0^t \langle w - P_H^{\partial} u \,,\, \tau(e_u - e_{\widehat{u}}) \rangle_{\partial \mathcal{T}_H},$$
$$\mathbb{S}_7 = \int_0^t \langle w - P_H^{\partial} u \,,\, \tau(P_h^{\partial} u - u) \rangle_{\partial \mathcal{T}_H}.$$

*Proof.* Taking $(w, \boldsymbol{v}, \mu) = (e_u, \boldsymbol{e}_q, e_{\widehat{u}})$ in (5.10a)-(5.10c), respectively. Adding the resulting three equations, we get, after some algebraic manipulation,

$$\begin{aligned}
&\|\boldsymbol{e}_q\|_{\alpha}^2 + \frac{1}{2}\frac{d}{dt}\|e_u\|^2 + \langle \boldsymbol{e}_{\widehat{q}} \cdot \boldsymbol{n} - \boldsymbol{e}_q \cdot \boldsymbol{n} \,,\, e_u - e_{\widehat{u}} \rangle_{\partial \mathcal{T}_h} \\
&= -(\alpha \boldsymbol{\delta}_q \,,\, \boldsymbol{e}_q)_{\mathcal{T}_h} - (\partial_t \delta_u \,,\, e_u)_{\mathcal{T}_h} - \langle (I - P_M) u \,,\, \boldsymbol{e}_q \cdot \boldsymbol{n} \rangle_{\partial \mathcal{T}_h} - \langle (I - P_M)(\boldsymbol{q} \cdot \boldsymbol{n}) \,,\, e_u \rangle_{\partial \mathcal{T}_h}.
\end{aligned}$$

Inserting the identity (5.10f) in the above equation, we have

$$\begin{aligned}
\|\boldsymbol{e}_q\|_{\alpha}^2 + \frac{1}{2}\frac{d}{dt}\|e_u\|^2 + \|e_u - e_{\widehat{u}}\|_{\tau}^2 &= -(\alpha \boldsymbol{\delta}_q \,,\, \boldsymbol{e}_q)_{\mathcal{T}_h} - (\partial_t \delta_u \,,\, e_u)_{\mathcal{T}_h} \\
&\quad - \langle (I - P_M) u \,,\, \boldsymbol{e}_q \cdot \boldsymbol{n} \rangle_{\partial \mathcal{T}_h} - \langle (I - P_M)(\boldsymbol{q} \cdot \boldsymbol{n}) \,,\, e_u \rangle_{\partial \mathcal{T}_h} \\
&\quad + \langle (P_h^{\partial} - P_M)(\boldsymbol{q} \cdot \boldsymbol{n} + \tau u) \,,\, e_u - e_{\widehat{u}} \rangle_{\partial \mathcal{T}_h}.
\end{aligned}$$

Now using the fact that $\langle P_M(\boldsymbol{q} \cdot \boldsymbol{n}) \,,\, e_{\widehat{u}} \rangle_{\partial \mathcal{T}_h} = \langle \boldsymbol{q} \cdot \boldsymbol{n} \,,\, e_{\widehat{u}} \rangle_{\partial \mathcal{T}_h}$, we observe that

$$\begin{aligned}
&-\langle (I - P_M)(\boldsymbol{q} \cdot \boldsymbol{n}) \,,\, e_u \rangle_{\partial \mathcal{T}_h} + \langle (P_h^{\partial} - P_M)(\boldsymbol{q} \cdot \boldsymbol{n} + \tau u) \,,\, e_u - e_{\widehat{u}} \rangle_{\partial \mathcal{T}_h} \\
&= -\langle (I - P_M)(\boldsymbol{q} \cdot \boldsymbol{n}) \,,\, e_u - e_{\widehat{u}} \rangle_{\partial \mathcal{T}_h} + \langle (P_h^{\partial} - P_M)(\boldsymbol{q} \cdot \boldsymbol{n}) \,,\, e_u - e_{\widehat{u}} \rangle_{\partial \mathcal{T}_h} \\
&\quad + \langle P_h^{\partial} u - P_M u \,,\, \tau(e_u - e_{\widehat{u}}) \rangle_{\partial \mathcal{T}_h} \\
&= -\langle (I - P_h^{\partial})(\boldsymbol{q} \cdot \boldsymbol{n}) \,,\, e_u - e_{\widehat{u}} \rangle_{\partial \mathcal{T}_h} + \langle P_h^{\partial} u - P_M u \,,\, \tau(e_u - e_{\widehat{u}}) \rangle_{\partial \mathcal{T}_h}.
\end{aligned}$$

Since for any $F \in \mathcal{E}_h^0$, $P_M = P_h^\partial$, we get the identity

$$\begin{aligned}
\langle (I - P_M)u \,,\, \boldsymbol{e}_q \cdot \boldsymbol{n} \rangle_{\partial \mathcal{T}_h} &= \langle (I - P_H^\partial)u \,,\, \boldsymbol{e}_q \cdot \boldsymbol{n} \rangle_{\partial \mathcal{T}_H}, \\
\langle (I - P_h^\partial)(\boldsymbol{q} \cdot \boldsymbol{n}) \,,\, e_u - e_{\widehat{u}} \rangle_{\partial \mathcal{T}_h} &= \langle (I - P_h^\partial)(\boldsymbol{q} \cdot \boldsymbol{n}) \,,\, e_u - e_{\widehat{u}} ) \rangle_{\partial \mathcal{T}_H}, \\
\langle (P_h^\partial - P_M)u \,,\, \tau(e_u - e_{\widehat{u}} \rangle_{\partial \mathcal{T}_h} &= \langle (P_h^\partial - P_H^\partial)u \,,\, \tau(e_u - e_{\widehat{u}}) \rangle_{\partial \mathcal{T}_H}.
\end{aligned}$$

For any $w \in M_H$, we only need to rewrite $\langle (I - P_H^\partial)u \,,\, \boldsymbol{e}_q \cdot \boldsymbol{n} \rangle_{\partial \mathcal{T}_H}$. By the proof of Lemma 4.6.5,

$$\begin{aligned}
\langle (I - P_H^\partial)u \,,\, \boldsymbol{e}_q \cdot \boldsymbol{n} \rangle_{\partial \mathcal{T}_H} =& \langle u - w \,,\, \boldsymbol{e}_q \cdot \boldsymbol{n} \rangle_{\partial \mathcal{T}_H} - \langle w - P_H^\partial u \,,\, \tau(e_u - e_{\widehat{u}}) \rangle_{\partial \mathcal{T}_H} \\
&+ \langle w - P_H^\partial u \,,\, \tau(P_h^\partial u - u) \rangle_{\partial \mathcal{T}_H}.
\end{aligned}$$

Then, we have

$$\begin{aligned}
\|\boldsymbol{e}_q\|_\alpha^2 + \frac{1}{2}\frac{d}{dt}\|e_u\|^2 + \|e_u - e_{\widehat{u}}\|_\tau^2 =& -(\alpha \boldsymbol{\delta}_q \,,\, \boldsymbol{e}_q)_{\mathcal{T}_h} - (\partial_t \delta_u \,,\, e_u)_{\mathcal{T}_h} \\
&- \langle u - w \,,\, \boldsymbol{e}_q \cdot \boldsymbol{n} \rangle_{\partial \mathcal{T}_H} - \langle \boldsymbol{q} \cdot \boldsymbol{n} - P_h^\partial(\boldsymbol{q} \cdot \boldsymbol{n}) \,,\, e_u - e_{\widehat{u}} \rangle_{\partial \mathcal{T}_H} \\
&+ \langle P_h^\partial u - P_H^\partial u \,,\, \tau(e_u - e_{\widehat{u}}) \rangle_{\partial \mathcal{T}_H} + \langle w - P_H^\partial u \,,\, \tau(e_u - e_{\widehat{u}}) \rangle_{\partial \mathcal{T}_H} \\
&+ \langle w - P_H^\partial u \,,\, \tau(P_h^\partial u - u) \rangle_{\partial \mathcal{T}_H}.
\end{aligned}$$

Integrating in time over the interval $(0, t)$ and using $e_u(0) = 0$, we get the identity of the lemma and this completes the proof. □

Now we derive the error estimate for $e_u$ with the multiscale space II-a in Section 4.3.2.1. To get this estimate, we need Assumption 4.6.9, which is related to the spectral expansion of exact solution on the common coarse face. We can also prove the error estimate for another multiscale spaces with the same procedure.

**Theorem 5.4.5.** *Let Assumptions 4.6.1 and 4.6.9 be satisfied and the local space be*

*the type of* $\mathbf{HDG}_k$*. Then, we have*

$$\begin{aligned}\|e_u\|_{L^\infty(L^2)} \leq & Ch^s \left(\|\boldsymbol{q}\|_{L^2(H^s)} + \|u_t\|_{L^2(H^s)} + \|\boldsymbol{q}_t\|_{L^2(H^s)}\right) \\ & + Ch^s H^{-\frac{1}{2}} \left(\|u\|_{L^2(H^{s+1})} + \|\boldsymbol{q}\|_{L^2(H^{s+1})}\right) + C\left(\frac{H}{h\Lambda_1^*}\right)^{\frac{1}{2}} \|\kappa^{\frac{1}{2}}\nabla u\|_{L^2(L^2)},\end{aligned} \tag{5.11}$$

*Moreover, for any time* $t \in (0, t_F]$*, we have*

$$\int_0^t \|\boldsymbol{e}_q(s)\|_\alpha^2 ds + \int_0^t \|e_u(s) - e_{\widehat{u}}(s)\|_\tau^2 ds \leq C\|e_u\|_{L^\infty(L^2)}^2.$$

*Proof.* We estimate the right hand side terms in Lemma 5.4.4 one by one. since $0 < \alpha \leq \alpha_0 = 1/\kappa_0$, we get

$$\begin{aligned}|\mathbb{S}_1| &\leq \int_0^t |(\alpha\boldsymbol{\delta}_q\,,\,\boldsymbol{e}_q)_{\mathcal{T}_h}| \leq \frac{1}{2\epsilon_1}\int_0^t \|\boldsymbol{\delta}_q\|^2 + \frac{\epsilon_1}{2}\int_0^t \|\boldsymbol{e}_q\|_\alpha^2 \\ &\leq Ch^{2s}\|\boldsymbol{q}\|_{L^2(H^s)}^2 + \frac{\epsilon_1}{2}\int_0^t \|\boldsymbol{e}_q\|_\alpha^2\end{aligned}$$

for all $1 \leq s \leq k+1$. Similarly, we have

$$\begin{aligned}|\mathbb{S}_2| &\leq \int_0^t |(\partial_t\delta_u\,,\,e_u)_{\mathcal{T}_h}| \leq \frac{1}{2}\int_0^t \|\partial_t\delta_u\|^2 + \frac{1}{2}\int_0^t \|e_u\|^2 \\ &\leq Ch^{2s}\left(\|u_t\|_{L^2(H^s)}^2 + \|\boldsymbol{q}_t\|_{L^2(H^s)}^2\right) + \frac{1}{2}\int_0^t \|e_u\|^2\end{aligned}$$

for all $1 \leq s \leq k+1$. By the trace inequality and the estimate in Lemma 4.6.11, we

obtain

$$
\begin{aligned}
|\mathbb{S}_3| &\le \int_0^t |\langle u-w\,,\, \boldsymbol{e}_q\cdot\boldsymbol{n}\rangle_{\partial\mathcal{T}_H}| = \int_0^t |\langle \kappa^{\frac{1}{2}}(u-w)\,,\, \alpha^{\frac{1}{2}}\boldsymbol{e}_q\cdot\boldsymbol{n}\rangle_{\partial\mathcal{T}_H}| \\
&\le Ch^{-\frac{1}{2}}\int_0^t \|\kappa^{\frac{1}{2}}(u-w)\|_{\partial\mathcal{T}_H}\|\boldsymbol{e}_q\|_\alpha \\
&\le \frac{C}{h}\int_0^t \|\kappa^{\frac{1}{2}}(u-w)\|^2_{\partial\mathcal{T}_H} + \frac{\epsilon_1}{2}\int_0^t \|\boldsymbol{e}_q\|^2_\alpha \\
&\le C\frac{H}{h\Lambda_1^*}\|\kappa^{\frac{1}{2}}\nabla u\|^2_{L^2(L^2)} + \frac{\epsilon_1}{2}\int_0^t \|\boldsymbol{e}_q\|^2_\alpha.
\end{aligned}
$$

For $\mathbb{S}_4$, since $\tau$ is positive constant, we have

$$
\begin{aligned}
|\mathbb{S}_4| &\le \int_0^t |\langle \boldsymbol{q}\cdot\boldsymbol{n} - P_h^\partial(\boldsymbol{q}\cdot\boldsymbol{n})\,,\, e_u - e_{\widehat{u}}\rangle_{\partial\mathcal{T}_H}| \\
&\le \tau^{-\frac{1}{2}}\int_0^t \|\boldsymbol{q}\cdot\boldsymbol{n} - P_h^\partial\boldsymbol{q}\cdot\boldsymbol{n}\|_{\partial\mathcal{T}_H}\|e_u - e_{\widehat{u}}\|_\tau \\
&\le \frac{C}{\epsilon_2}\int_0^t \|\boldsymbol{q}\cdot\boldsymbol{n} - P_h^\partial\boldsymbol{q}\cdot\boldsymbol{n}\|^2_{\partial\mathcal{T}_H} + \frac{\epsilon_2}{2}\int_0^t \|e_u - e_{\widehat{u}}\|^2_\tau \\
&\le C\frac{h^{2s}}{H}\|\boldsymbol{q}\|^2_{L^2(H^{s+1})} + \frac{\epsilon_2}{2}\int_0^t \|e_u - e_{\widehat{u}}\|^2_\tau.
\end{aligned}
$$

For $\mathbb{S}_5$ and $\mathbb{S}_6$, we use the fact that $P_H^\partial$ is the $L^2$ projection onto $M_H$ so that $\|u - P_H^\partial\|_{\partial\mathcal{T}_H} \le \|u-w\|_{\partial\mathcal{T}_H}$ for any $w \in M_H$. Then, we get

$$
\begin{aligned}
|\mathbb{S}_5| &\le \int_0^t |\langle (P_h^\partial - P_H^\partial)u\,,\, \tau(e_u - e_{\widehat{u}})\rangle_{\partial\mathcal{T}_H}| \\
&\le \int_0^t |\langle P_h^\partial u - u\,,\, \tau(e_u - e_{\widehat{u}})\rangle_{\partial\mathcal{T}_H}| + \int_0^t |\langle (u - P_H^\partial u\,,\, \tau(e_u - e_{\widehat{u}})\rangle_{\partial\mathcal{T}_H}| \\
&\le \frac{\tau}{2\epsilon_2}\int_0^t \|P_h^\partial u - u\|^2_{\partial\mathcal{T}_H} + \frac{\alpha_0\tau}{2\epsilon_2}\int_0^t \|\kappa^{\frac{1}{2}}(u-w)\|^2_{\partial\mathcal{T}_H} + \epsilon_2\int_0^t \|e_u - e_{\widehat{u}}\|^2_\tau \\
&\le C\frac{h^{2s}}{H}\|u\|^2_{L^2(H^{s+1})} + C\frac{H}{\Lambda_1^*}\|\kappa^{\frac{1}{2}}\nabla u\|^2_{L^2(L^2)} + \epsilon_2\int_0^t \|e_u - e_{\widehat{u}}\|^2_\tau
\end{aligned}
$$

and

$$
\begin{aligned}
|\mathbb{S}_6| &\le \int_0^t |\langle w - P_H^{\partial} u \,,\, \tau(e_u - e_{\widehat{u}})\rangle_{\partial\mathcal{T}_H}| \\
&\le \int_0^t |\langle w - u \,,\, \tau(e_u - e_{\widehat{u}}\rangle_{\partial\mathcal{T}_H}| + \int_0^t |\langle u - P_H^{\partial} u \,,\, \tau(e_u - e_{\widehat{u}}\rangle_{\partial\mathcal{T}_H}| \\
&\le 2\tau^{-\frac{1}{2}} \int_0^t \|u - w\|_{\partial\mathcal{T}_H} \|e_u - e_{\widehat{u}}\|_{\tau} \\
&\le \alpha_0 \tau \int_0^t \|\kappa^{\frac{1}{2}}(u - w)\|^2_{\partial\mathcal{T}_H} + \frac{\epsilon_2}{2} \int_0^t \|e_u - e_{\widehat{u}}\|^2_{\tau} \\
&\le C \frac{H}{\Lambda_1^*} \|\kappa^{\frac{1}{2}} \nabla u\|^2_{L^2(L^2)} + \frac{\epsilon_2}{2} \int_0^t \|e_u - e_{\widehat{u}}\|^2_{\tau}.
\end{aligned}
$$

For the last term, we get

$$
\begin{aligned}
|\mathbb{S}_7| &\le \int_0^t |\langle w - P_H^{\partial} u \,,\, \tau(P_h^{\partial} u - u)\rangle_{\partial\mathcal{T}_H}| \le 2\tau \int_0^t \|u - w\|_{\partial\mathcal{T}_H} \|P_h^{\partial} u - u\|_{\partial\mathcal{T}_H} \\
&\le \alpha_0 \tau^2 \int_0^t \|\kappa^{\frac{1}{2}}(u - w)\|^2_{\partial\mathcal{T}_H} + \frac{1}{2} \int_0^t \|P_h^{\partial} u - u\|_{DTH} \\
&\le C \frac{H}{\Lambda_1^*} \|\kappa^{\frac{1}{2}} \nabla u\|^2_{L^2(L^2)} + C \frac{h^{2s}}{H} \|u\|_{L^2(H^{s+1})}.
\end{aligned}
$$

Then, for any time $t \in (0, t_F]$, we obtain

$$
\begin{aligned}
\frac{1}{2}\|e_u(t)\|^2 + (1 - \epsilon_1) \int_0^t \|\boldsymbol{e}_q\|^2_{\alpha} + (1 - 2\epsilon_2) \int_0^t \|e_u - e_{\widehat{u}}\|^2_{\tau} & \\
\le C h^{2s} \left( \|\boldsymbol{q}\|^2_{L^2(H^s)} + \|u_t\|^2_{L^2(H^s)} + \|\boldsymbol{q}_t\|^2_{L^2(H^s)} \right) + C \frac{H}{h\Lambda_1^*} \|\kappa^{\frac{1}{2}} \nabla u\|^2_{L^2(L^2)} & \\
+ C h^{2s} H^{-1} \left( \|u\|^2_{L^2(H^{s+1})} + \|\boldsymbol{q}\|^2_{L^2(H^{s+1})} \right) + \frac{1}{2} \int_0^t \|e_u\|^2. &
\end{aligned}
$$

Taking $\epsilon_1 = 1, \epsilon_2 = 2$ and applying the Gronwall's lemma, we have

$$
\begin{aligned}
\|e_u(t)\| \le & C h^s \left( \|\boldsymbol{q}\|_{L^2(H^s)} + \|u_t\|_{L^2(H^s)} + \|\boldsymbol{q}_t\|_{L^2(H^s)} \right) \\
& + C h^s H^{-\frac{1}{2}} \left( \|u\|_{L^2(H^{s+1})} + \|\boldsymbol{q}\|_{L^2(H^{s+1})} \right) + C \left( \frac{H}{h\Lambda_1^*} \right)^{\frac{1}{2}} \|\kappa^{\frac{1}{2}} \nabla u\|_{L^2(L^2)},
\end{aligned}
$$

for all $t \in (0, T]$. Taking the maximum in both side of the inequality, we get the

error estimates. Taking $\epsilon_1 < 1, \epsilon_2 < 2$, we can get the second estimates and this completes the proof. □

### *5.4.3 Estimate of $\boldsymbol{e}_q$ in $L^\infty(L^2)$*

The goal of this section is to derive an error bound of the $L^\infty$-norm of $\boldsymbol{e}_q$.

**Lemma 5.4.6.** *Let Assumption 4.6.1 be satisfied. Then, for any time $t \in (0, t_F]$, we have*

$$\frac{1}{2}\|\boldsymbol{e}_q(t)\|_\alpha^2 + \frac{1}{2}\|e_u(t) - e_{\widehat{u}}(t)\|_\tau^2 + \int_0^t \|\partial_t e_u\|^2 = \sum_{i=1}^{10} \mathbb{T}_i,$$

*where*

$$\mathbb{T}_1 = -\int_0^t (\alpha \partial_t \boldsymbol{\delta}_q \,,\, \boldsymbol{e}_q)_{\mathcal{T}_h},\ \mathbb{T}_2 = -\int_0^t (\partial_t \delta_u \,,\, \partial_t e_u)_{\mathcal{T}_h},\ \mathbb{T}_3 = -\int_0^t \langle u_t - w \,,\, \boldsymbol{e}_q \cdot \boldsymbol{n} \rangle_{\partial\mathcal{T}_H},$$
$$\mathbb{T}_4 = \int_0^t \langle w - P_H^\partial u_t \,,\, \tau(e_u - e_{\widehat{u}}) \rangle_{\partial\mathcal{T}_H},\quad \mathbb{T}_5 = -\int_0^t \langle w - P_H^\partial u_t \,,\, \tau(P_h^\partial u - u) \rangle_{\partial\mathcal{T}_H},$$
$$\mathbb{T}_6 = -\int_0^t \frac{d}{dt} \langle \boldsymbol{q} \cdot \boldsymbol{n} - P_h^\partial(\boldsymbol{q} \cdot \boldsymbol{n}) \,,\, e_u - e_{\widehat{u}} \rangle_{\partial\mathcal{T}_H},$$
$$\mathbb{T}_7 = \int_0^t \langle \boldsymbol{q}_t \cdot \boldsymbol{n} - P_h^\partial(\boldsymbol{q}_t \cdot \boldsymbol{n}) \,,\, e_u - e_{\widehat{u}} \rangle_{\partial\mathcal{T}_H},$$
$$\mathbb{T}_8 = \int_0^t \frac{d}{dt} \langle P_h^\partial u - P_H^\partial u \,,\, \tau(e_u - e_{\widehat{u}}) \rangle_{\partial\mathcal{T}_H},\ \mathbb{T}_9 = -\int_0^t \langle P_h^\partial u_t - P_H^\partial u_t \,,\, \tau(e_u - e_{\widehat{u}}) \rangle_{\partial\mathcal{T}_H},$$
$$\mathbb{T}_{10} = \frac{1}{2}\left(\|\boldsymbol{e}_q(0)\|_\alpha^2 + \|e_u(0) - e_{\widehat{u}}(0)\|_\tau^2\right).$$

*Proof.* We keep all of error equations except for (5.10a) and (5.10d), which are re-

placed by the equations obtained by differentiating them with respect to time:

$$\begin{aligned}
(\alpha\partial_t \boldsymbol{e}_q\,,\,\boldsymbol{v})_{\mathcal{T}_h} - (\partial_t e_u\,,\,\nabla\cdot\boldsymbol{v})_{\mathcal{T}_h} + \langle\partial_t e_{\widehat{u}}\,,\,\boldsymbol{v}\cdot\boldsymbol{n}\rangle_{\partial\mathcal{T}_h} &= -(\alpha\partial_t\boldsymbol{\delta}_q\,,\,\boldsymbol{v})_{\mathcal{T}_h} \\
&\quad - \langle(I-P_M)u_t\,,\,\boldsymbol{v}\cdot\boldsymbol{n}\rangle_{\partial\mathcal{T}_h} \\
(\partial_t e_u\,,\,w)_{\mathcal{T}_h} - (\boldsymbol{e}_q\,,\,\nabla w)_{\mathcal{T}_h} + \langle\boldsymbol{e}_{\widehat{q}}\cdot\boldsymbol{n}\,,\,w\rangle_{\partial\mathcal{T}_h} &= -(\partial_t\delta_u\,,\,w)_{\mathcal{T}_h} \\
&\quad - \langle(I-P_M)(\boldsymbol{q}\cdot\boldsymbol{n})\,,\,w\rangle_{\partial\mathcal{T}_h} \\
\langle\boldsymbol{e}_{\widehat{q}}\cdot\boldsymbol{n}\,,\,\mu\rangle_{\partial\mathcal{T}_h} &= 0 \\
\partial_t e_{\widehat{u}}|_{\partial\Omega} &= 0 \\
e_u|_{t=0} &= 0
\end{aligned}$$

for all $(w,\boldsymbol{v},\mu)\in W_h\times\boldsymbol{V}_h\times M_{h,H}$, where

$$\boldsymbol{e}_{\widehat{q}}\cdot\boldsymbol{n} = \boldsymbol{e}_q\cdot\boldsymbol{n} + \tau(e_u - e_{\widehat{u}}) - (P_h^{\partial} - P_M)(\boldsymbol{q}\cdot\boldsymbol{n} + \tau u) \quad \text{on} \quad \partial\mathcal{T}_h.$$

Taking $(w,\boldsymbol{v},\mu) = (\partial_t e_u, \boldsymbol{e}_q, \partial_t e_{\widehat{u}})$ in first three equations. Adding the resulting four equations, we get, after some algebraic manipulation,

$$\begin{aligned}
\frac{1}{2}\frac{d}{dt}\|\boldsymbol{e}_q\|_\alpha^2 + \|\partial_t e_u\|^2 + \langle\boldsymbol{e}_{\widehat{q}}\cdot\boldsymbol{n} - \boldsymbol{e}_q\cdot\boldsymbol{n}\,,\,\partial_t e_u - \partial_t e_{\widehat{u}}\rangle_{\partial\mathcal{T}_h} &= -(\alpha\partial_t\boldsymbol{\delta}_q\,,\,\boldsymbol{e}_q)_{\mathcal{T}_h} \\
-(\partial_t\delta_u\,,\,\partial_t e_u)_{\mathcal{T}_h} - \langle(I-P_M)u_t\,,\,\boldsymbol{e}_q\cdot\boldsymbol{n}\rangle_{\partial\mathcal{T}_h} - \langle(I-P_M)(\boldsymbol{q}\cdot\boldsymbol{n})\,,\,\partial_t e_u\rangle_{\partial\mathcal{T}_h}.
\end{aligned}$$

Inserting the identity (5.10f) in the above equation, we have

$$\begin{aligned}
\frac{1}{2}\frac{d}{dt}\|\boldsymbol{e}_q\|_\alpha^2 + \|\partial_t e_u\|^2 + \|e_u - e_{\widehat{u}}\|_\tau^2 &= -(\alpha\partial_t\boldsymbol{\delta}_q\,,\,\boldsymbol{e}_q)_{\mathcal{T}_h} - (\partial_t\delta_u\,,\,\partial_t e_u)_{\mathcal{T}_h} \\
&\quad -\langle(I-P_M)u_t\,,\,\boldsymbol{e}_q\cdot\boldsymbol{n}\rangle_{\partial\mathcal{T}_h} - \langle(I-P_M)(\boldsymbol{q}\cdot\boldsymbol{n})\,,\,\partial_t e_u\rangle_{\partial\mathcal{T}_h} \\
&\quad +\langle(P_h^{\partial} - P_M)(\boldsymbol{q}\cdot\boldsymbol{n} + \tau u)\,,\,\partial_t(e_u - e_{\widehat{u}})\rangle_{\partial\mathcal{T}_h}.
\end{aligned}$$

Since $\langle P_M(\boldsymbol{q}\cdot\boldsymbol{n})\,,\,\partial_t e_{\widehat{u}}\rangle_{\partial\mathcal{T}_h} = \langle\boldsymbol{q}\cdot\boldsymbol{n}\,,\,\partial_t e_{\widehat{u}}\rangle_{\partial\mathcal{T}_h}$ and for any $F\in\mathcal{E}_h^0$, $P_M = P_h^{\partial}$, we

observe that

$$
\begin{aligned}
&-\langle (I-P_M)(\boldsymbol{q}\cdot\boldsymbol{n})\,,\,\partial_t e_u\rangle_{\partial\mathcal{T}_h} + \langle (P_h^\partial - P_M)(\boldsymbol{q}\cdot\boldsymbol{n}+\tau u)\,,\,\partial_t(e_u - e_{\widehat{u}})\rangle_{\partial\mathcal{T}_h}\\
&= -\langle (I-P_h^\partial)(\boldsymbol{q}\cdot\boldsymbol{n})\,,\,\partial_t(e_u-e_{\widehat{u}})\rangle_{\partial\mathcal{T}_h} + \langle P_h^\partial u - P_M u\,,\,\tau\partial_t(e_u-e_{\widehat{u}})\rangle_{\partial\mathcal{T}_h}
\end{aligned}
$$

and

$$
\begin{aligned}
\langle (I-P_M)u_t\,,\,\boldsymbol{e}_q\cdot\boldsymbol{n}\rangle_{\partial\mathcal{T}_h} &= \langle u_t - P_H^\partial u_t\,,\,\boldsymbol{e}_q\cdot\boldsymbol{n}\rangle_{\partial\mathcal{T}_H},\\
\langle (I-P_h^\partial)(\boldsymbol{q}\cdot\boldsymbol{n})\,,\,\partial_t(e_u-e_{\widehat{u}})\rangle_{\partial\mathcal{T}_h} &= \langle \boldsymbol{q}\cdot\boldsymbol{n} - P_h^\partial(\boldsymbol{q}\cdot\boldsymbol{n})\,,\,\partial_t(e_u-e_{\widehat{u}})\rangle_{\partial\mathcal{T}_H},\\
\langle P_h^\partial u - P_M u\,,\,\tau\partial_t(e_u-e_{\widehat{u}})\rangle_{\partial\mathcal{T}_h} &= \langle P_h^\partial u - P_H^\partial u\,,\,\tau\partial_t(e_u-e_{\widehat{u}})\rangle_{\partial\mathcal{T}_H}.
\end{aligned}
$$

To rewrite $\langle u_t - P_H^\partial u_t\,,\,\boldsymbol{e}_q\cdot\boldsymbol{n}\rangle_{\partial\mathcal{T}_H}$, we do the same way of Lemma 5.4.4. Then, we get

$$
\begin{aligned}
\langle u_t - P_H^\partial u_t\,,\,\boldsymbol{e}_q\cdot\boldsymbol{n}\rangle_{\partial\mathcal{T}_H} =& \langle u_t - w\,,\,\boldsymbol{e}_q\cdot\boldsymbol{n}\rangle_{\partial\mathcal{T}_H} - \langle w - P_H^\partial u_t\,,\,\tau(e_u-e_{\widehat{u}})\rangle_{\partial\mathcal{T}_H}\\
&+ \langle w - P_H^\partial u_t\,,\,\tau(P_h^\partial u - u)\rangle_{\partial\mathcal{T}_H}.
\end{aligned}
$$

Also, we observe that

$$
\begin{aligned}
\langle \boldsymbol{q}\cdot\boldsymbol{n} - P_h^\partial(\boldsymbol{q}\cdot\boldsymbol{n})\,,\,\partial_t(e_u-e_{\widehat{u}})\rangle_{\partial\mathcal{T}_H} =& \frac{d}{dt}\langle \boldsymbol{q}\cdot\boldsymbol{n} - P_h^\partial(\boldsymbol{q}\cdot\boldsymbol{n})\,,\,e_u-e_{\widehat{u}}\rangle_{\partial\mathcal{T}_H}\\
&- \langle \boldsymbol{q}_t\cdot\boldsymbol{n} - P_h^\partial(\boldsymbol{q}_t\cdot\boldsymbol{n})\,,\,e_u-e_{\widehat{u}}\rangle_{\partial\mathcal{T}_H}
\end{aligned}
$$

and

$$
\begin{aligned}
\langle P_h^\partial u - P_H^\partial u\,,\,\tau\partial_t(e_u-e_{\widehat{u}})\rangle_{\partial\mathcal{T}_H} =& \frac{d}{dt}\langle P_h^\partial u - P_H^\partial u\,,\,\tau(e_u-e_{\widehat{u}})\rangle_{\partial\mathcal{T}_H}\\
&- \langle P_h^\partial u_t - P_H^\partial u_t\,,\,\tau(e_u-e_{\widehat{u}})\rangle_{\partial\mathcal{T}_H}.
\end{aligned}
$$

Finally, we obtain the identity in the lemma by integrating in time over the interval $(0,t)$ and arrange the terms. This completes the proof. □

Now we state the error estimate for $\boldsymbol{e}_q$:

**Theorem 5.4.7.** *Let Assumptions 4.6.1 and 4.6.9 be satisfied and the local space be the type of* $\mathbf{HDG}_k$*. Then, we have*

$$\begin{aligned}\|\boldsymbol{e}_q\|_{L^\infty(L^2_\alpha)} &\le Ch^s\left(\|\boldsymbol{q}(0)\|_s + \|u_t\|_{L^2(H^s)} + \|\boldsymbol{q}_t\|_{L^2(H^s)}\right)\\ &+ Ch^sH^{-\frac{1}{2}}\left(\|\boldsymbol{q}(0)\|_{s+1} + \|u\|_{L^2(H^{s+1})} + \|u_t\|_{L^2(H^{s+1})} + \|\boldsymbol{q}_t\|_{L^2(H^{s+1})}\right)\\ &+ Ch^sH^{-\frac{1}{2}}\left(\|u\|_{L^\infty(H^{s+1})} + \|\boldsymbol{q}\|_{L^\infty(H^{s+1})}\right)\\ &+ C\left(\frac{H}{h\Lambda_1^*}\right)^{\frac{1}{2}}\|\kappa^{\frac{1}{2}}\nabla u_t\|_{L^2(L^2)} + C\left(\frac{H}{\Lambda_1^*}\right)^{\frac{1}{2}}\|\kappa^{\frac{1}{2}}\nabla u\|_{L^\infty(L^2)}\end{aligned} \tag{5.12}$$

*Proof.* We get the estimate, we consider the identity of Lemma 5.4.6. For $\mathbb{T}_1 \sim \mathbb{T}_9$, we execute the similar steps of Theorem 5.4.5. For any $1 \le s \le k+1$, we get

$$\begin{aligned}|\mathbb{T}_1| &\le \int_0^t |(\alpha\partial_t\boldsymbol{\delta}_q\,,\,\boldsymbol{e}_q)_{\mathcal{T}_h}| \le \frac{\alpha_0}{2}\int_0^t \|\partial_t\boldsymbol{\delta}_q\|^2 + \frac{1}{2}\int_0^t \|\boldsymbol{e}_q\|_\alpha^2\\ &\le Ch^{2s}\|\boldsymbol{q}_t\|^2_{L^2(H^s)} + \frac{1}{2}\int_0^t \|\boldsymbol{e}_q\|_\alpha^2\end{aligned}$$

and

$$\begin{aligned}|\mathbb{T}_2| &\le \int_0^t |(\partial_t\delta_u\,,\,\partial_t e_u)_{\mathcal{T}_h}| \le \frac{1}{2\epsilon_1}\int_0^t \|\partial_t\delta_u\|^2 + \frac{\epsilon_1}{2}\int_0^t \|\partial_t e_u\|^2\\ &\le Ch^{2s}\left(\|u_t\|^2_{L^2(H^s)} + \|\boldsymbol{q}_t\|^2_{L^2(H^s)}\right) + \frac{\epsilon_1}{2}\int_0^t \|\partial_t e_u\|^2.\end{aligned}$$

Note that $\mathbb{T}_3 \sim \mathbb{T}_5$ is the similar to $\mathbb{S}_3$, $\mathbb{S}_6$, and $\mathbb{S}_7$ in Theorem 5.4.5, respectively. It is the only changes to exist $u_t$ in these terms instead of $u$ and to apply Young's inequality with a different weight. Then, we obtain

$$\begin{aligned}|\mathbb{T}_3| &\le C\frac{H}{h\Lambda_1^*}\|\kappa^{\frac{1}{2}}\nabla u_t\|^2_{L^2(L^2)} + C\int_0^t \|\boldsymbol{e}_q\|_\alpha^2,\\ |\mathbb{T}_4| &\le C\frac{H}{\Lambda_1^*}\|\kappa^{\frac{1}{2}}\nabla u_t\|^2_{L^2(L^2)} + C\int_0^t \|e_u - e_{\widehat{u}}\|_\tau^2,\end{aligned}$$

and

$$|\mathbb{T}_5| \leq C\frac{H}{\Lambda_1^*}\|\kappa^{\frac{1}{2}}\nabla u_t\|^2_{L^2(L^2)} + C\frac{h^{2s}}{H}\|u\|^2_{L^2(H^{s+1})}.$$

For $\mathbb{T}_6$ and $\mathbb{T}_7$,

$$\begin{aligned}
|\mathbb{T}_6| &\leq |\langle \boldsymbol{q}(t)\cdot\boldsymbol{n} - P_h^{\partial}(\boldsymbol{q}(t)\cdot\boldsymbol{n})\,,\, e_u(t) - e_{\widehat{u}}(t)\rangle_{\partial\mathcal{T}_H}| \\
&\quad + |\langle \boldsymbol{q}(0)\cdot\boldsymbol{n} - P_h^{\partial}(\boldsymbol{q}(0)\cdot\boldsymbol{n})\,,\, e_u(0) - e_{\widehat{u}}(0)\rangle_{\partial\mathcal{T}_H}| \\
&\leq \frac{1}{2\epsilon_2\tau}\|\boldsymbol{q}(t)\cdot\boldsymbol{n} - P_h^{\partial}(\boldsymbol{q}(t)\cdot\boldsymbol{n})\|^2_{\partial\mathcal{T}_H} + \frac{\epsilon_2}{2}\|e_u(t) - e_{\widehat{u}}(t)\|^2_{\tau} \\
&\quad + \frac{1}{2\tau}\|\boldsymbol{q}(0)\cdot\boldsymbol{n} - P_h^{\partial}(\boldsymbol{q}(0)\cdot\boldsymbol{n})\|^2_{\partial\mathcal{T}_H} + \frac{1}{2}\|e_u(0) - e_{\widehat{u}}(0)\|^2_{\tau} \\
&\leq C\frac{h^{2s}}{H}\|\boldsymbol{q}\|^2_{L^\infty(H^{s+1})} + \frac{\epsilon_2}{2}\|e_u(t) - e_{\widehat{u}}(t)\|^2_{\tau} \\
&\quad + C\frac{h^{2s}}{H}\|\boldsymbol{q}(0)\|^2_{s+1} + \frac{1}{2}\|e_u(0) - e_{\widehat{u}}(0)\|^2_{\tau}
\end{aligned}$$

and

$$\begin{aligned}
|\mathbb{T}_7| &\leq \frac{1}{2\tau}\int_0^t \|\boldsymbol{q}_t\cdot\boldsymbol{n} - P_h^{\partial}(\boldsymbol{q}_t\cdot\boldsymbol{n})\|^2_{\partial\mathcal{T}_H} + \frac{1}{2}\int_0^t \|e_u - e_{\widehat{u}}\|^2_{\tau} \\
&\leq C\frac{h^{2s}}{H}\|\boldsymbol{q}_t\|^2_{L^2(H^{s+1})} + \frac{1}{2}\int_0^t \|e_u - e_{\widehat{u}}\|^2_{\tau}.
\end{aligned}$$

Similar to the estimate of $\mathbb{S}_6$ in Theorem 5.4.5, we obtain an upper bound of $\mathbb{T}_8$ and $\mathbb{T}_9$. Then, we have

$$\begin{aligned}
|\mathbb{T}_8| &= |\langle P_h^{\partial}u(t) - P_H^{\partial}u(t)\,,\, \tau(e_u(t) - e_{\widehat{u}}(t))\rangle_{\partial\mathcal{T}_H}| \\
&\leq \frac{\tau}{2\epsilon_2}\|P_h^{\partial}u(t) - u(t)\|^2_{\partial\mathcal{T}_H} + \frac{\tau\alpha_0}{2\epsilon_2}\|\kappa^{\frac{1}{2}}(u(t) - w(t))\|^2_{\partial\mathcal{T}_H} \\
&\quad + \epsilon_2\|e_u(t) - e_{\widehat{u}}(t)\|^2_{\tau} \\
&\leq C\frac{h^{2s}}{H}\|u\|_{L^\infty(H^{s+1})} + C\frac{H}{\Lambda_1^*}\|\kappa^{\frac{1}{2}}\nabla u\|_{L^\infty(L^2)} + \epsilon_2\|e_u(t) - e_{\widehat{u}}(t)\|^2_{\tau}.
\end{aligned}$$

by $u(0)=0$, and

$$
\begin{aligned}
|\mathbb{T}_9| &\le \frac{\tau}{2}\int_0^t \|P_h^{\partial}u_t - u_t\|^2_{\partial\mathcal{T}_H} + \frac{\tau\alpha_0}{2}\int_0^t \|\kappa^{\frac{1}{2}}(u_t - P_H^{\partial}u_t)\|^2_{\partial\mathcal{T}_H} + \int_0^t \|e_u - e_{\widehat{u}}\|^2_{\tau} \\
&\le C\frac{h^{2s}}{H}\|u_t\|_{L^2(H^{s+1})} + C\frac{H}{\Lambda_1^*}\|\kappa^{\frac{1}{2}}\nabla u_t\|_{L^2(L^2)} + \int_0^t \|e_u - e_{\widehat{u}}\|^2_{\tau}
\end{aligned}
$$

The last term can be estimated that if we differentiate the identity in Lemma 5.4.4 with $w = P_H^{\partial}u$ and evaluate the result at $t=0$, we get

$$
\begin{aligned}
\|\boldsymbol{e}_q(0)\|^2_{\alpha} + \|e_u(0) - e_{\widehat{u}}(0)\|^2_{\tau} &= -(\alpha\boldsymbol{\delta}_q(0)\,,\,\boldsymbol{e}_q(0))_{\mathcal{T}_h} \\
&\quad - \langle \boldsymbol{q}(0)\cdot\boldsymbol{n} - P_h^{\partial}(\boldsymbol{q}(0)\cdot\boldsymbol{n})\,,\, e_u(0) - e_{\widehat{u}}(0)\rangle_{\partial\mathcal{T}_H} \\
&\le \frac{1}{2}\left(\|\boldsymbol{e}_q(0)\|^2_{\alpha} + \|e_u(0) - e_{\widehat{u}}(0)\|^2_{\tau}\right) \\
&\quad + \frac{1}{2}\left(\|\boldsymbol{\delta}_q(0)\|^2 + \frac{1}{\tau}\|\boldsymbol{q}(0)\cdot\boldsymbol{n} - P_h^{\partial}(\boldsymbol{q}(0)\cdot\boldsymbol{n})\|^2_{\partial\mathcal{T}_H}\right)
\end{aligned}
$$

since $u(0)=0$ and $e_u(0)=0$. So, for $\mathbb{T}_6$, we obtain

$$
\begin{aligned}
\|\boldsymbol{e}_q(0)\|^2_{\alpha} + \|e_u(0) - e_{\widehat{u}}(0)\|^2_{\tau} &\le \|\boldsymbol{\delta}_q(0)\|^2 + C\|\boldsymbol{q}(0)\cdot\boldsymbol{n} - P_h^{\partial}(\boldsymbol{q}(0)\cdot\boldsymbol{n})\|^2_{\partial\mathcal{T}_H} \\
&\le Ch^{2s}\|\boldsymbol{q}(0)\|_s + C\frac{h^{2s}}{H}\|\boldsymbol{q}(0)\|^2_{s+1}.
\end{aligned}
$$

Then, for any time $t\in(0,t_F]$, we have

$$
\begin{aligned}
&\frac{1}{2}\|\boldsymbol{e}_q(t)\|^2_{\alpha} + \left(\frac{1}{2} - \frac{3\epsilon_2}{2}\right)\|e_u(t) - e_{\widehat{u}}(t)\|^2_{\tau} + \left(1 - \frac{\epsilon_1}{2}\right)\int_0^t \|\partial_t e_u\|^2 \\
&\qquad \le Ch^{2s}\left(\|\boldsymbol{q}(0)\|^2_s + \|u_t\|^2_{L^2(H^s)} + \|\boldsymbol{q}_t\|^2_{L^2(H^s)}\right) \\
&\qquad\quad + Ch^{2s}H^{-1}\left(\|\boldsymbol{q}(0)\|^2_{s+1} + \|u\|^2_{L^2(H^{s+1})} + \|u_t\|^2_{L^2(H^{s+1})} + \|\boldsymbol{q}_t\|^2_{L^2(H^{s+1})}\right) \\
&\qquad\quad + Ch^{2s}H^{-1}\left(\|u\|^2_{L^\infty(H^{s+1})} + \|\boldsymbol{q}\|^2_{L^\infty(H^{s+1})}\right) + C\frac{H}{\Lambda_1^*}\|\kappa^{\frac{1}{2}}\nabla u\|^2_{L^\infty(L^2)} \\
&\qquad\quad + C\frac{H}{h\Lambda_1^*}\|\kappa^{\frac{1}{2}}\nabla u_t\|^2_{L^2(L^2)} + C\int_0^t \left(\|\boldsymbol{e}_q\|^2_{\alpha} + \|e_u - e_{\widehat{u}}\|^2_{\tau}\right).
\end{aligned}
$$

Taking $\epsilon_1 = 2, \epsilon_2 < \frac{1}{3}$ and applying Gronwall's lemma, we have

$$\begin{aligned}
\|\boldsymbol{e}_q(t)\|_\alpha + \|e_u(t) - e_{\widehat{u}}(t)\|_\tau &\leq Ch^s \left(\|\boldsymbol{q}(0)\|_s + \|u_t\|_{L^2(H^s)} + \|\boldsymbol{q}_t\|_{L^2(H^s)}\right) \\
&+ Ch^s H^{-\frac{1}{2}} \left(\|\boldsymbol{q}(0)\|_{s+1} + \|u\|_{L^2(H^{s+1})} + \|u_t\|_{L^2(H^{s+1})} + \|\boldsymbol{q}_t\|_{L^2(H^{s+1})}\right) \\
&+ Ch^s H^{-\frac{1}{2}} \left(\|u\|_{L^\infty(H^{s+1})} + \|\boldsymbol{q}\|_{L^\infty(H^{s+1})}\right) \\
&+ C\left(\frac{H}{h\Lambda_1^*}\right)^{\frac{1}{2}} \|\kappa^{\frac{1}{2}}\nabla u_t\|_{L^2(L^2)} + C\left(\frac{H}{\Lambda_1^*}\right)^{\frac{1}{2}} \|\kappa^{\frac{1}{2}}\nabla u\|_{L^\infty(L^2)}
\end{aligned}$$

Taking the maximum in both side of the inequality, we get the estimates. This completes the proof. □

# 6. CONCLUSIONS

In the dissertation, we propose generalized multiscale methods in the framework of the discontinuous Galerkin and the hybridizable discontinuous Galerkin finite element methods for solving steady-state and transient flows in highly heterogeneous porous media.

Within discontinuous Galerkin Simmetric Penalty (SIPG) framework we propose two different types of multiscale spaces on the coarse mesh. The first type of spaces is based on the solutions of some local spectral problem, uses the sum of a weighted $L^2$-norm and a penalty term for computing the mass matrix. For the construction of the second space, a local spectral problem is solved in the snapshot space where the snapshots are chosen as harmonic extensions of unitary boundary functions. These multiscale basis functions are inherently discontinuous and SIPG is used to produce consistent finite element approximation.

Similarly, within the hybridizable discontinuous Galerkin framework, we propose several multiscale spaces for the numerical traces. The main contribution is the construction of a low dimensional trace space that brings some of the fine-scale features of the exact solution. We present a general framework for construction the trace spaces. This procedure consists of three steps: (1) a partition of the coarse skeleton; (2) a construction of a local snapshot space; (3) a construction of an offline space and consequently a construction of the numerical trace space. Within this framework, we proposed and test three different types of trace spaces. The first class uses the boundaries of the coarse-grid subdomain. The second class is constructed by using the traces on the faces that are strictly within coarse blocks. In this regard, the second approach uses an oversampling techniques where the information in larger

domains is used in the construction. For the construction of the last class, we use the boundaries on some specially chosen subdomains. Comparing with the previous classes, the local spectral problem is posed on the smaller domains and we can save significantly on the computational cost.

Further, we extend the multiscale HDG method to nonlinear time-dependent problems. To solve time-dependent problems, we derive the upscale structure with backward Euler time-discretization. For nonlinear problems, we use the local spectral problem with a parameter dependent coefficient instead of a nonlinear coefficient and do Richardson iteration to find a numerical solution. Furthermore, we investigate an optimal stabilization parameter $\tau$ defined on fine and coarse gird. As a working value of the stabilization parameter for nonlinear problems, we choose either 1 and $h$ as stabilization parameter on a fine and coarse grids, respectively.

Finally, investigate the stability of the proposed methods and derive error estimate. In the case of multiscale SIPG method the analysis shows that one needs to amend the mass matrix with the penalty term to obtain good error estimates. In HDG method, we show that the stability is independent of the choice of multiscale space, but the error estimates depends on a local spectral problem. Also, we provide error estimates of the linear parabolic problem.

In our future work, we plan to develop error analysis for nonlinear problems. Our numerical results show that all methods achieve a good accuracy with a few degrees of freedom on various permeability examples presented in the dissertation. We note that the multiscale HDG methods with using snapshot spaces are recommended if one can estimate the error between the solution and its projection onto the snapshot space and reduce the dimension of the local spectral problems.

# REFERENCES


[1] J. Aarnes. On the use of a mixed multiscale finite element method for greater flexibility and increased speed or improved accuracy in reservoir simulation. *Multiscale Modeling and Simulation*, 2(3):421–439, 2004.

[2] J. Aarnes and Y. Efendiev. Mixed multiscale finite element for stochastic porous media flows. *SIAM Journal on Scientific Computing*, 30 (5):2319–2339, 2008.

[3] T. Arbogast. Analysis of a two-scale, locally conservative subgrid upscaling for elliptic problems. *SIAM Journal on Numerical Analysis*, 42(2):576–598, 2004.

[4] T. Arbogast. Homogenization-based mixed multiscale finite elements for problems with anisotropy. *Multiscale Modeling and Simulation.*, 9(2):624–653, 2011.

[5] T. Arbogast and K. Boyd. Subgrid upscaling and mixed multiscale finite elements. *SIAM Journal on Numerical Analysis*, 44(3):1150–1171, 2006.

[6] T. Arbogast and D. Brunson. A computational method for approximating a Darcy-Stokes system governing a vuggy porous medium. *Computational Geosciences*, 11(3):207–218, 2007.

[7] T. Arbogast, L. Cowsar, M. Wheeler, and I. Yotov. Mixed finite element methods on nonmatching multiblock grids. *SIAM Journal on Numerical Analysis*, 37(4):1295–1315, 2000.

[8] T. Arbogast and M. Gomez. A discretization and multigrid solver for a Darcy-Stokes system of three dimensional vuggy porous media. *Computational Geosciences*, 13(2):331–343, 2009.

[9] T. Arbogast, G. Pencheva, M. Wheeler, and I. Yotov. A multiscale mortar mixed finite element method. *Multiscale Modeling and Simulation*, 6(1):319–346, 2007.

[10] T. Arbogast and H. Xiao. A multiscale mortar mixed space based homogenization for heterogeneous elliptic problems. *SIAM Journal on Numerical Analysis*, 51(1):377–399, 2013.

[11] D. Arnold. An interior penalty finite element method with discontinuous elements. *SIAM Journal on Numerical Analysis*, 19(4):742–760, 1982.

[12] D. Arnold, F. Brezzi, B. Cockburn, and L. Marini. Unified analysis of discontinuous Galerkin methods for elliptic problems. *SIAM Journal on Numerical Analysis*, 39(5):1749–1779, 2001/02.

[13] C. Bernardi, Y. Maday, and A. Patera. Domain decomposition by the mortar element method. In H. Kaper, M. Garbey, and G. Pieper, editors, *Asymptotic and Numerical Methods for Partial Differential Equations with Critical Parameters*, volume 384 of *NATO ASI Series*, pages 269–286. Springer Netherlands, 1993.

[14] S. Boyaval, C. LeBris, T. Lelièvre, Y. Maday, N. Nguyen, and A. Patera. Reduced basis techniques for stochastic problems. *Archives of Computational Methods in Engineering*, 17(4):435–454, 2010.

[15] F. Brezzi and M. Fortin. *Mixed and hybrid finite element methods*, volume 15 of *Springer Series in Computational Mathematics*. Springer-Verlag, New York, 1991.

[16] C. Chu, I. G. Graham, and T. Hou. A new multiscale finite element method for high-contrast elliptic interface problems. *Mathematics of Computation*, 79(272):1915–1955, 2010.

[17] E. Chung, Y. Efendiev, and W. Leung. Generalized multiscale finite element methods for wave propagation in heterogeneous media. *Multiscale Modeling and Simulation*, 12(4):1691–1721, 2014.

[18] P. Ciarlet. *The finite element method for elliptic problems*. Elsevier North-Holland, New York, 1978.

[19] B. Cockburn, B. Dong, and J. Guzmán. A superconvergent LDG-hybridizable Galerkin method for second-order elliptic problems. *Mathematics of Computation*, 77(264):1887–1916, 2008.

[20] B. Cockburn, B. Dong, J. Guzmán, M. Restelli, and R. Sacco. A hybridizable discontinuous Galerkin method for steady-state convection-diffusion-reaction problems. *SIAM Journal on Scientific Computing*, 31(5):3827–3846, 2009.

[21] B. Cockburn and J. Gopalakrishnan. A characterization of hybridized mixed methods for second order elliptic problems. *SIAM Journal on Numerical Analysis*, 42(1):283–301, 2004.

[22] B. Cockburn, J. Gopalakrishnan, and R. Lazarov. Unified hybridization of discontinuous Galerkin, mixed, and continuous Galerkin methods for second order elliptic problems. *SIAM Journal on Numerical Analysis*, 47(2):1319–1365, 2009.

[23] B. Cockburn, J. Gopalakrishnan, and F. Sayas. A projection-based error analysis of HDG methods. *Mathematics of Computation*, 79(271):1351–1367, 2010.

[24] B. Cockburn, W. Qiu, and K. Shi. Conditions for superconvergence of HDG methods for second-order elliptic problems. *Mathematics of Computation*, 81(279):1327–1353, 2012.

[25] B. Cockburn, W. Qiu, and K. Shi. Superconvergent HDG methods on isoparametric elements for second-order elliptic problems. *SIAM Journal on Numerical Analysis*, 50(3):1417–1432, 2012.

[26] J. Douglas and T. Dupont. Interior penalty procedures for elliptic and parabolic Galerkin methods. In *Computing methods in applied sciences*, pages 207–216. Springer, 1976.

[27] M. Dryja. On discontinuous Galerkin methods for elliptic problems with discontinuous coefficients. *Computational Methods in Applied Mathematics*, 3(1):76–85, 2003. Dedicated to Raytcho Lazarov.

[28] J. Eberhard and G. Wittum. A coarsening multigrid method for flow in heterogeneous porous media. In *Multiscale methods in science and engineering*, volume 44 of *Lecture Notes in Computational Science and Engineering*, pages 111–132. Springer, Berlin, 2005.

[29] Y. Efendiev and J. Galvis. A domain decomposition preconditioner for multiscale high-contrast problems. In *Domain Decomposition Methods in Science and Engineering XIX*, pages 189–196. Springer, 2011.

[30] Y. Efendiev and J. Galvis. Coarse-grid multiscale model reduction techniques for flows in heterogeneous media and applications. In *Numerical Analysis of Multiscale Problems*, pages 97–125. Springer, 2012.

[31] Y. Efendiev, J. Galvis, and T. Hou. Generalized multiscale finite element methods (GMsFEM). *Journal of Computational Physics*, 251:116–135, 2013.

[32] Y. Efendiev, J. Galvis, R. Lazarov, and J. Willems. Robust domain decomposition preconditioners for abstract symmetric positive definite bilinear forms. *ESAIM. Mathematical Modelling and Numerical Analysis*, 46(5):1175–1199, 2012.

[33] Y. Efendiev, J. Galvis, and F. Thomines. A systematic coarse-scale model reduction technique for parameter-dependent flows in highly heterogeneous media and its applications. *Multiscale Modeling and Simulation*, 10(4):1317–1343, 2012.

[34] Y. Efendiev, J. Galvis, and X. Wu. Multiscale finite element methods for high-contrast problems using local spectral basis functions. *Journal of Computational Physics*, 230(4):937–955, 2011.

[35] Y. Efendiev and T. Hou. *Multiscale Finite Element Methods: Theory and Applications*, volume 4 of *Surveys and Tutorials in the Applied Mathematical Sciences*. Springer, New York, 2009.

[36] Y. Efendiev, T. Hou, and V. Ginting. Multiscale finite element methods for nonlinear problems and their applications. *Communications in Mathematical Sciences*, 2(4):553–589, 2004.

[37] J. Galvis and Y. Efendiev. Domain decomposition preconditioners for multiscale flows in high contrast media. *Multiscale Modeling and Simulation*, 8(4):1461–1483, 2010.

[38] I. Graham, P. Lechner, and R. Scheichl. Domain decomposition for multiscale PDEs. *Numerische Mathematik*, 106(4):589–626, 2007.

[39] P. Grisvard. *Elliptic problems in nonsmooth domains*, volume 24 of *Monographs and Studies in Mathematics*. Pitman (Advanced Publishing Program), Boston, MA, 1985.

[40] M. Hinze and S. Volkwein. Proper orthogonal decomposition surrogate models for nonlinear dynamical systems: error estimates and suboptimal control. In P. Benner, V. Mehrmann, and D. Sorensen, editors, *Dimension Reduction of Large-Scale Systems*, volume 45 of *Lecture Notes in Computational Science and Engineering*, pages 261–306. Springer Berlin Heidelberg, 2005.

[41] T. Hou and X. Wu. A multiscale finite element method for elliptic problems in composite materials and porous media. *Journal of Computational Physics*, 134(1):169–189, 1997.

[42] T. Hughes, G. Feijoo, L. Mazzei, and J. Quincy. The variational multiscale method - a paradigm for computational mechanics. *Computer Methods in Applied Mechanics and Engineering*, 166(1):3–24, 1998.

[43] O. Iliev, R. Lazarov, and J. Willems. Variational multiscale finite element method for flows in highly porous media. *Multiscale Modeling and Simulation*, 9(4):1350–1372, 2011.

[44] P. Jenny, S. Lee, and H. Tchelepi. Multi-scale finite volume method for elliptic problems in subsurface flow simulation. *Journal of Computational Physics*, 187(1):47–67, 2003.

[45] S. Kaulmann, M. Ohlberger, and B. Haasdonk. A new local reduced basis discontinuous galerkin approach for heterogeneous multiscale problems. *Comptes Rendus Mathematique*, 349(23):1233–1238, 2011.

[46] N. Nguyen, J. Peraire, and B. Cockburn. An implicit high-order hybridizable discontinuous galerkin method for linear convection–diffusion equations. *Journal of Computational Physics*, 228(9):3232–3254, 2009.

[47] J. Nitsche. Über ein variationsprinzip zur lösung von dirichlet-problemen bei verwendung von teilräumen, die keinen randbedingungen unterworfen sind. In *Abhandlungen aus dem mathematischen Seminar der Universität Hamburg*, volume 36, pages 9–15. Springer, 1971.

[48] J. Nitsche. On dirichlet problems using subspaces with nearly zero boundary conditions. *The mathematical foundations of the finite element method with applications to partial differential equations*, pages 603–627, 1972.

[49] J. Oden, I. Babuŝka, and C. Baumann. A discontinuoushpfinite element method for diffusion problems. *Journal of Computational Physics*, 146(2):491–519, 1998.

[50] D. Pietro and A. Ern. *Mathematical aspects of discontinuous Galerkin methods*, volume 69. Springer Science and Business Media, 2011.

[51] W. Reed and T. Hill. Triangular mesh methods for the neutron transport equation. *Los Alamos Report LA-UR-73-479*, 1973.

[52] B. Rivière, M. Wheeler, and V. Girault. A priori error estimates for finite element methods based on discontinuous approximation spaces for elliptic problems. *SIAM Journal on Numerical Analysis*, 39(3):902–931, 2001.

[53] A. Toselli and O. Widlund. *Domain decomposition methods – Algorithms and Theory*, volume 34 of *Computational Mathematics*. Springer-Verlag, 2005.

[54] P. Vassilevski. *Multilevel block-factrorization preconditioners. Matrix-based analysis and algorithms for solving finite element equations*. Springer-Verlag, New York, 2008.

[55] P. Vassilevski. Coarse spaces by algebraic multigrid: multigrid convergence and upscaling error estimates. *Advances in Adaptive Data Analysis. Theory and Applications*, 3(1-2):229–249, 2011.

[56] M. Wheeler. An elliptic collocation-finite element method with interior penalties. *SIAM Journal on Numerical Analysis*, 15(1):152–161, 1978.

[57] M. Wheeler, G. Xue, and I. Yotov. A multiscale mortar multipoint flux mixed finite element method. *ESAIM. Mathematical Modelling and Numerical Analysis*, 46(4):759–796, 2012.